Aus dem Institut für Biochemie

der Medizinischen Fakultät Charité - Universitätsmedizin Berlin

DISSERTATION

A systems biology approach to model cardiomyocyte metabolism

zur Erlangung des akademischen Grades
Doctor medicinae (Dr. med.)

vorgelegt der Medizinischen Fakultät
Charité – Universitätsmedizin Berlin

von
Frau Anja Karlstädt

aus Perleberg

Datum der Promotion: 25.10.2013

To C.K., M.K., G.E.K., J.K., E.K. and R.K.

Contents

Tables and Figures

Tables

Figures

Abbreviations and variables

Abbreviations

ACC	Acetyl-CoA carboxylase
ANF	Atrial natriuretic factor
BRENDA	Braunschweig Enzyme Database
CHF	Congestive heart failure
CPT-1	Carnitine palmitoyl transferase I
CVD	Cardiovascular diseases
EC	Enzyme Commission
FBA	Flux Balance Analysis
FCA	Flux Coupling Analysis
FVA	Flux Variability Analysis
G6PDH	Glucose-6-phosphate dehydrogenase
GEO	Gene Expression Omnibus
GLUT1	Glucose Transporter 1
GS	Glycogen synthase
KEGG	Kyoto Encyclopedia of Genes and Genome
KO	KEGG Orthology
LCAD	Long-chain acyl-CoA dehydrogenase
LP	Linear Programming

$m\dot{V}O_2$	myocardial oxygen consumption
MCAD	Medium-chain acyl-CoA dehydrogenase
MCD	Malonyl-CoA decarboxylase
MHC-α	Myosin heavy chain α
MHC-β	Myosin heavy chain β
MILP	Mixed-integer linear problem
MPI	Math Program Instructions
MPS	Mathematical Programming System
ODE	Ordinary differential equation
PDK2	Pyruvate dehydrogenase kinase 2
PGC-1	Coactivator PPAR-γ 1
PPAR-α	Peroxisome proliferator-activated receptor α
ROS	Reactive oxygen species
SBML	Systems Biology Markup language
SEM	Supporting electronic material
TCA	Tricyclic acid cycle
TCD	Transport Classification Database
UniprotKB	Uniprot Knowledgebase
XML	Extensible Markup Language

Variables

β	is a coefficient
[E]	represents an enzyme concentration
[P]	represents a product concentration
[S]	represents a substrate concentration

c	is a stoichiometric coefficient
C_i^+	is the efficiency index
$f(v)$	is the objective function in the optimization problem
kcat	represents the turnover number for a enzyme
k_+	represents a kinetic or rate constant for a forward reaction
k_-	represents a kinetic or rate constant for a backward reaction
K_m	is the Michaelis constant
N	represents the stoichiometric matrix
q_j	identifies criteria
S	is a single substrate
S_i	represent a distance
t	represents a time point
v	is a flux vector
V_{max}	represents a substrate concentration
V_{myo}	is the cardiomyocyte volume
v_m	is a single external substrate uptake flux vector
v_r	is a single target flux vector
v_s	identifies a vector of all substrate uptake fluxes, total substrate uptake flux
v_t	identifies a vector of all target fluxes
z^*	is a constraint in the optimisation problem

Zusammenfassung

Kardiovaskuläre Erkrankungen zählen weiterhin zu den Haupttodesursachen weltweit. Trotz umfangreicher Forschungsbemühungen ist eine umfassende Behandlung, insbesondere eines kongestiven Herzversagens (congestive heart failure, CHF), zur Zeit nicht möglich da molekulare sowie zelluläre Mechanismen für deren Entstehung noch nicht vollständig geklärt wurden. In diesem Kontext bieten mathematische Modelle die Möglichkeit molekularen Mechanismen und metabolische Veränderungen unter hämodynamischer Stresssituationen und veränderter Substratversorgung des Herzen zu analysieren und die Entwicklung neuer Therapien zu unterstützen.

Die vorliegende Arbeit präsentiert eine umfangreiche metabolische Netzwerkrekonstruktion des humanen Kardiomyozyten (CardioNet) und beschreibt einen systembiologischen Ansatz zur Analyse der Effizienz des kardialen Metabolismus. Das rekonstruierte Netzwerk besteht aus 1793 metabolischen Reaktionen, darunter 560 Transportprozesse, die sich auf 6 verschiedene Kompartimente verteilen. Mit Hilfe dieses Models ist es möglich 368 verschiedene metabolische Funktionen des Kardiomyozyten zu simulieren.

In dieser Arbeit wird analysiert, inwiefern eine variable Substratversorgung von Glukose, Laktat, Fettsäuren und Ketonkörpern die Effizienz des kardialen Metabolismus beeinflussen könnte. Dabei wird ein im Rahmen dieser Arbeit entwickeltes Konzept verwendet, das ausgehend von der jeweiligen Substratversorgung Flussverteilungen ableitet und einen entsprechenden Effizienzwert ermittelt. Das entwickelte Effizienzmaß(C_{i^+}), basiert auf der Annahme, dass zelluläre Funktionen optimiert werden und der Verbrauch von exogenen und endogenen Substraten sowie Sauerstoff auch bei veränderten Umgebungsbedingungen möglichst minimal ist. Insgesamt wurden mehr als 400000 Einzelsimulationen unter Verwendung einer metabolischen Zielfunktion des humanen Kardiomyozyten, basierend auf experimentellen Ergebnissen, durchgeführt. Anhand von Simulationen kann gezeigt werden, dass eine balancierte Substratkombination aus allen betrachteten Substanzklassen eine höhere Effizienz des kardialen Stoffwechsels ermöglicht als unter Verwendung nur einzelner Substrate.

Abschließend kann festgestellt werden, dass mit CardioNet ein funktionelles und valides Netzwerk des humanen Kardiomyozyten vorgestellt wird. Darüberhinaus ermöglicht der in dieser Arbeit präsentierte mathematische Ansatz

weiterführende theoretische Studien des kardialen Metabolismus und Analysen der kardialen Effizienz.

Abstract

Cardiovascular diseases are still among the main causes of death worldwide. Yet in spite of enormous and broad efforts to develop treatments, in particular, for congestive heart failure no such cures are currently available, because underlying molecular and cellular mechanism are still not completely understood.

This thesis presents a comprehensive metabolic network reconstruction of the human cardiomyocyte and establishes a concept to analyse cardiac efficiency in nutritional stress. The reconstructed network comprises of 1793 metabolic reactions, including 560 transport processes in six compartments. The network is capable to accomplish a set of 368 metabolic functions of the cardiomyocyte.

This study aims to analyse how variations in the substrate supply of glucose, lactate, fatty acids and ketone bodies may influence the efficiency of cardiac performance. A concept is developed to estimate flux distributions in varied substrate availability and determine cardiac efficiency. This measure of cardiac efficiency (C_{i^+}) is based on the assumption that cellular functions are optimized and given exogenous and endogenous resources (substrates, oxygen) are used at minimal cost.

In total more than 400 000 simulations of altered substrate supply have been performed, while applying a metabolic target function of the human cardiomyocyte based on experimental data, including the formation of ATP, production of NADPH and important membrane lipids such as ceramide, cardiolipin and sphingomyelin.

In conclusion, CardioNet is a functionally and validated metabolic network of the human cardiomyocyte. The presented mathematical approach enables theoretical studies of the cardiomyocyte metabolism and analysis of cardiac efficiency.

1 Introduction

Cardiovascular diseases (CVD) are among the main causes of death worldwide [1], in particular myocardial infarction and stroke. Major risk factors for development of cardiovascular diseases have been identified as tobacco abuse, physical inactivity, unhealthy diet and genetic predisposition.

Frequently, CVD results in the development of congestive heart failure (CHF), in particular hypertension, myocardial ischemia and infarction [2], diabetes and cardiomyopathies are known precipitants. In the progress of CHF the heart initially undergoes compensatory mechanisms, including myocardial hypertrophy and cardiac remodelling to maintain cardiac output. These adaptations are characterized by signal transduction mechanisms and alterations in cardiac energy metabolism by increased expression of embryonic genes [3, 4].

Despite enormous and broad efforts to unveil the underlying mechanisms for the development of CHF, there is still no treatment available. A complete understanding of molecular mechanisms and metabolic changes in cardiomyocytes during nutritional and hemodynamic stress might lead to better treatment and prevention of heart failure, thus eventually decreasing the death rate.

In this context, systems biology enables to analyse cardiac metabolism and to identify potential drug targets, thus perturbate in-silico studies prior time-consuming and expensive animal studies [5]. Systems biology is an integrative research field aiming to investigate complex biological systems by analysing their behaviour at all levels of cellular organization in different environments. Advances in high-throughput technology offer to integrate large sets of data collected from genome sequencing (genomics), gene expression levels (transcriptomics, e.g. microarrays) and protein levels (proteomics) or determination of present metabolites (metabolomics). These advances enable to define mathematical and computational models of biological networks in order to test and design hypothesis-driven experiments. A necessary prerequisite to study molecular mechanisms and metabolic changes in cardiomyocytes is to reconstruct a complete network of the cardiomyocyte. This network may contribute to elucidate the underlying biological

processes perturbed in cardiac diseases.

The rationale arises from previously reported comprehensive network reconstructions of biological systems, which revealed new biological insight into metabolic changes in altered extra- and intracellular conditions [6–10]. In general, network reconstructions can be divided into two approaches: a data-driven or bottom-up approach compared to a hypothesis-driven or top-down approach. Both methods aim to reconstruct functional and complete networks of the respective biological system to enable mathematical predictions of the system's behaviour. Taking the advantage of high-throughput technology, recent mathematical approaches [5, 11] enable to integrate gene expression information from high-throughput technologies, e.g. microarrays, to reconstruct networks which are consistent with the given gene expression state.

However, fully automated network reconstructions have been shown to lack functionality and consistency to cover important cellular processes [6]. One known limitation of automated reconstructions is the quality of applied high-throughput data and the variable annotation resources [12, 13]. This enhances the need of combining automated reconstruction methods with human-supervised curation. In the recent past different tools [14–16] and resources have been developed to aid researchers to integrate multiple data with varying levels of evidence. These resources provide information about metabolic reactions [17–19], compounds [20, 21], thermodynamics [22] as well as gene and protein alignment from different tissues and cell types [23–26]. Together this enables the reconstruction and comparison of specific cellular networks even of higher organisms. Work in the field of cardiology has uncovered many interactions between metabolic energy provision and cardiac contraction following the hypothesis of energy depletion in the failing heart. This concept was first proposed in 1939 by Herrman and Decherd [27, 28] based on their observation of depleted creatine content in the failing myocardium. However, the impact of nutritional stress on cardiac efficiency has never been systematically analysed for a large set of substrates, neither for the intact nor diseased heart.

This thesis presents a comprehensive metabolic network reconstruction of the human cardiomyocyte and establishes a concept to analyse cardiac efficiency in nutritional stress. The following sections of this introduction provide the biological and mathematical background for modelling cardiac metabolism.

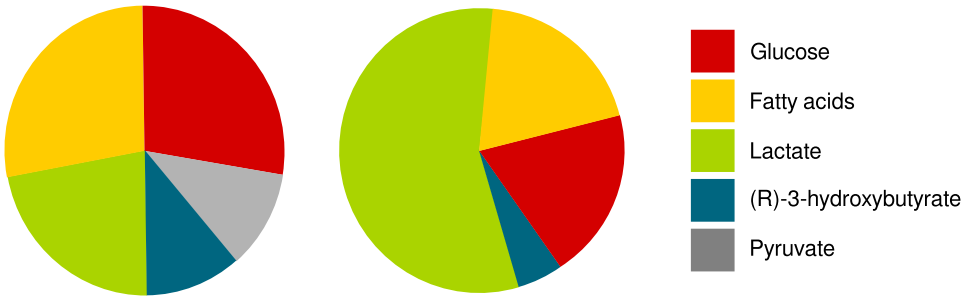

Figure 1.1: ***A.*** *Under normal physiological conditions, fatty acids are the preferred substrates followed by glucose. Unlike other tissues, cardiac metabolism is able to shift the substrate preference according to substrate availability and cardiac workload.*
B. *Increased lactate availability as observed with physical activity will enhance substrate uptake.*

1.1 Cardiac metabolism and substrate utilisation

To understand the mechanism underlying pathological conditions, it is important to first consider the intact cardiac metabolism. The heart is a functional syncytium of highly specialised cells (cardiomyocytes) responsible for cardiac contraction. Even under normal physiological conditions, cardiomyocytes have to fulfil a wide range of metabolic functions, serving cellular integrity and energy demands to maintain contractile activity for the cardiac cycle. Optimal cardiomyocyte function depends on a critical balance of energy production (e.g. ATP), replenishment and biosynthesis of macromolecules (e.g. protein, membrane lipids). Consequently, it is hypothesized that an imbalance of energy production and use on the cellular level due to changes in energy substrate metabolism may explain the development of CHF [29, 30]. This imbalance may increase the susceptibility of cardiac metabolism under stress, such as ischemia or increased work load.

Among all human organs, the heart is very unique in terms of its substrate utilisation preference. Metabolic functions greatly depend on the availability of oxygen and external substrates, including fatty acids, glucose, lactate, pyruvate

and amino acids [31]. However, the contribution of each substrate for a metabolic process greatly depends its extracellular availability, on the cellular state (cell cycle), oxygen supply and endocrine conditions [32, 33].

The energy for cardiac contraction is mostly derived from oxidative phosphorylation of ADP to ATP. Therefore, ATP turnover and myocardial oxygen consumption are commonly used to estimate cardiac metabolic activity and determine cardiac efficiency. One definition of cardiac efficiency is the ratio of cardiac work (pressure-volume area) and myocardial oxygen consumption, which directly reflects the relation between $m\dot{V}O_2$ and oxidative phosphorylation. Hence, alterations in cardiac energy-substrate metabolism, e.g. nutrient supplies, may affect cardiac efficiency.

Under normal physiological conditions, in particular in the fasted state when fatty acid plasma levels are high, fatty acids are the preferred substrates followed by glucose. Therefore, the β-oxidation of fatty acids derives 60% to 90% of the ATP production, while glucose and lactate contribute up to 40% (see Figure 1.1). However, unlike in other tissues, cardiac metabolism is able to shift the substrate preference, according to the substrates' availability in the blood stream and cardiac workload. A switch from predominately fatty acid oxidation to increased oxidation of carbohydrates, in particular glucose, is observed under hypoxic and hypertrophic conditions, but can also occur under normal physical activity.

Depending on the substrate class (lipids, carbohydrates, amino acids), myocardial oxygen consumption ($m\dot{V}O_2$) and ATP yield differ [34]. Due to its anatomical localisation, the adult heart receives an optimal oxygen supply, which enables a highly oxygen demanding degradation of long-chain fatty acids. Therefore, substrate oxidation can become a limiting factor for cardiac function in the event of nutritional deprivation, impaired substrate oxidation or decreased oxygen supply. Influenced by these intrinsic and extrinsic environmental conditions, the heart might utilise carbohydrates to a greater extent to make efficient use of the given substrate and oxygen supply. In this context, experiments in the working heart ex vivo showed that a short-term increase in workload shifts substrate preference towards increased oxidation of endogenous glucose from glycogen degradation, lactate and exogenous glucose [34].

Furthermore, with increased contractile activity of skeletal muscles, lactate concentration increases in the blood, thus initiating enhanced uptake and oxidation of lactate due to a better supply (see Figure 1.1). Likewise, glucose is increasingly utilised under continuous hemodynamic stress. These changes in

cardiac substrate oxidation are accompanied with altered oxygen consumption, thus either impaired or improved cardiac efficiency. In fact, experiments in the working heart in vivo showed profound shifts in glucose and fatty acid oxidation [35]. This study demonstrated an increased cardiac performance with glucose (up to 40%) compared with fatty acids as the main energy-providing substrate for a limited oxygen supply.

Further adaptations to metabolic stress influence the fatty acid composition of myocardial membrane phospholipids, which is known to alter with dietary fatty acid availability and oxygen supply [36, 37]. Another structural adaptation to hypoxia was shown to be associated with increased incorporation of long-chain omega-3 polyunsaturated fatty acids (e.g. eicosapentaenoic acid, docosahexaenoic acid), which mostly derived from dietary essential α-linoleic acid (C18:3 n-3, ALA) [36, 38]. These mechanisms seem to offer protection from oxidative damage, thus have beneficial effects against the risk of primary cardiac arrest [39, 40]. In the event of hypoxia, remodelling processes are initiated resulting in a shift in substrate preference from predominately fatty acid to glucose utilisation. In addition, the expression of genes is enhanced, which are specific for the fetal heart. Together these adaptation mechanisms enable cardiac metabolism to react promptly and flexibly to changing environmental conditions.

1.2 Stress response mechanisms and fetal gene profile

The initial response of cardiac metabolism during continuous stress is regulated by different factors, including transcriptional down regulation of adult gene transcripts. In particular, genes encoding for metabolic enzymes involved in fatty acid metabolism [41, 42], especially in the fatty acid β-oxidation, are down regulated. It is important to consider that in contrast to the rodent heart, the human heart does not show a switch to fetal isogenes [41], it rather shows a down or up regulation of genes resulting in a fetal metabolic gene profile.

Changes on the transcription level involve metabolic genes, including the glucose transporter GLUT1, pyruvate dehydrogenase kinase 2 (PDK2), glycogen synthase (GS), carnitine palmitoyl transferase I (CPT-1), medium chain acyl-CoA dehydrogenase (MCAD) and acetyl-CoA carboxylase (ACC). Decreased PDK2 enzyme levels result in decreased inhibition of the pyruvate dehydrogenase complex and

lead to enhanced carbohydrate oxidation, especially glucose and lactate.

Recent investigations have shown that the transcription levels in the failing and fetal heart [41, 43, 44] correspond to each other. Therefore, studies of the fetal heart enable implications for the failing heart. Studies of substrate utilisation in the fetal heart demonstrated an increased reliance of cardiac metabolism on carbohydrate utilisation in contrast to the non-failing adult heart. This is in concordance with studies in the failing heart showing a decreased fatty acid utilisation in favour of glucose. To understand the difference between adult and fetal heart, it is necessary to consider that in utero the heart is exposed to a reduced amount of oxygen compared to postnatal conditions. Therefore, the ability to efficiently oxidise fatty acids is likewise reduced. Hemodynamic changes 24h after birth cause a shifting from predominately glucose oxidation to fatty acid β-oxidation [45] due to increased oxygen supply.

In contrast to other organs, the fetal and adult heart has little capacity for short-term energy storage such as glycogen, which enables bypassing of any shortage of substrates. Therefore, cardiac metabolism is strongly dependent on constant nutritional supply and close regulation of energy demand with energy production to maintain cardiac function. In this context, recent findings of studies in the fetal heart demonstrated the lack of compensatory mechanisms of cardiac metabolism in an environment with impaired fatty acid utilisation and deprivation of carbohydrate utilisation. In fact, a reduction of glycogen synthase level and activity during the early phase of cardiac development was associated with high death rate in an animal study [46, 47]. Due to congenital heart defects, 90% of the animals die prenatally.

Although there is evidence for increased glucose utilisation in heart failure [48–50], recent findings indicate an increased development of insulin-resistance and decline in glucose oxidation in advanced heart failure [41, 51]. In this context, recent studies demonstrated the importance of insulin for cardiac metabolism and proposed that accumulation of non-oxidative metabolic intermediates and reactive oxygen-species may affect cardiac fatty acid and carbohydrate oxidation [52].

1.3 Regulators of cardiac metabolism

In addition to oxygen and substrate supply, there are further modulators such as nuclear-receptor transcription factors which are activated by lipid metabolites. Among these transcription factors, the most widely studied are the peroxisome

proliferator-activated receptor α (PPAR-α) family, including three isoforms: PPAR-α, PPAR-β and PPAR-γ.

Especially the fatty acid metabolism is highly regulated by PPAR-α and its coactivator PPAR-γ 1 (PGC-1), which control both fatty acid uptake and oxidation. PGC-1 promotes mitochondrial biogenesis and activation of PPAR-α, resulting in an increase of CPT-1 expression and activity.

Additionally, CPT-1 mediates the mitochondrial transport of fatty acids and by that regulates fatty acid β-oxidation. The activity of CPT-1 is regulated by cytosolic malonyl-CoA, which promotes inhibition of the enzyme [53]. Consequently, increasing the cytosolic level of malonyl-CoA results in inhibition of fatty acid β-oxidation. The level of cytosolic malonyl-CoA is regulated by the enzymatic activity of Malonyl-CoA decarboxylase and Acetyl-CoA carboxylase (ACC). PPAR-α is a known transcriptional regulator of Malonyl-CoA decarboxylase (MCD) [54]. Consequently, activation of PPAR-α increases the formation of acetyl-CoA through ACC activity, thus enhances the biosynthesis of fatty acids. This interplay of fatty acid biosynthesis and degradation is of particular importance in the impaired myocardium and in reduced carbohydrate supply.

Investigations on potential therapeutic targets to treat heart failure focus on changes in metabolic signalling mediated by these transcription factors and changes in creatine kinase activity. Furthermore, the inhibition of myocardial fatty acid oxidation has been of interest in order to improve left ventricular pump function [55]. The underlying hypothesis is that failure or maladaptations of cardiac metabolism are related to impaired myocardial energy metabolism, thus leading to heart failure. Therefore, calculated influence of cardiac metabolism might correct these maladaptations, increase cardiac efficiency and hence cardiac performance.

Among investigated pharmacological agents are (1) partial inhibitors of fatty acid β-oxidation or (2) agents which reduce the free fatty acid concentration in plasma. However, recent investigations found evidence that a certain level of fatty acid utilisation is required to maintain cardiac function in acute pressure overload [56]. Under experimental conditions, cardiac dysfunction increased under long-term reduction of lipoprotein fatty acid uptake despite a compensatory increase in glucose utilisation [56, 57]. Hence, initially beneficial effects of reduced fatty acid oxidation might result in the opposite.

The complexity of metabolism and cellular systems in general makes it difficult to study the cardiac efficiency under normal and diseased conditions in order to find balanced substrate combinations. Furthermore, experimental studies of cellular

systems and animal models are time consuming, expensive and are often limited to a small number of analysed parameters due to the work effort. Here, mathematical modelling and approaches in the field of systems biology offer to detect and understand cardiac adaptations and maladaptations on different stress factors instead of focusing only on single failing components.

1.4 Mathematical modelling of biological systems

Mathematical modelling of biological systems aims to study how related components cause specific behaviours of a system and how systems interact with and relate towards its environment. This enables to predict the behaviour of systems under different defined conditions and give rise to modify the systems behaviour by identifying causative factors. The resulting concepts aim to enhance the understanding of biological systems and to design hypothesis-driven experimental studies.

Models can be classified by different criteria: (1) qualitative or quantitative, (2) deterministic or stochastic and (3) discrete or continuous. Furthermore, processes can be described as either reversible or irreversible, depending on whether a process can proceed in either forward or backward direction or only in one direction. These criteria are used to describe biological models and help to make comparisons.

1. Qualitative or quantitative models describe relations on a nominal scale between the observed variables by using, e.g. partial derivatives. These definitions of qualitative relations may describe a function as being in either positive or negative relation with a variable over a specific region if the partial derivative itself, with respect to the variable, is positive or negative over the entire region [58]. Such models investigate if a certain condition or behaviour is possible or not. On the other hand a **quantitative model** assigns intervals, ratios or ordinal values on model elements and their interactions. In biological systems these values are often functional parameters, such as concentrations, specific activities or kinetic parameters (e.g. K_m values). Quantitative models aim to make reliable predictions for biological systems, thus it is essential to integrate a large number of biological parameters into the model and mathematical computations.

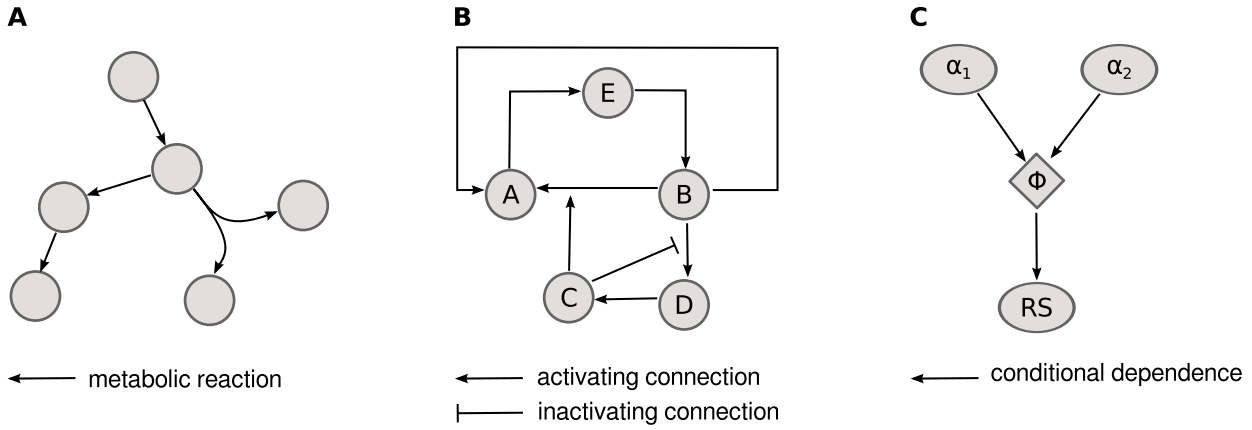

Figure 1.2: *Different types of networks have to be distinguished: linear networks or non-linear dynamic models, such as dynamic networks, Boolean networks or Bayesian networks.*
A. *Example of a graph representing a linear or non-linear model describing the dynamics of a biological system.*
B. *Boolean network describing a gene regulatory network with activating and inactivation connections between components A to E.*
C.*Bayesian network describing the probabilistic relationships between* α_1 *and* α_2 *to cause a certain response (RS).*

2. Deterministic or stochastic models follow the concept that any state or event of a given system follows specific laws which make the outcome predictable. Applying these laws enables to predict any other state. An example for deterministic modelling is the kinetic modelling of biochemical reactions. Here, based on the law of mass action, the assumption is made that the reaction rate v at a certain time point t and space can be expressed as a unique fraction of the concentrations of all substances at this point in time and space. By contrast, indeterministic processes are considered as **stochastic**, which evolve according to probabilistic laws to define probabilistic models of reaction kinetics [59]. One example for a stochastic process is the Bernoulli process, which describes a finite or infinite sequence of binary random variables as being either 0 or 1.

3. Discrete or continuous models are based on difference equations on a discrete time scale or ordinary differential equations (ODE) on a continuous time scale. These concepts are applied to dynamical systems, which change over time. Examples of discrete models are the Ricker model (1954) and Beverton-Holt model (1981) [60], which describe the expected number of individuals in a given generation.

Table 1.1: *Mathematical models in biological systems.*

Type	Biological system	Reference
Linear network		
genome-scale metabolic networks		
•homo sapiens	global network	[61]
	hepatocyte	[6]
•microorganisms	E. coli K-12 MG1655	[10]
	Plasmodium falciparum	[5]
Boolean network		
genetic regulatory networks (GRN)		
•homo sapiens	neuron	[62]
	T-helper GRN	[63]
•microorganisms	yeast	[64]
Dynamic network		
kinetic modelling glucose metabolism		
•homo sapiens	erythrocyte	[65]
		[66]
	hepatocyte	[67]
dynamic causal modelling (DCM)	neural responses	[68]
recurrent artificial neural network	neural network	[69]
Bayesian networks		
	saccadic responses	[70]
	neural network	[71]

Models are often represented by networks or graphs which describe the interconnections of elements within a model. In such graphs molecules are depicted by nodes, points or vertices and the reactions are depicted by lines or edges (see Figure 1.2). Here, different types of networks have to be distinguished: linear networks or non-linear dynamic models, such as dynamic networks, Boolean networks or bayesian networks. In Table 1.1 these network types are summarised and examples for different mathematical models are given.

The relation between components in a linear network are based on linear equations, while Boolean networks assign to each connection a Boolean value such as 0 or 1 and true or false, which corresponds to an on or off state in a biological system (see Figure 1.2-B). A Bayesian network describes the probabilistic relationship between variables and their conditional dependencies. Recent studies have used the Bayesian inference to mathematically describe sensory causes and the learning causal regularities in the sensorium (see Figure 1.2-C, [72, 73]).

Finally, dynamic networks describe the dynamics of a biological system in a continuous, deterministic approach through ODE, while systems employing on a discrete time scale are modelled through difference equations. Among mathematical modelling of biological systems, deterministic kinetic models are of great importance. These models aim to define ODEs, which describe the kinetics of enzymatic reactions (see Table 1.1). In general, biochemical kinetics are based on the mass action law [74] which states that the reaction rate v is proportional to the concentration of reactants ([S]).

Based on this concept, the rate of enzymatic reactions can be determined by assuming a quasi-equilibrium state between free enzyme (E) and the enzyme-substrate complex (ES) as proposed by Michaelis and Menten [75, 76]. The Michaelis-Menten equation describes a state when the enzyme is completely saturated with substrate and a maximal rate (V_{max}) for the reaction is reached:

$$v = k_{cat} \cdot [E] \frac{[S]}{[S] + K_m} = \frac{V_{max} \cdot [S]}{[S] + K_m} \tag{1.1}$$

The Michaelis constant (K_m) describes the substrate concentrations yield at half-maximal reaction rate, while the turnover number k_{cat} describes the ratio of maximal velocity of the total enzyme concentration.

Based on these concepts, it is possible to define dynamic biochemical processes such as accumulation of substrates or substrate inhibition. Furthermore, kinetic models enable to make time dependent predictions about substrate changes for variable environmental conditions. However, depending on the scale and complexity of the cellular systems, these models require the incorporation of multiple and often unknown parameters. This makes it difficult to define large-scale kinetic models.

1.4.1 Linear modelling

An alternative to dynamic modelling is offered by linear modelling. Here, complex reactions of biological systems are described by linear equations in which stoichiometric coefficients denote the proportion of each substance S involved in n network reactions (see Figure 1.3-A). The system dynamic where a substance S changes

A

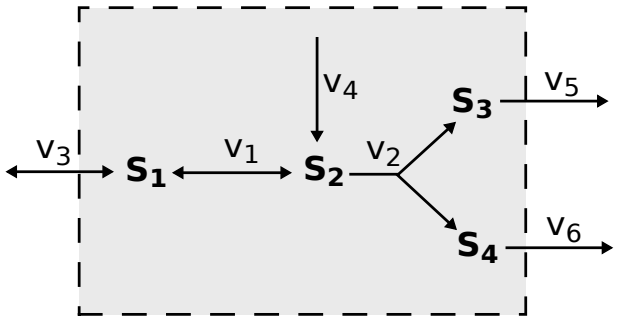

B

$$\mathbf{N} = \begin{pmatrix} -1 & 0 & 1 & 0 & 0 & 0 \\ 1 & -1 & 0 & 1 & 0 & 0 \\ 0 & 1 & 0 & 0 & -1 & -1 \\ 0 & 1 & 0 & 0 & 0 & -1 \end{pmatrix}$$

Figure 1.3: ***A.*** *Example of a reaction network with m metabolites (j=1,2,...,m) and n reactions (i=1,2,...,n). Each metabolite S is assigned to a metabolic reaction with a specific flux rate v. Dashed lines indicate system boundaries.*
B. *Stoichiometric matrix with stoichiometric coefficients of the given metabolic network.*

with a rate v is described by the system equations:

$$\frac{d\mathrm{S_j}}{d\mathrm{t}} = \sum_{\mathrm{i=1}}^{\mathrm{n}} (\mathrm{c_{ij}} \cdot \mathrm{v_i}) \text{ for j=1,2,...m} \tag{1.2}$$

where c denotes for the stoichiometric coefficients of the respective metabolite j in the reaction i. Together all stoichiometries are represented by the stoichiometric matrix N (see Figure 1.3-B). The stoichiometric matrix denotes for m rows and n columns representing n network reactions with v_i variables (i=1,2,...n) and m participating substances. The system of linear equations reads as follows:

$$\mathrm{c_{11}} \cdot \mathrm{v_1} + \mathrm{c_{12}} \cdot \mathrm{v_2} + ...\mathrm{c_{1i}} \cdot \mathrm{v_i} = \mathrm{S_1} \tag{1.3}$$

$$\mathrm{c_{11}} \cdot \mathrm{v_1} + \mathrm{c_{12}} \cdot \mathrm{v_2} + ...\mathrm{c_{1i}} \cdot \mathrm{v_i} = \mathrm{S_1} \tag{1.4}$$

$$\vdots \tag{1.5}$$

$$\mathrm{c_{m1}} \cdot \mathrm{v_i} + \mathrm{c_{m2}} \cdot \mathrm{v_i} + ...\mathrm{c_{mi}} \cdot \mathrm{v_{mi}} = \mathrm{S_m} \tag{1.6}$$

In summary, a metabolic system can be described by different vectors: (1) a vector S of concentration values, (2) a vector v of reaction rates, (3) a parameter vector and (4) the stoichiometric matrix N. In case the system is in a steady-state, we further consider a vector containing the steady-state fluxes. The rates of change

of a molecular substance S can then be described by:

$$\frac{d\mathrm{S}}{d\mathrm{t}} = \mathrm{N} \cdot \mathrm{v} = 0 \tag{1.7}$$

where v defines the flux vector v through a specific reaction n.

1.5 Mathematical optimisation and systems biology

Mathematical optimisation deals with finding an optimal solution of a defined problem from a given set of available alternatives with respect to certain criteria. The objective of each optimisation problem is to find optimal solutions for a vector x in a given problem either to find the minimal usage of resources (e.g. cost function) or to identify a maximal coverage from a given set of resources. The general form for an optimisation problem to minimize or maximize an objective function is:

$$\underset{\mathrm{x}\in\mathbb{R}^{\mathrm{n}}}{\text{minimize/ maximize}} \quad \mathrm{f(x)} \tag{1.8}$$

$$\mathrm{x} \in \mathrm{M} \tag{1.9}$$

where $\mathrm{M} \in \mathbb{R}^n$ is the feasible region and f(x) the objective function. The feasible region M is further defined by constraints and predominantly describes a closed aggregate or convex region. The feasible region M applies if constraints $g_i(x)$ are constant with the form:

$$g_i(x) \leq c_i, \ \text{i=1,2,...,k.} \tag{1.10}$$

However, M can be unlimited or non-convex, which may lead to the problem becoming infeasible.

In biological systems the concept of optimality plays an important role. This concept is based on the assumption that in any environment with restricted or limited access to resources, e.g. nutritional supply, each biological system has to make efficient use of the given resources [77]. Here the objective function represents cellular functions reflecting the synthesis of important precursors for cellular building blocks such as membrane lipids and proteins or formation of

energy-rich phosphates, in particular ATP. As a consequence, optimisation problems for biological systems are not only defined with respect to known intrinsic factors representing the robustness and versatility of the respective system. Moreover extrinsic factors such as adaptations to environmental conditions or limited access to resources affect the definition of the optimisation problem. Therefore, assumptions or side-constraints about the internal structure of the biological system and its surrounding external environment have to be made.

Constraint-based modelling of biological systems uses stoichiometric information about biological processes to define a mathematical model. This requires the definition of physicochemical and environmental constraints ($g_i(x)$) to define the system boundaries. In the past different approaches have been developed to enable optimality based simulations. In flux balance analysis (FBA) it is assumed that a given system is in a steady state. Depending on the scope of the study FBA enables to predict flux distributions with respect to the applied constraints. In the recent past it has been shown that this method is capable of accurate predictions for intracellular metabolic flux states in microorganisms [9, 10] and human cells such as erythrocytes [77]. Taking together optimisation-based modelling of cellular systems enables to simulate metabolic responses in conditions of restricted substrate supply or inhibition of enzymatic reactions observed in diabetes, starvation and cardiovascular diseases [9, 11, 14, 77].

1.6 Statement of problem

The objective of this thesis is to reconstruct the metabolic network of the human cardiomyocyte and determine how nutritional stress may affect cardiac efficiency.

To approach this question, gene expression information and data from biochemical and molecular studies are integrated to reconstruct the cellular network in a combined bottom-up and top-down approach. In this context, linear optimisation problems are applied according to the flux balance principle to test the consistency and capability of the model to achieve known metabolic and physiological functions of the cardiomyocyte.

On the basis of this comprehensive network, the metabolic efficiency of cardiomyocytes to maintain mechanisms, which are directly or indirectly involved in cardiac contraction, are studied in varied substrate availability. For this purpose a metabolic target function of the human cardiomyocyte is defined and the capability of nine different substrates to maintain this function is tested.

The following questions are examined:

1. How is the efficiency of cardiac metabolism to be measured with respect to each substrate?
2. Are the calculated flux estimations in concordance with experimental results?
3. What is the contribution of each substrate to the ATP formation?
4. Is there a glycogen turnover and what is the contribution of glycogenolysis to the predefined metabolic target function, in particular ATP formation?

1.7 Thesis content

The following chapters 2 and 3 summarise materials and methods in-depth which were used for the network reconstruction and mathematical computations. Chapter 4.1 presents the network reconstruction and testing for functionality as well as validation of the network. Chapter 4.2 specifies and outlines the mathematical approach implemented for simulations of variable substrate supply and evaluation of metabolic efficiency. Chapter 4.3 summarizes the computational results.

The text of Chapter 4.3, in parts, contains material as it appears in A. Karlstaedt, D. Fliegner, G. Kararigas, H. Sanchez Ruderisch, V. Regitz-Zagrosek, H.G. Holzhütter. CardioNet: A human metabolic network suited for the study of

cardiomyocyte metabolism, BMC Systems Biology, 2012(6):114. I was the primary author of this publication and the co-authors participated and directed the research which forms the basis for Chapter 4.3.

2 Materials

This chapter presents available metabolic network reconstructions and summarizes database resources, software and experimental parameters which were used for the network reconstruction and mathematical computations.

2.1 Consulted metabolic networks

2.1.1 Recon 1: The global human network

Recon 1 [8] is a comprehensive genome-scale metabolic reconstruction of the global human network. The model was reconstructed with a bottom-up approach by using genomic and bibliomic data. Recon 1 accounts for 2766 metabolites and 3311 metabolic as well as transport reactions. Metabolites are assigned to either the extracellular environment or to seven intracellular compartments: cytoplasm, mitochondrion, nucleus, endoplasmic reticulum, Golgi apparatus, lysosome and peroxisome. Additionally, confidence scores are provided for biological evidence obtained for genes, proteins and reactions. The network has been validated through simulation of 288 metabolic functions [8].

2.1.2 HepatoNet 1: The metabolic network of the human hepatocyte

HepatoNet 1 [6] is a manually curated and functional model of the human hepatocyte metabolism. This network comprises 777 metabolites and 2539 reactions, including 1466 transport reactions. The model is fully compartmentalized with six intracellular (cytosol, mitochondrion, endoplasmic reticulum and Golgi apparatus, lysosome, nucleus, peroxisome) and two extracellular compartments (bile canaliculus, sinusoidal space). The network has been validated through simulation of 319 metabolic objectives and tested for functionality through simulation of 123 physiological functions known for the human hepatocyte.

2.2 Experimental data

2.2.1 High-throughput data: Transcriptomic data

An important tool for investigating transcriptional activity in biological samples is the high-throughput profiling of gene expressions. Among others microarray technology enables to investigate a large set of samples and analyse different biological states from various organisms. We obtained these datasets by accessing the “Gene Expression Omnibus” (GEO) database [26, 78] (see Table 2.3).

GDS181

An approach to investigate gene expression profiles from 91 human and mouse samples of different tissues, organs and cell lines from mostly normal physiological state has been published by Su et al [79]. This dataset is part of the BioGPS database [80] and gives a comprehensive description of the normal mammalian transcriptome. The samples were labelled and hybridized to either human (U95A) or mouse (U74A) high-density oligonucleotide arrays. The primary image analysis was performed by using the genechip 3.2 (Affymetrix, Santa Clara, CA). Based on the absence and presence call provided by the genechip software package and additional PCR-validation of oligonucleotide array data, an average difference (AD) value of 200 was defined. Gene expression values above this threshold were considered present [79].

GSE1145

In this study changes in cardiac transcription profiles during heart failure in humans were investigated. Myocardial tissue samples were collected from patients undergoing cardiac transplantation. The causes of heart failure differed between patients including idiopathic dilated cardiomyopathy, ischemic cardiomyopathy and hypertrophic cardiomyopathy. The control samples were collected from organ donors whose hearts could not be used for transplantation. The samples were labelled and hybridized to human (U95A and U133) high-density oligonucleotide arrays. This dataseries is part of the CardioGenomics database [81].

Table 2.1: *Substrate utilisation in the isolated working rat heart.*

Exp.	Substrate	v_{O_2}	v_s
1	Glucose	4.280 ± 0.860	0.758 ± 0.123
2.1	Lactate	4.710 ± 0.590	1.410 ± 0.137
2.2	Glucose	4.70 ± 0.51	0.369 ± 0.088
	Lactate		1.220 ± 0.223
3.1	Oleate	4.940 ± 0.530	0.176 ± 0.330
3.2	Glucose	4.360 ± 0.920	0.643 ± 0.133
	Oleate		0.115 ± 0.037
4.1	Acetate	4.280 ± 0.035	1.677 ± 0.223
4.2	Glucose	4.690 ± 0.223	0.251 ± 0.086
	Acetate		1.391 ± 0.174
5.1	Acetoacetate	4.200 ± 0.223	0.645 ± 0.107
5.2	Glucose	4.950 ± 0.390	0.486 ± 0.053
	Acetoacetate		0.979 ± 0.166

Flux rates for v_{O_2} and v_s are given in mmol $\cdot$ h^{-1} $\cdot$ (g dry wt.) $^{-1}$. v_{O_2} indicates oxygen demand; v_m, substrate uptake rate.

2.2.2 Metabolic parameters

Taegtmeyer, H et al 1980 [82] In this study a new improved perfusion system is presented for the Langendorff mode in the isolated working rat heart. The oxygen demand and substrate utilisation were determined while monitoring the cardiac output. In total, uptake rates for six different substrates (glucose, oleate, lactate, acetate, acetoacetate and β-hydroxybutyrate) were measured while workload and cardiac output were estimated during the perfusion experiment (see Table 2.1). Most substrates were determined by using enzymatic methods (glucose, lactate,acetoacetate and β-hydroxybutyrate). Oleate and acetate utilisation were measured by measuring the [1-^{14}C] oleate level and the [1-^{14}C]acetate level in the perfusate, respectively.

Hatch, GM et al 1994 [83] The objective of this study was to investigate the cardiolipin biosynthesis pathway in the heart and determine rate-limiting steps.
For this purpose the level of incorporated radioactive tracers ([^{32}P]P_i and [U-^{14}C]-glycerol) was measured in the isolated working rat heart to estimate the synthesis rate of cardiolipin, phosphatidylcholine, phosphatidylethanolamine and sphingomyeline (see Table 2.2).

Table 2.2: *Substrate biosynthesis and degradation rates in the heart.*

Dobrzyn et.al. 2010 [84]	$\mathbf{v_t}$
Phosphatidylcholine	2.98E-006
Phosphatidylethanolamine	2.00E-006
Sphingomyelin	1.94E-008
Cardiolipin	5.69E-008
Ceramide	1.58E-009
Goodwin et.al. 1995 [85]	$\mathbf{v_t}$
Glycogenolysis	1.50E-003 $\pm$ 0.18E-003
Glycogen synthesis	0.17E-003 $\pm$ 0.04E-003
Glycolytic flux	
Total	5.09E-003 $\pm$ 0.70E-003
From exogenous glucose	3.59E-003 $\pm$ 0.63E-003
Wu, F et.al. 2008 [86]	$\mathbf{v_t}$
ATP Hydrolysis	21.6

Substrate biosynthesis and degradation rates (v_t) are given in mmol $\cdot$ min^{-1} $\cdot$ (g dry wt.) $^{-1}$ except for ATP Hydrolysis, which is given in mmol $\cdot$ min^{-1} $\cdot$ (l cell) $^{-1}$.

Dobrzyn et al 2010 [84] Using an ob/ ob; SCD1^{-}/$^{-}$ mouse model, the hypothesis is tested that lack of SCD1 could improve steatosis and left ventricle function in leptin deficiency. For this purpose, different parameters of cardiac lipid metabolism were determined such as total lipid synthesis and cardiac free fatty acid level and ceramide level. In addition, the incorporation of palmitic acid into ceramide was determined by using a radioactive tracer ([^{14}C]palmitic acid) (see Table 2.2).

Goodwin et al 1995 [85] In this study the effect of glucagon and insulin on cardiac glycogen synthesis and degradation was investigated. The experiments were performed on isolated working rat hearts by using a Langendorff mode. The glycogenolysis and glycogen synthesis rates were determined by measuring the incorporation of radioactive labels ([U-^{14}C] glucose, see Table 2.2).

Wu, F et al 2008 [86] In this study, a ^{31}Phosphate-magnetic resonance spectroscopy (^{31}P-MRS) was performed on dog hearts at different cardiac work-loads. For each condition, concentrations of creatinephosphate, ATP levels and myocardial blood flow were determined. In combination with a model of cardiac

energy metabolism, predictions of the ATP hydrolysis potential, cytoplasmic free P_i and ADP concentrations as a function of oxygen consumption were estimated.

2.3 Consulted databases

Table 2.3

Database	Link	Reference
Genes and Genome		
UniGene	http://www.ncbi.nlm.nih.gov/unigene	[23]
NCBI Entrez Gene	http://www.ncbi.nlm.nih.gov/gene	[87]
Ensembl	http://www.ensembl.org/index.html	[25]
BioMart project	http://www.biomart.org/	[88]
Gene Expression Omnibus	http://www.ncbi.nlm.nih.gov/geo/	[26, 78]
Proteins		
Reactome	http://www.reactome.org	[89]
UniProt Knowledgebase	http://www.uniprot.org	[24]
Enzymes		
BRENDA	http://www.brenda-enzymes.info/	[17]
KEGG	http://www.genome.jp/kegg/	[18]
MetaCyc	http://metacyc.org/	[90]
Metabolites		
LIPID MAPS	http://www.lipidmaps.org/	[20]
HMDB	http://www.hmdb.ca/	[21]
PubChem	http://pubchem.ncbi.nlm.nih.gov/	[91]
Transporter		
TCDB	http://www.tcdb.org/	[19]
TransportDB	http://www.membranetransport.org/	[92]

2.4 Software

Table 2.4

Software	Description	Resource
CPLEX 10.1	commercial mathematical solver for linear programming, mixed integer programming, quadratic programming and quadratically constrained programming problems	IBM ILOG Incorporation
FASIMU	Flux Balance Analysis simulation software	Hoope A., 2011 [16]
Metannogen	Software to manage information for metabolic networks reconstruction	Gille C., 2007 [93]
PSQL	object-relational database system	The PostgreSQL Global Development Group
R Project	software environment for statistical computing	R Foundation for Statistical Computing

3 Methods

This chapter presents methods and general strategies for metabolic network reconstructions and summarises computational methods for functional testing and validation of such models.

The methodology of network reconstructions can be divided into two different types: a top-down and a bottom-up approach. In a top-down approach, high-throughput molecular biology data such as gene expression information and proteomic information is used to identify network components. This process is supported by statistical and computational methods. It is an advantage of the top-down approach that no prior knowledge of a biological system is required to perform a reconstruction. Thus, unbiased analysis of biological systems is possible and discovery of new biological features is more likely. In contrast, a bottom-up approach place emphasis on manual curation of biological evidence obtained from scientific literature and genome annotation. This approach is mainly hypothesis-driven and focuses on specific aspects of molecular cell biology such as metabolism, transcription regulation or signalling.

Depending on the scope of the study, experimental evidence, such as genome or gene expression information, has to be evaluated regarding which reactions are to be included. This is of great importance for network reconstructions taking into account the maturation state of a cellular system, because a selection of potential reactions has to be done which reflect different biological features as found between f.exp., myeloid progenitor cells compared to monocytes or fetal cardiomyocytes compared to adult cardiomyocytes.

Irrespective of the approach which is eventually adopted, the integration of data from multiple resources and different levels of evidence is required. This includes high-throughput genome data, multiple types of experimental data and bibliomic information. There are a number of public databases available providing genomic and molecular information about different organisms and tissues, including human cells. Among these are resources providing information about metabolic reactions and compounds such as the Kyoto Encyclopedia of Genes and Genomes (KEGG)

[18], Reactome [89] and HumanCyc [94]. While other databases focus on gene and protein alignment such as PRIDE [95], Uniprot Knowledgebase (UniprotKB, [24]) or Ensembl [25]. Together these databases offer researchers a good basis to perform reconstructions of cell and tissue type specific human networks.

The following sections summarise a general protocol and tools for the reconstruction of cellular networks and present computational methods for testing models for their functionality and consistency.

3.1 Methods for a metabolic network reconstruction

In the recent past, different protocols have been introduced for the reconstruction of cellular networks [11, 15, 96]. All these protocols share a basic concept: an initial set of genes is obtained from genome annotation or high-throughput data and assigned to enzymes which carry enzymatic reactions. Each identified enzyme is than evaluated regarding its biochemical characteristics such as subcellular localisation, required cofactors and metabolic activity. For this purpose specialised databases such as the Braunschweig Enzyme Database (BRENDA)[17] and KEGG [18] are consulted or evidence from experimental data and scientific literature is collected. The generated reaction scheme is than further evaluated regarding consistency and admissibility of its contents. In summary the general strategy for a comprehensive model reconstruction requires the following steps:

1. Definition of a preliminary reaction list
2. Extension of composed reaction list by missing reactions and metabolites
3. Generating the mathematical representation of the network
4. Evaluation, validation and consistency check of the reconstructed network

These steps form the backbone of each reconstruction and should be regarded as guidance, whether a top-down or a bottom-up approach was chosen.
However, to reconstruct a functional and valid model of a cellular system is it essential to iterate each of the given steps multiple times to include all wanted biological processes. In case missing reactions are identified then the whole process starts again from the beginning including constant re-evaluation.

3.1.1 Reaction list

Irrespective of the chosen approach, either top-down or bottom-up, the initial step aims to generate a preliminary reaction list. For this purpose it is necessary to collect genomic, bibliomic or high-throughput data which are specific for the respective organism or cell type. This list will form a preliminary network functioning as a starting point for further data integration. Previous investigations mostly started with a fully annotated genome [10, 61] which can be automatically generated by using databases providing genomic sequence information such as UniGene [23], NCBI Entrez Gene [87] or Ensembl [25].
The obtained gene information is subsequently linked to the encoded enzymatic function. Finally this allows to automatically or to manually determine which reactions are carried out by these enzymes and by which stoichiometries. In this context, databases such as BRENDA [17], KEGG [18], MetaCyc [90] or TransportDB [92] provide metabolic information to generate these network reactions.

3.1.2 Extension of composed reaction list

The composed reaction list requires further manual curation and careful revision to create a reliable network for mathematical simulations of cellular or tissue-specific behaviour. In this step the focus is on the verification and reconciliation of collected information about metabolites, enzymes and reactions from literature or experimental evidence. The collected meta-information can be stored in a network database to support the curation process and further revision.
Additional information about every incorporated metabolite should be obtained including charge, stoichiometric formula and identifier. The charge balance of reactions has to be ensured and checked. The subcellular localisation of each reaction should be determined as well as the reaction directionality. This process can be supported by external database and methods to determine $\triangle G$ values in order to set the directionality, such as the group contribution method [97, 98].

3.1.3 Generating the mathematical representation of the network

Following the manual curation and revision, the network has to be converted into a format enabling mathematical computations. The file format syntax is dependent on the respective mathematical solver and characteristic of the model (e.g. non-linear, linear). The most common file formats used by solvers such as CPLEX [99] and LINDO API [100] are the Mathematical Programming System (MPS) format, the Linear Programming (LP) format and the Math Program Instructions (MPI) format. It is possible to use programs written in a standard programming language such as Perl or Python to convert the drafted network into the required file format.

In the recent past tools have been developed to provide platforms for direct use of a reconstructed network to solve optimisation problems with different FBA algorithms. For example, the openCOBRA project [101] and the CellNetAnalyzer [102] provide a toolbox for use in Matlab, while FASIMU [16] is a command line oriented software. These software packages enable the incorporation of a reconstructed network in a plain reaction scheme, Extensible Markup Language (XML) format or Systems Biology Markup Language (SBML) format. In the past, SBML developed into a standard representation format for communicating and storing mathematical models of biological systems. Together with software packages such as Metannogen [93] or the SQL database system, it is possible to generate biological networks and directly link the respective knowledge-base with mathematical computations through the SBML file format.

3.1.4 Evaluation, validation and consistency check of the reconstructed network

It is important to evaluate the network capability to fulfil tissue or organism specific biological functions in order to seek functionality and consistency of the reconstruction. Each function is incorporated as an objective function into the optimisation problem and flux distributions are predicted for the respective cellular state. These objectives might represent certain important cellular processes such as ATP formation, detoxification or protein synthesis. However, the set of biological functions is based on the scope of the respective study, thus it might be limited and has to be carefully defined. Therefore, it is necessary to ensure the production of included metabolites and further evaluate

network reactions for (1) dead-ends, (2) incorrect directionality or (3) isolated reactions. The constraints and system boundaries for the network have to be defined and evaluated for feasible solutions while applying a set of biological functions.

3.2 Methods for analysing network states and estimation of stationary fluxes

This section presents computational methods which are widely used to determine flux distributions in metabolic networks and analyse cellular states.

3.2.1 Flux Balance Analysis

Flux Balance Analysis (FBA) is a linear programming (LP) based method for flux prediction and analysis of biological system. In contrast to kinetic modelling, no enzymatic kinetic data is included to calculate flux distributions. A linear programming problem is defined to find optimal solutions for corresponding network states. In FBA it is proposed that all internal fluxes fulfil the steady-state condition with respect to all metabolites and applied constraints. The linear optimisation problem is then solved to find optimal solutions while maximising or minimizing an objective function f(v). The general LP in FBA reads as follows:

$$\text{maximize/ minimize} \qquad f(v) = \sum_{i=1}^{r} c_i \cdot v_i \tag{3.1}$$

$$\text{subject to} \qquad N \cdot v = 0, \tag{3.2}$$

$$v_{min,i} \leq v_i \leq v_{max,i} \tag{3.3}$$

where $v \in \mathbb{R}^n$ is the flux vector and N is the m $\times$ n stoichiometric matrix of the network, with m metabolites and n reactions. The objective function is represented by a linear combination of metabolic fluxes v_i with the coefficient c_i representing weights. The lower and upper bounds on each reaction are represented by $v_{min,i}$ and $v_{max,i}$, respectively. Objective functions match cellular functions such as ATP formation, maximisation of biomass or minimisation of external substrate uptake. However, each function depends on the scope of the study, thus might be incomplete. All possible flux distributions for a given network in a steady-state

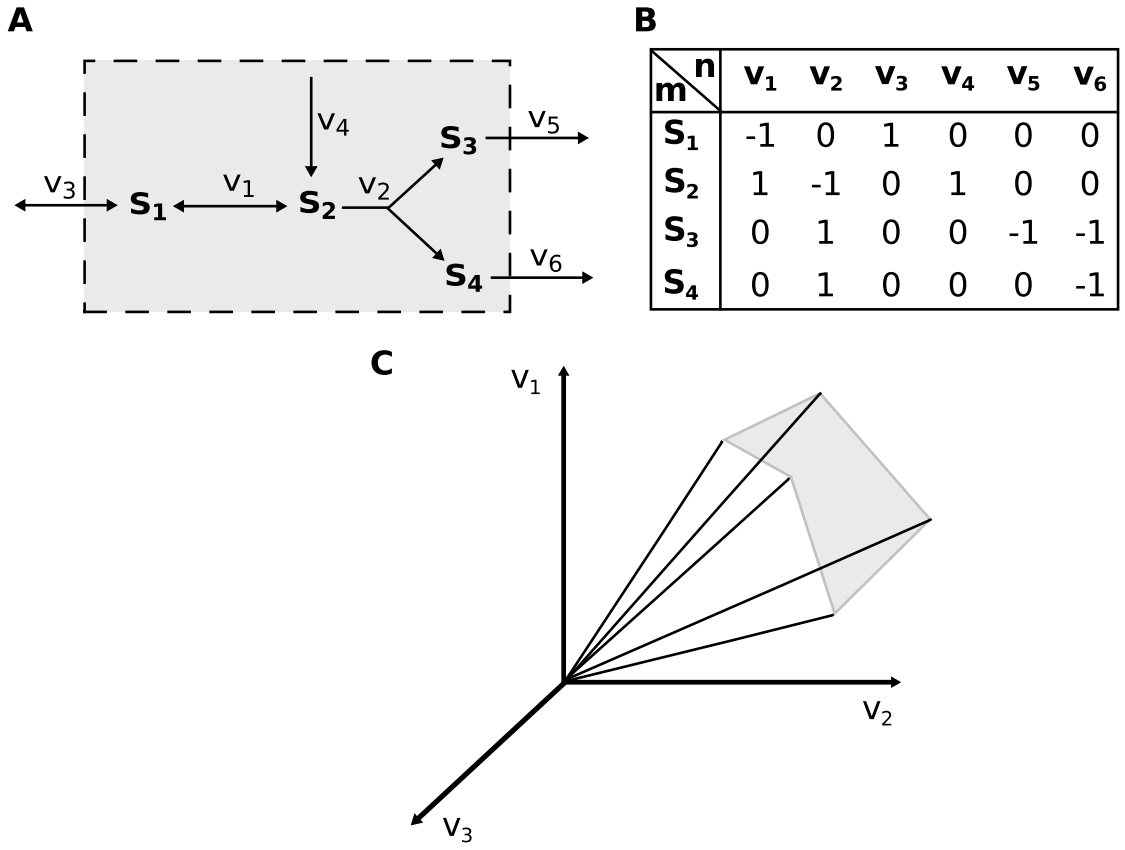

m \ n	v_1	v_2	v_3	v_4	v_5	v_6
S_1	-1	0	1	0	0	0
S_2	1	-1	0	1	0	0
S_3	0	1	0	0	-1	-1
S_4	0	1	0	0	0	-1

Figure 3.1: ***A.*** *Example for a reaction network with m metabolites (j=1,2,...,m) and n reactions (i=1,2,...,n). Each metabolite S is assigned to a metabolic reaction with a specific flux rate v. Dashed lines indicate system boundaries.* ***B.*** *Stoichiometric matrix with stoichiometric coefficients of the given metabolic network.* ***C.*** *The steady-state flux cone.*

condition define a polyhedral cone or the *steady-state flux cone* (see Figure 3.1).

3.2.2 Flux Variability Analysis

In some cases, linear problems have more than one optimal solution [103, 104]. Most solvers, e.g. CPLEX, terminate as soon as an optimal solution to an optimisation problem is found. Especially, CPLEX does not automatically provide methods to find alternate optimal solutions. However, a recently developed method, the Flux Variability Analysis (FVA), aims to estimate alternative optima for different network states [105, 106]. Using FVA it is possible to determine the robustness of a metabolic network and possibly identify network redundancy. The existence of such alternative reaction sets could compromise predictions for network states regarding:

1. optimal flux distributions for different biological states,
2. estimated substrate requirement or biosynthesis of different metabolites and
3. process optimisation.

In the FVA approach as proposed by Mahadevan et al [105] the optimality condition is relaxed for calculating the maximal and minimal values of all fluxes. The objective function f(v) is to be constrained as above 95% of the optimal achievable growth rate z_{obj}. The linear optimisation problem reads as follows:

$$\begin{aligned} &\text{maximize/ minimize} && v_i && (3.4)\\ &\text{subject to} && N \cdot v = 0, && (3.5)\\ & && f(v) \geq 0.95 \cdot z_{obj} && (3.6)\\ & && 0 \leq v_i \leq v_{max,i} && (3.7) \end{aligned}$$

where v (i=1,2, ... n) denotes for all network reactions and N describes the stoichiometric matrix.

3.2.3 Flux Coupling Analysis

The Flux Coupling Analysis (FCA) aims to identify (1) coupled and (2) blocked reactions in metabolic networks [107] while assuming steady-state condition. Here, a linear fractional programming is employed to compare calculated flux ratios for every pair of metabolic fluxes within a network.

Blocked reactions are defined as fluxes whose maximum and minimum values equal zero, thus blocked reactions are incapable of carrying any flux in the given scenario. The linear optimisation problem reads as follows:

$$\begin{aligned} &\text{maximize} && v_i && (3.8)\\ &\text{subject to} && N \cdot v = 0, && (3.9)\\ & && v_{uptake,i} \leq v_{uptake\text{-}max,i} \text{ for all transport reactions} && (3.10)\\ & && v_i \geq 0 && (3.11) \end{aligned}$$

where N denotes for the stoichiometric matrix and v for the flux through reaction i. In this approach reversible reactions are expressed as two separate irreversible

reactions. In the FCA method all reversible reactions are split into a forward and a backward reaction, which are constrained to carry a non-negative flux.

It is further possible to differentiate three types of coupled reactions with this method: reactions are (i) directional, (ii) partial or (iii) fully coupled. Here, fully coupled reactions are fixed fluxes where a flux v_1 has the samel value as v_2 and vice versa. The identification of coupled reactions can either occur by a (1) nonlinear optimisation problem or through variable transformation by a (2) linear optimisation problem. In the nonlinear optimisation problem, upper and lower limits of flux ratios for every flux pair in the network are calculated. However, this nonlinear problem can be transformed into a linear problem by setting a constrained reference flux $\hat{v}_2$ to 1 and normalizing flux v_1 to v where $\hat{v} = v \cdot t$. By applying this variable transformation a linear problem is obtained which reads as follows:

$$\begin{aligned}
&\text{maximize/ minimize} && \hat{v_1} && (3.12)\\
&\text{subject to} && N \cdot v = 0, && (3.13)\\
& && \hat{v_2} \geq 0, && (3.14)\\
& && \hat{v}_{\text{uptake,i}} \leq v_{\text{uptake-max,i}} \cdot t \text{ for all transport reactions}, && (3.15)\\
& && \hat{v}_i \geq 0, && (3.16)\\
& && t \geq 0 && (3.17)
\end{aligned}$$

By comparing the calculated flux ratios it is possible to decide how reactions are coupled. Consequently, the amount of linear optimisation problems to be solved increases with this method, which requires a large computing capacity in dependence on the network. Since in large-scale networks the identification of blocked reactions can support the reconstruction process, another method has been developed to aid this [108]. Network pruning aims to create a smaller subnetwork which contains no dead ends and blocked reactions, thereby generating a network in which all reactions are coupled. The resulting sub-network can then be analysed regarding consistency and functionality to model the respective cellular system. However, the set of blocked reactions should be evaluated regarding (1) missing links to other network reactions, (2) missing transport reactions or (3) missing metabolites. The revision process can be supported by bibliomic data and may lead to reintegration of reactions into the network. Both approaches, FCA and network pruning, are functions included in the FASIMU software package.

3.3 Integration of gene expression data into mathematical modelling

3.3.1 Functional annotation of gene expression data

Microarray technology is a hybridization technique for the simultaneous monitoring of expression levels of thousands of genes or detection of variations in a gene sequence. DNA microarrays consist of a glass slide on to which DNA molecules are fixed at specific locations (spots). A single microarray may contain thousands of spots which in turn contain copies of identical DNA molecules which should equally correspond to an administrated probe. Most widely used DNA microarrays are cDNA arrays, oligonucleotide arrays and single nucleotide polymorphism (SNP) arrays.

Administrated nucleic acid samples (target) are then hybridised to the probes on the array by forming complementary nucleotide base pairs. After washing off of non-specific bonding sequences, fluorescently labelled target sequences bind to a probe sequence which generates a signal. The signal intensity varies depending on the amount of target sample bound to a specific probe. The signal validity in Affymetrix oligo-chip design is judged by a comparison of perfect match (PM) to mismatch (MM) pairs to identify spot artefacts. By analysing the relation of PM to MM differences it is possible to calculate a single expression value for a specific probe. However, it is important to note that cross-hybridization may influence the signal validity, thus alternative statistical analysis such as comparison of adjacent probes have been developed.

In order to integrate the gene expression information from microarrays into mathematical computations, each probe has to be linked to a gene. Based on this information encoded enzymes can be identified and integrated into network reconstructions.

The annotation of gene expression information in the current study is guided by the following protocol [6]:

1. Collection of probeset identifier from the dataset and obtaining information on the microarray platform type

2. Annotation of probesets from the given microarray platform to Ensembl transcripts (ENST, ENSMUST) by filtering the Ensembl database.

3. Each transcript is linked to an ENSMBL gene identifier. These identifiers are

species specific (e.g. ENSG for homo sapiens, ENSMUSG for mus musculus), thus enable to clearly identify each gene.

4. Collected ENSMBL gene identifier should further be linked to additional gene annotation databases such as NCBI, entrez gene or unigene. This enables a good coverage of the dataset and increases the possibility of retrieving annotation for every given probeset.

5. Linking each gene identifier to a protein and, if available, enzyme classification number (EC number) by using UniProt, KEGG or Vega [1]

The entire process can be automatically performed through script-based accessing of the Ensembl database by using the Perl-API. Furthermore, Ensembl Biomart [88] provides a comprehensive data mining tool which efficiently links information from different databases. However, manual linking of genes to enzymes might be required for a complete and comprehensive annotation. Results can be stored as either plain text file or in a database to enable later integration of data and amplification of generated gene annotation. Depending on the scope of the study, it might be important to define each expression state as either present, absent or marginal through f.exp. Boolean values.

3.3.2 Shlomi approach

Recently Shlomi et al. introduced a new method of defining a reaction list by integrating tissue-specific gene- and protein-expression data with an existing reconstructed metabolic network [11]. By using the global human metabolic network [8] it was possible to identify tissue-specific metabolic activities in ten different human tissues. This algorithm aims to integrated gene expression data with linear optimisation problem as follows:

[1] http://vega.sanger.ac.uk/index.html

$$\text{maximize} \quad \sum_{i \epsilon R_H} (y_i^+ + y_i^-) + \sum_{i \epsilon R_L} y_i^+ \tag{3.18}$$

$$\text{subject to} \quad N \cdot v = 0 \tag{3.19}$$

$$v_{min} \leq v \leq v_{max} \tag{3.20}$$

$$v_i + y_i^+ (v_{min,i} - \varepsilon) \geq v_{min,i}, \; i \epsilon R_H \tag{3.21}$$

$$v_i + y_i^- (v_{max,i} - \varepsilon) \geq v_{max,i}, \; i \epsilon R_H \tag{3.22}$$

$$v_{min,i}(1\text{-}y_i^+) \leq v_{max,i}(1 - y_i^+), \; i \epsilon R_L \tag{3.23}$$

$$v \epsilon R^m \tag{3.24}$$

$$y_i^+, y_i^-, \epsilon [0,1] \tag{3.25}$$

with the flux vector v and the stoichiometric matrix N. Stationary flux distributions are determined while maximising the number of reactions whose activity is consistent with their corresponding gene expression state. These states are expressed as Boolean values as 1, -1 and 0 to account for highly, lowly and moderately expressed genes, respectively. In this approach, highly expressed reactions are considered to be active (y^+) if the carried flux is greater than a threshold ε (see equation 3.21 and 3.22). The resulting subsets of reactions are considered as highly expressed (R_H) and lowly expressed (R_L). The objective of the linear optimisation problem is to maximize the amount of highly expressed (R_H), active reactions and lowly expressed (R_L), inactive reactions. Such drafted sub networks could act as a good starting point for further tissue-specific network reconstruction.

3.4 Statistical analysis

Statistical analysis was performed by using the statistical package provided by R Statistics. All values were tested for a normal distribution and a t-Test was performed. A p-value less than 0.05 was considered as statistically significant.

For graphical presentation boxplots were used, which present the numerical data through specific observations: the smallest observation (data minimum), lower quartile or 25th percentile (Q1), median or 50th percentile (Q2), upper quartile or 75th percentile (Q3) and largest observation (data maximum). The median, lower and upper quartiles represent the middle 50% of the data and are plotted

through a box which length represents the interquantile distance. The variability of the underlying data can be described by the distance between upper and lower quartile. Further, the median is displayed as a band inside the plotted box and is a non-parametric method. The median is obtained by sorting values of a given observation from its lowest value to its highest value and picking the middle one. In particular the median is used in observations with skewed distributions or to reduce the importance of extreme values (outliers), which would affect the mean value of an observation. However, in case 50% of the values are equal to 0, the median cannot be used. Instead, the arithmetic mean enables to measure the central tendency of a sample. The whiskers of the boxplot display the lowest and highest data points within 1.5 interquantile range of the lower and upper quartile, respectively. Any outliers in a sample which were not included in this range were plotted as single values above or below the whiskers of the boxplot.

4 Results

This chapter presents the reconstruction process for the fully compartmentalized network of the human cardiomyocyte - CardioNet. Furthermore, an overview of the validation and functional testing of the drafted network is given. Subsquently, the reconstructed network is compared to previously reported mitochondrial models of the cardiomyocyte and a genome-scale reconstruction of the human heart. Finally, an approach to determine the cardiac efficiency in varied substrate supplies is presented and flux distributions determined.

4.1 Reconstruction of the human cardiomyocyte network: CardioNet

A genome-scale network aims to represent all cellular functions in order to form a reliable basis for further computational simulations of cellular behaviour. These cellular functions include metabolic reactions such as those from intermediary metabolism. Metabolic reactions can be divided into two different types: (1) anabolic and (2) catabolic reactions. Anabolic reactions comprise for the synthesis of building blocks such as fatty acids, amino acids and nucleic acids, while catabolic pathways break down molecules into smaller units or monomers. These monomers again can act as substrates in anabolic reactions or are excreted from the cell. Together these pathways function as the engine of a cell to either maintain cellular integrity or enable cellular growth.

However, proteins are not only involved in metabolic reactions. Moreover proteins participate in the formation of cellular membranes. They form transport and signalling systems such as ion-carriers or hormonal receptors and enable important cellular functions such as muscular contractions. In order to fully understand a specific cell type it is important to incorporate the entire process of protein synthesis and regulation into a cellular model. However, this would require a comprehensive description of the DNA and RNA replication, repair and

recombination system. Furthermore, the complex transcriptional regulatory processes which control the expression of genes have to be included into a fully genome-scale network. Although huge efforts have been undertaken to fully reconstruct these transcriptional regulatory processes, not all details for a comprehensive network reconstruction are yet available.

This thesis does not aim not to give a fully reconstruction of the transcriptional regulatory processes of the human cardiomyocyte. Instead, the stated objective is to include metabolic reactions to form a basis for further studies of cardiomyocyte metabolism and physiological functions of the human heart.

4.1.1 Definition of a preliminary reaction list

First, a tissue specific set of metabolic reactions was identified by applying the algorithm by Shlomi et al [11] as described in Chapter 3.3.2. This approach aims to integrate gene expression data with linear optimisation problem. A stationary flux distribution is determined while maximizing the number of reactions whose activity is consistent with their gene expression state. Gene expression information in normal human heart tissue samples was obtained from two different datasets, the Geo Dataset (GDS) GDS181 [79] and the Geo Series (GSE) GSE1145, which are publicly available from the GEO database [26] (see Chapter 2.2.1).

A gene was considered to be expressed if the expression value for the respective transcript was equal to or greater than a threshold value of 100 or the Affymetrix Call indicated a present (P) expression. Each expression type was assigned a Boolean value of 1 or 0 representing either present or absent expression, respectively.

By using the Ensembl Homo sapiens database [25] and KEGG orthology records (KO, [18]), Affymetrix probeset identifier indicating present expression were assigned to reactions of the global reconstruction of the human metabolic network - Recon1 [8]. The optimisation problem based on the Shlomi et al approach [11] was solved to find a steady-state flux distribution while satisfying, first, the steady-state condition of all internal fluxes and second, maximizing the number of reactions carrying a flux which is consistent with the respective gene expression state. The resulting flux distribution reflected the tissue specific metabolic activity in human heart based on the gene expression state under normal physiological conditions. This subnetwork comprised 972 reactions for which corresponding reactions in KEGG were identified based on the Enzyme

Commission (EC). All obtained reactions were integrated into a preliminary network which formed the basis for our network reconstruction. For a complete list of annotated gene expression data see Additional file 1 of the SEM.

4.1.2 Extension of composed reaction list by missing reactions and metabolites

The reaction list was extended by including KEGG reactions [18], which are annotated as present in human heart tissue, but were not part of the initial subnetwork. All reactions were evaluated and analysed for tissue specificity and subcellular localisation according to evidence from scientific literature and databases such as the BRENDA [17], KEGG [18] and UniProtKB [24]. Only reactions with evidence for occurrence in human cardiomyocyte or human heart tissue (keywords: heart muscle, myocardium, cardiac tissue) were included. In case no evidence was found for occurrence in humans, information from other mammalian species and human orthologous genes was obtained allowing inference of the reaction.

At the current state the synthesis of biopolymers such as DNA and RNA is not part of the metabolic network, therefore no reactions were considered in the network reconstruction which are localised in the nucleus, e.g. DNA transcription and translation. Instead the objectives of the metabolic network were restrained to the production of building blocks, e.g. amino acids and nucleotides. Any changes in enzyme activity or occurrence, such as in heart failure, have to be included as additional constraints into the optimisation problem.

In addition, missing metabolites were integrated by using the Human Metabolome Database (HMDB) [21] and Lipid Maps Classification System [20]. Here, a special focus was given to fatty acids, glycerolipids, glycerophospholipids and sphingolipids. In order to describe the variable composition of lipoprotein particles such as LDL particles, nine generic metabolites were defined following the concept of pooled metabolites as described in previous investigations [6]. Instead of including every possible composition of the respective particles these pooled metabolites were used. For each metabolite the chemical formula, IUPAC name and additional external database cross-references were obtained such as CAS-identifier, HMDB identifier or KEGG compound identifier where available (see Additional file 2 of the SEM for a complete list of metabolites).

The system boundaries were set by including further information on transport

Table 4.1: *Overview of the metabolic network of the human cardiomyocyte: CardioNet.*

	Compartments	Reactions	Transporters	Metabolites	Genes	Literature references
N	6	1793	560	728	951	363

reactions from the Transport Classification Database (TCD) [19], Reactome database [89] and another metabolic network of the human hepatocyte, HepatoNet1 [6], providing a large set of manually curated transport processes. Here, transport processes were only included in case evidence for occurrence in human cardiomyocytes was found. The following types of transport processes were included:

1. ATP-dependent transporters (e.g. ABC family for transport of long-chain and very long-chain fatty acids)

2. Secondary transport processes (e.g. SLC25 family for amino acid transport) and

3. Simple diffusion processes.

The resulting network totals 1793 reactions, including 560 transport reactions and 728 metabolites assigned to 6 sub-cellular localisations: external, cytosol, mitochondrion, lysosome, peroxisome and microsome (see Table 4.1). This determination was based on experimental evidence (protein localisation, targeting sequences and subcellular fractionation) and indirect physiological or biochemical evidence as reported in scientific literature. In the absence of information, reactions were assigned to the cytosol. The microsome refers to a combination of three different compartments: endoplasmic reticulum (ER), Golgi apparatus and microsome. This simplification was used as the communication among endoplasmic reticulum, Golgi apparatus and microsome is mediated by vesicular transport processes which can be only inadequately included in the FBA methodology. In addition, recent studies demonstrated the experimental difficulty of proteomic profiling of the microsomes [109, 110] which would lead to missing transport processes between these compartments. In the modelling of complex biological systems it is often beneficial to set the directionality of reactions within a network. According to the second law of thermodynamics the spontaneity of a

reaction is defined by its change in Gibbs energy ($\triangle$G) with. However, for large-scale networks it is often difficult to obtain these parameters for every single reaction. The group contribution method [97, 98] allows estimating Gibbs energies. This method decomposes compound structures from a given set of reactions according to a basic set of groups.

The directionality of included network reactions was set according to Jankowski et.al.[98] or evidence from literature where available (see Additional file 3 of the SEM for a complete list of references and $\triangle$G values).

4.1.3 Generating the mathematical representation of the network

All reactions and different levels of evidence were documented during the network reconstruction process by using the Java-based Metannogen software [93]. At a later point the network and all meta-information, including metabolomic, transcriptomic and bibliomic data was stored in a PostgreSQL database (see Figure 4.1). This database functions as the knowledge-base for the network and enables subsequent integration of experimental data into mathematical computations.

Furthermore, a plain SBML representation of the network was generated for the following computational simulations and to make the network available to the scientific community (see Additional file 4 of the SEM). As mentioned earlier the SBML file format developed into a standard format for models within the systems biology community. Various mathematical software enable to incorporate SBML models and perform further computations. The linear programming files for all optimisation problems were generated by using FASIMU [16] and later computed with CPLEX [99].

4.1.4 Evaluation, validation and consistency check of the reconstructed network

The consistency and full functionality of the metabolic network was ensured by performing an extensive testing of physiological functions based on knowledge of the cardiac metabolism by using FBA. For each function linear optimisation problems were defined, which tested the biosynthesis of phospholipids (e.g. cardiolipin), conversion of amino acids into citric acid cycle intermediates by transamination or oxidative deamination as well as nucleotide synthesis (see Table 4.2).

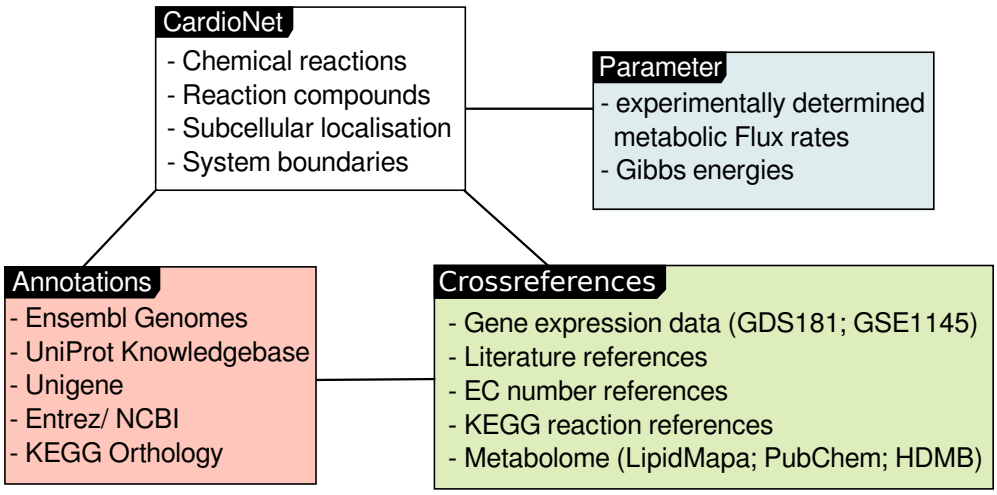

Figure 4.1: *Schematic overview of the PostgreSQL database. Boxes illustrate properties represented by the database.*

In total more than 400 single objective functions were defined.

The simulations were performed while restricting the import of metabolites to 27 compounds present in the plasma. This set included oxygen, glucose, lactate, ketone bodies (acetoacetate, (R)-3- hydroxybutanoate), essential amino and fatty acids as well as vitamins, while the release of intermediates was restricted to metabolic end products, e.g. lactate and glutamine (see Appendix, Table 1 or Additional file 5 of the SEM for applied constraints and Additional file 6 of the SEM for calculated flux distributions). In case the network failed to fulfil a required function, related reactions and metabolites were critically evaluated. Particular emphasis was given to ensuring the generation of each metabolite through direct synthesis or uptake from the extracellular space. In case a metabolite could not be produced, precursors of the metabolite were checked regarding their synthesis and the directionality of the reactions involved revised.

Additionally, the network was checked for any blocked reactions through FCA and network pruning. In case included reactions were not capable of carrying any non-zero flux, these candidates were critically evaluated regarding (i) missing metabolites, (ii) inaccurate systems boundaries or (iii) directionality of related reactions. It is important to mention, that every linear optimisation problem being applied is depend upon the imposed constraints including exchange of metabolites, steady-state assumption and fixed flux rates such as ATP formation or biosynthesis rates of biomolecules.

During this testing process, primary missing intracellular transport reactions and incomplete pathways (e.g. lipid metabolism) were revealed, which required further

manual literature review to complete the network functionality. These reactions were revised and eventually the metabolic network expanded based on additional evidence for occurrence in the human cardiomyocyte from experimental studies.

Table 4.2: *Metabolic and physiological functions tested for the metabolic network.*

Classification	Metabolic function	Cellular function	Reference
1. Carbohydrates			
• **Monosaccharides**	Glucose and fructose metabolism	Energy production	[111, 112]
	Glycogen formation	short-term energy storage	[113]
	Ribose metabolism	Energy production Formation of ribonucleotides	[114, 115]
2. Carboxylic acids	Degradation of ketone bodies	Energy production during fasting and diabetes	[116, 117]
3. Lipids			
• **Cholesterol**	De novo synthesis (cytosol, peroxisome)	Membrane synthesis	[118, 119]
• **Fatty acids**	Formation of (semi)-essential fatty acids	Membrane synthesis	[120, 121]
	β-oxidation of (non)-essential fatty acids	Energy production	[48, 122, 123]
• **Triacylglycerides**	De novo synthesis/ degradation of Mono-, Di- and Triacylglycerides	Membrane synthesis	[124, 125]
• **Phospholipids**	De novo synthesis/ degradation of:	Membrane formation	[39, 40, 124, 126–128]
	Phosphatidylserines		
	Phosphatidylcholines		
	Lysophosphatidylcholines		
	Phosphatidylethanolamines		

continues on next page

Table 4.2 – continued from previous page

Classification	Metabolic function	Cellular function	Reference
	Phosphatidylinositol		
	Sphingomyelin		
	Cardiolipin		
• **Sphingolipids**	Ceramides	Membrane formation, apoptosis	[84]
4. Proteins			
• **Amino acids**	Formation of (non)-essential amino acids	Precursors of cellular proteins, nucleic acids,glutathione and thioredoxin	[129, 130]
	Degradation of (non)-essential amino acids	Amino acid homoeostasis, anaplerotic reactions of TCA cycle	[131]
	Glutamine formation	Ammonia detoxification, Protein de novo synthesis	[132]
• **Tripeptide**	De novo synthesis of Glutathione	Prevention of cellular damage due to ROS	[133]
• **Polyamines**	Formation/ degradation of Prutescine and Spermidine	Cell growth and division	[134, 135]
• **Proteins**	De novo synthesis of: Myosin, Titin, α-Sarcoglycan, Tropomyosin, Troponin T	Contractile apparatus, enabling muscular contraction	[136, 137]
	De novo synthesis of Thioredoxin	Prevention of cellular damage due to ROS	[129, 130]
5. Nucleic acids			
• **Nucleobases**	De novo synthesis/ degradation of purine and pyrimidine nucleotides	Precursors of nucleosides, deoxyribonulceotides and ribonucleotides	[138, 139]
	Salvage of purine and pyrimidine nucleotides	Maintaining energy state	[140]

continues on next page

Table 4.2 – continued from previous page

Classification	Metabolic function	Cellular function	Reference
	De novo synthesis/ rephosphorylation of: nucleosides (ATP, CTP, GTP, TTP, UTP)	Energy production for muscular contraction	[139, 141–143]
	NADH, NADPH	Energy production and providing redox-state	[144, 145]

4.1.5 Comparison to other heart models

Recently, two mitochondrial network reconstructions [61, 146] and one genome-scale reconstruction of the human heart [147] have been reported. The reconstructed network of the cardiomyocyte was compared to these networks. All studies used different types of evidence during the reconstruction process, such as transcriptomic, metabolomic and proteomic data. However, in contrast to both mitochondrial networks [61, 146] and this study, the genome-scale reconstruction of the human heart [147] does not provide any cross-references for included reactions from experimental studies, databases or scientific literature.

A large alignment between CardioNet and both mitochondrial networks were found, with 90.48% and 92.49% of the mitochondrial network reactions being represented in CardioNet (see Table 4.3). Absent reactions included the heme biosynthesis pathway and the conversion of L-arginine into L-ornithine by arginase-II. The current network reconstruction is based on evidence in the normal human cardiomyocyte, thus reactions (e.g. arginase-II) belonging to genes, which are not expressed normally, were not included in the model. Further, previous studies reported an absent expression of arginase-II in the normal human cardiomyocyte [148] with up-regulation only during pathological states such as heart failure [149]. In order to perform simulations of pathological conditions, additional reactions such as arginase-II have to be included to reflect the changed gene expression.

The analysis revealed that 228 additional mitochondrial reactions have been considered in the network reconstruction, which is not part of the previous mitochondrial network reconstructions. These additional reactions include the metabolism of 26 fatty acids and the biosynthesis of important phospholipids such as cardiolipin, phosphatidylserine and phosphatidylcholine. Furthermore, the metabolism of amino acids has been reconstructed to a greater extent, for example, by including the synthesis of non-essential amino acids (e.g. glycine), which is not part of both mitochondrial networks.

Finally, CardioNet was compared to a genome-scale reconstruction of the human heart [147]. For the comparison the ”Human heart partial” network was used as provided in the supplemental material (Human_heart_partial.xml, [147]). Only cytosolic reactions and exchange reactions with the extracellular space are considered in this model. The fatty acid metabolism is represented in the human heart model to a greater extent compared to both mitochondrial networks

Table 4.3: *Comparison of cardiac metabolic networks.*

	CardioNet	**Smith AC 2011,[146]**	**Vo TD 2004, [61]**	**Zhao Y 2011,[147]**
Reactions, total	1793	253	189	2803
Compartments				
cytosol	745	-	45	1850
mitochondrion	257	164	74	-
lysosome	147	-	-	-
peroxisome	48	-	-	-
microsome	36	-	-	-
Transport reactions	560	89	70	953
extracellular	120	-	-	496
Metabolites	728	245	148	1494
CardioNet				
included reactions, N		234	171	395
included reactions, %		92.49%	90.48%	14.09%

[61, 146]. However, important phospholipids such as cardiolipin and the cholesterol biosynthesis in the peroxisome are missing. The localisation of citric acid cycle compounds such as fumarate and succinate is restricted to the cytosol and does not involve the mitochondrion. A functional testing of the human heart model has been performed for the same physiological functions of the cardiomyocyte as presented earlier in this chapter (see Table 4.2). Of the 110 functions tested 53 had no feasible solution, this included important cellular functions such as the citric acid cycle (see Additional file 7 of the SEM for a complete overview of all tested functions). These findings are in concordance with previous studies showing that fully automatic network reconstructions based on Recon1 not necessarily lead to a functional network [6, 150].

The comparison revealed that significantly more metabolic reactions of the mitochondrion were considered in the metabolic network reconstruction of the cardiomyocyte compared to previously reported mitochondrial reconstructions. Most strikingly, it was demonstrated that CardioNet is able to accomplish essential cellular functions while the genome-scale human heart model failed to fulfil all required objectives.

4.2 The determination of cardiac efficiency in varied substrate supplies

This section presents the developed approach to determine the cardiac efficiency in conditions of varied substrate availability and defines a metabolic target function for the cardiomyocyte.

4.2.1 Approach

The objective was to determine the efficiency of cardiac metabolism in varied substrate supplies. The difficulty here is to define input and output variables which are used to analyse this efficiency. Cardiomyocytes have to maintain an adequate energy formation, notably ATP synthesis, together with a multitude of metabolic functions including abundance of contractile proteins, membrane integrity and protection against reactive oxygen species. Irrespective of the external substrate supply and composition, these functions should be maintained in order to preserve cellular integrity. Simulations should not only reflect the combinatory complexity of potential substrates, but also take into account a comprehensive set of metabolic functions to describe real cellular conditions as closely as possible.

Cardiac efficiency can be determined by the ratio of cardiac work (pressure-volume-area) and myocardial oxygen requirement ($m\dot{V}O_2$). This definition directly reflects the relation between $m\dot{V}O_2$ and oxidative phosphorylation of ADP to ATP. In order to enable cardiac contraction, energy-delivering substrates such as glucose and fatty acids have to be oxidised by the heart. Any intrinsic or extrinsic changes in the substrate metabolism directly affect cardiac performance. This rationale arises from previous experimental studies showing preserved or altered cardiac performance in dependence on external substrate supply in the normal and failing heart [30, 35, 82].

In this study the efficiency of cardiac metabolism is defined by the myocardial oxygen consumption and the requirement of endogenous and exogenous substrates. It is further assumed that cardiomyocyte metabolism follows the principle of optimality, thus cellular functions are preserved while making minimal use of given resources. Based on these assumptions, cardiac efficiency is considered high if applied metabolic functions are maintained while making use of available substrates and oxygen at minimum cost. In following sections the developed approach to simulate altered substrate availability and the concept to

determine cardiac efficiency is presented.

The standard form for linear programming problems as used in flux balance analysis is:

$$\begin{aligned} &\underset{v\in\mathbb{R}^n}{\text{minimize}} && f(v) && (4.1)\\ &\text{subject to} && N \cdot v = 0, && (4.2)\\ & && v_{min,i} \leq v_i \leq v_{max,i}, \text{for i=1,2, ... n} && (4.3) \end{aligned}$$

where f(v) is the objective function, $v \in \mathbb{R}^n$ is the flux vector and N describes the m $\times$ n stoichiometric matrix. The lower and upper bounds on each reaction are represented by $v_{min,i}$ and $v_{max,i}$, respectively.

Experiments using the perfused isolated heart (e.g. Langendorff mode) showed that the relationship between measured uptake rates of substrates directly reflected the ratio of these substrates in the perfusion medium [82]. Therefore, the higher the share of substrate n in the external medium, the higher its share in the total substrate uptake space (v_s). The total substrate uptake flux (v_s) is defined as a linear combination of the external uptake rates v_m (m=1,2,...,ns) for each oxidized substrate n. The substrate availability in the external space is reflected by the coefficient β_m with

$$\sum_{m=1}^{ns} \beta_m = 1,\ 0 \leq \beta_m \leq 1. \tag{4.4}$$

The resulting substrate uptake rate for each simulated substrate composition i (i=1,2,...,ni) reads, as follows:

$$v_{m_i} = (\beta_{m_i} \cdot v_s). \tag{4.5}$$

Systematical variation of β_m enables to simulate all possible substrate relations, thus providing the testing of substrate combinations which so far have not been considered in experimental studies. This concept was applied to the metabolic network of the human cardiomyocyte, CardioNet, which is described later in more detail. Flux distributions were determined for the formation of (1) ATP and (2) important cellular components which have to be accomplished by the

cardiomyocyte to maintain cellular integrity and cardiac contractility. Both of these functions form the basis for the metabolic target function (v_t), which aims to reflect important metabolic functions of the cardiomyocyte such as contractility, membrane integrity and protection against reactive oxygen species.

$$v_t = \sum_{r=1}^{nt} v_r. \tag{4.6}$$

The metabolic target function (v_t) is a linear combination of selected metabolic flux rates v_r. To test this approach, a (1) simplified metabolic target function was defined, which is limited to the requirement of energy formation, in particular ATP. Cardiac contraction is mediated by the actin-myosin complex through ATP
hydrolysis. Therefore, a rate for ATP hydrolysis (v_{ATPase}) was demanded to reflect this important function and include ATP formation in the analysis. The simplified metabolic target function reads as follows:

$$v_t = v_{ATPase} \tag{4.7}$$

However, cellular functions cannot be limited to the simple assumption of energy production. Therefore, an extended metabolic target function (v_t) was defined as a linear combination of ATP formation and synthesis of important membrane lipids: ceramide (v_{cer}), cardiolipin (v_{cl}), phosphatidylcholine (v_{pc}), phosphatidylethanolamine (v_{pe}) and sphingomyelin (v_{sm}). The extended metabolic target function reads as follows:

$$v_t = v_{ATPase} + v_{cer} + v_{cl} + v_{pc} + v_{pe} + v_{sm} \tag{4.8}$$

Changes in fatty acid composition or content are known to reflect dietary supply and are associated with cellular damage [36, 37]. Therefore, acyl-chain compositions of every phospholipid and its percentage in the entire phospholipid fraction were included in the metabolic target function under normal dietary conditions. For each phospholipid species specific flux rates with respect to reported fatty acid composition of membrane lipids from normal human heart tissue [151, 152] were calculated. Each phospholipid species consists of a linear combination of specific acyl-chain compositions based on occurrence and reported range.

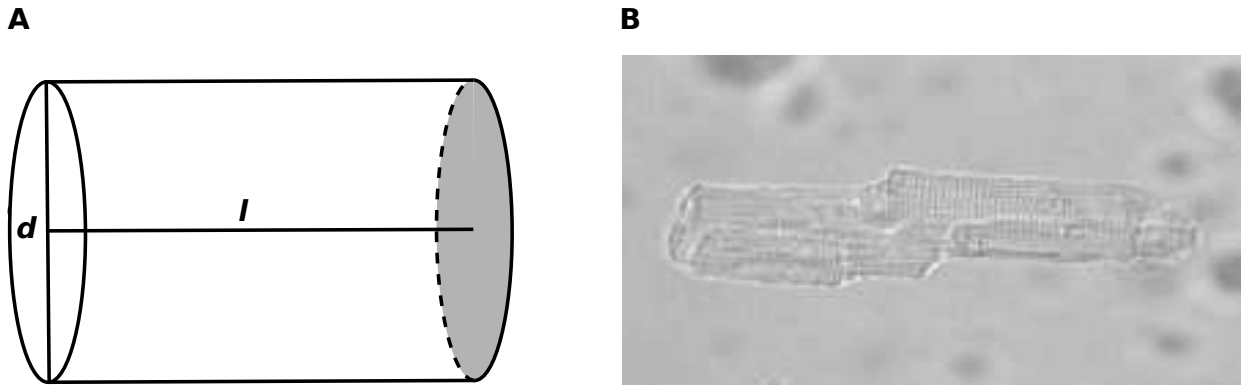

Figure 4.2: ***A.*** *Approximation of cardiomyocyte volume (V_{myo}) using the volume definition of a cylinder.*
B. *Cardiomyocytes in the bright-field microscope (Picture taken by Shokufeh Mahmoodzadeh, Charité - Universitätsmedizin Berlin).*

Another important aspect of cellular metabolism is the availability of endogenous short-term energy store such as glycogen and defence mechanisms against reactive oxygen species. To reflect these aspects, a limited cardiac glycogen store was assumed which could either (i) be resynthesized or (ii) degraded during the simulations. Hence, endogenous derived glucose could contribute to metabolic reactions. The maximal flux rate of glycogen degradation was set to experimentally determined values while the glycogen synthesis remained unrestricted. As in the case of glycogen turnover, a basal NADPH formation was demanded in order to reflect potential defence mechanisms against reactive oxygen species which have to be maintained irrespective of the external substrate supply.

All included metabolic flux rates v_r were obtained from experimental studies as given in Section 2.2.2 and Table 4.4. To consider flux rates from different sources, we decided to relate all parameters to the cell volume of a single cardiomyocyte. The unitary dimension for all included and calculated flux rates in this study is: mmol $\cdot$ min^{-1} $\cdot$ (l cell)$^{-1}$. Given the roughly cylindrical cell shape of cardiomyocytes in cardiac tissue (see Figure 4.2), the cell volume (V_{myo}) was approximated as follows:

$$V_{myo} = \frac{\pi}{4} \cdot d^2 \cdot l, \tag{4.9}$$

$$V_{myo} = 2.16e\text{-}11\ l \tag{4.10}$$

with a diameter (d) of 14 μm and length (l) of 140 μm [3, 4].

In summary, the objective of the linear programming problem is defined as finding the minimal total substrate uptake rate (v_s) and oxygen demand (v_{O_2}) while

accomplishing the metabolic target function and fulfilling all applied constraints.

$$f(v) = (v_s + v_{O_2}) \tag{4.11}$$

The modified optimization problem according to the flux-minimization principle for each simulated substrate composition i reads, as follows:

minimize	$f(v)$	(4.12)
subject to	$N \cdot v = 0,$	(4.13)
	$v_{min,j} \leq v \leq v_{max,j},$	(4.14)
	$v_t = \sum_{r=1}^{nt} v_r,$	(4.15)
	$v_m = (\beta_m \cdot v_s).$	(4.16)

4.2.2 Efficiency measure

To evaluate the cardiac efficiency and determine optimal substrate combinations, an efficiency measure was determined for each combination based on different input criteria q. These criteria were used to compare simulated external substrate availability with the worst-case and best-case solution to obtain a ratio measure of efficiency.

The following criteria q_j (j=1,2,...,nj) were applied: the oxygen demand (v_{O_2}, q_1), total substrate uptake rate (v_s, q_2) and endogenous glucose derived from glycogenolysis (v_{GL}, q_3). An optimal substrate combination should not only meet a minimal distance to the best achieved solution, but also a maximal distance to the worst achieved solution for each criterion. This takes into account that one solution could show minimal requirement of substrates while the oxygen demand and glycogenolysis increases.

The efficiency measure was calculated for every simulated substrate composition i (i=1,2,...,ni) as a Euclidean distance by, first, determining the best-case (q_j^+) and worst-case solution (q_j^-) from all simulations for each criterion as the minimal and maximal uptake rate, respectively. Secondly, the distances between actual flux rate (q_{ji}) to the best-case (q_j^+) and worst-case solution (q_j^-) were calcu-

lated.

$$S_{i^+} = \sqrt{\sum_{j=1}^{nj}(q_{ij} - q_j^+)^2} \qquad \forall\, i = 1,...,ni, \tag{4.17}$$

$$S_{i^-} = \sqrt{\sum_{j=1}^{nj}(q_{ij} - q_j^-)^2} \qquad \forall\, i = 1,...,ni. \tag{4.18}$$

The relative distance for each solution to the best-case solution is defined as the efficiency index C_{i^+} for the considered substrate combination:

$$C_{i^+} = \frac{S_{i^-}}{S_{i^+} + S_{i^-}} \tag{4.19}$$

with a maximal theoretical efficiency value C_{i^+} equal to 1. All substrate compositions with the highest overall match and efficiency values C_{i^+} close to 1 were considered as optimal solutions for the chosen metabolic objective. Further, the efficiency measure was tested for two criteria (q_1,q_2) showing several common relationship types. For each function we generated a dataset with an equal data size (n=2000, see Figure 4.3). These datasets showed either a (i) linear, (ii) exponential, (iii) quadratic or (iv) sinusoidal relationship between criteria q_1 and q_2. For each sample we determined the efficiency to demonstrate the behaviour of the measure. Figure 4.3 illustrates the calculated efficiency measure for each function type. For instance, a linear relationship between applied criteria q_1 and q_2 results in a corresponding linear representation of the efficiency measure. The sample minimum corresponds to an efficiency C_{i^+} score approaching 1. Similarly, an exponential relationship receives C_{i^+} scores showing a progressive proportionality in which sample minima and maxima equal maximal and minimal efficiency score, respectively. In a quadratic relation between criteria, calculated efficiency scores degrade and progress in an inversely proportionate manner to the sample. Here, the maximal efficiency score is less than 1.0, in contrast to a linear or exponential function type. Similarly, in a sinusoidal relationship the efficiency scores degrade and progress inversely. For a pair of criteria q_1 and q_2, if one criterion is a quadratic or sinusoidal function of the other criterion, then the same efficiency score can be received by more than one pair. For these noiseless (i.e, R^2 = 1.0) samples with equal size, the efficiency measure makes it easy to interpret and compare indices across and within function types given the data ranges are equal. It is important to note that a cut-off for optimal data points has to

be set. However, with this method it is not possible to determine a border indicating the efficient behaviour of a given dataset.

4.2.3 Alternate optima

Presumed a problem is feasible and a value for the objective can be calculated, then the solution for v (see equation 4.13) is not necessarily unique. Multiple solutions might occur to solve the problem and cause degeneration of the flux distribution. In order to identify alternate flux solutions that can equally satisfy the problem, i.e. yield the same optimal solution, additional simulations were performed. The mixed-integer linear problem (MILP) was resolved after adding a constraint (z^*) for a single flux of the original flux distribution which was set to either 1.01-fold (z_1^*) or 0.99-fold (z_2^*) of its original calculated flux value (v_0). This additional constraining was repeated for one flux after the other and the optimisation problem resolved.

$$z_1^* = 1.01 \cdot v_0, \tag{4.20}$$

$$z_2^* = 0.99 \cdot v_0. \tag{4.21}$$

The modified optimisation problem reads as follows:

minimize	$f(v)$	(4.22)
subject to	$N \cdot v = 0,$	(4.23)
	$v_{min,j} \leq v \leq v_{max,j},$	(4.24)
	$v_t = \sum_{r=1}^{nt} v_r,$	(4.25)
	$v_m = (\beta_m \cdot v_s),$	(4.26)
	$z_1^*, z_2^*.$	(4.27)

In case no feasible solution could be found, the respective original flux solution is dependent on one or more fixed fluxes of the target function and cannot be varied. Each feasible solution yielding the same optimum as the original solution was assigned to further statistical analysis (see Additional file 12 of the SEM). In case the variance is equal to zero the respective flux is uniquely defined. On

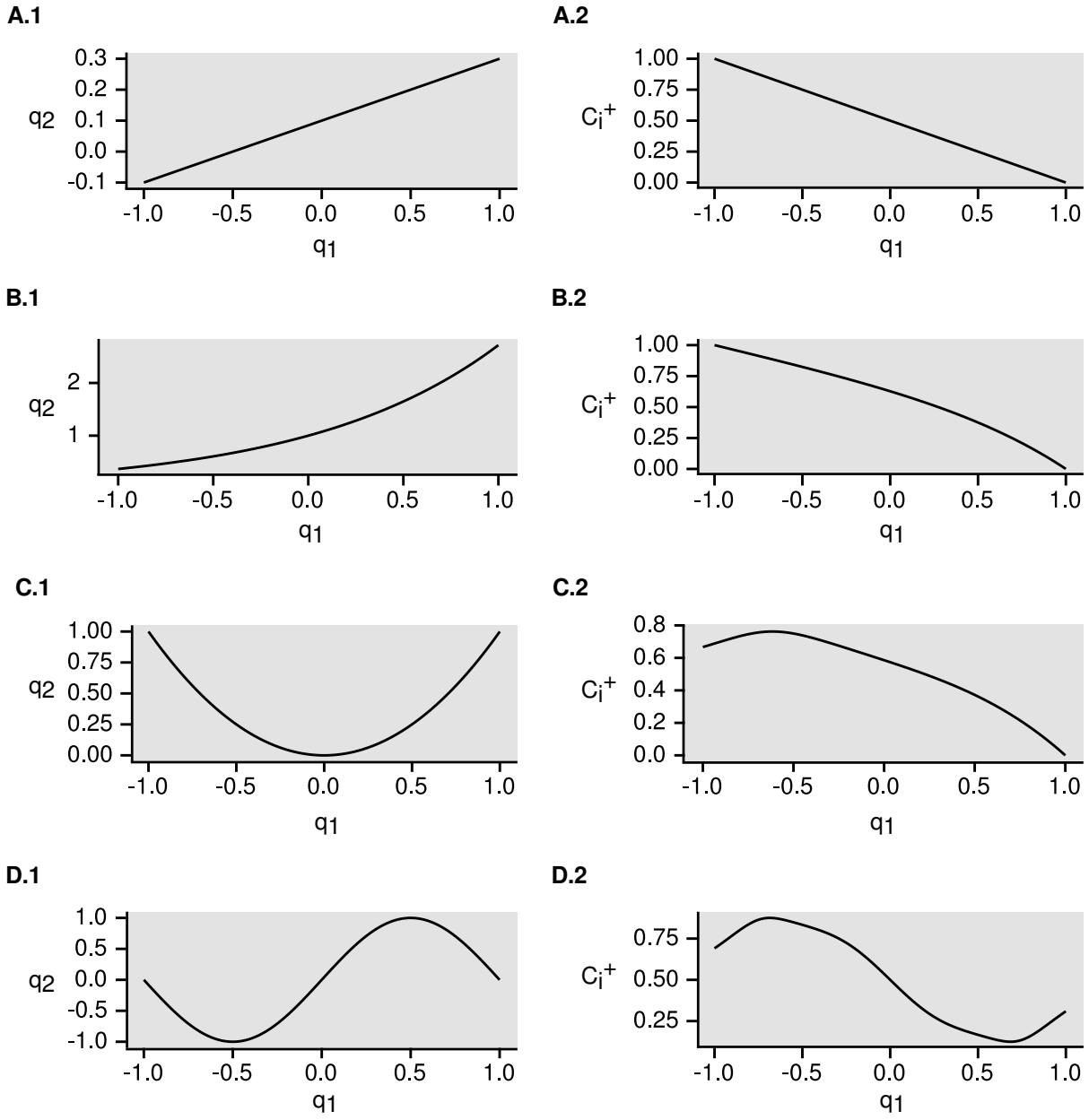

Figure 4.3: ***A to D.*** *Plots representing the characteristic efficiency measure (C_{i+}) for common function types. For each plot, datasets with the size n=2000 were generated. The following functions are presented: (A) f(x) = m·x+n, (B) $f(x)=x^2$, (C) $f(x)=e^x$ and (D) $f(x)=\sin(\pi \cdot x)$. The panels A.1 to D.1 refer to applied criteria q_1 and q_2, while panels A.2 to D.2 refer to calculated efficiency measures (C_{i+}).*

the other hand, a non-zero flux value indicates an unequivocal definition of the respective flux. These fluxes may vary without affecting the optimal behaviour of the metabolic network, based on the capability of the network to compensate these variations.

The optimisation problem was repeated for substrate combinations which were identified with the highest or lowest efficiency value while satisfying (1) a baseline ATP consumption rate and (2) a target function of the cardiomyocyte (see Additional file 12 of the SEM for calculated flux values). Based on the variance analysis for all four examples, no significant difference was found between the solutions. About one third of the fluxes cannot be changed without violating the demanded target function, thus leading to infeasibility of the problem.

Table 4.4: *Metabolic target function of the cardiomyocyte. Flux rates are given in mmol · min^{-1} · (l cell)$^{-1}$.*

	Acyl-Composition	**v_r**	**Ref.**
Cardiolipin (v_{cl})	C18:2, C18:2, C18:2, C18:2	3.38E-004	[83]
	C20:3, C18:2, C18:2, C18:2	2.56E-004	
	C20:4, C18:2, C18:2, C18:2	2.46E-004	
	C18:2, C18:1, C18:1, C18:1	1.72E-004	
Phosphatidylcholine (v_{pc})	C16:0, C16:1	2.51E-002	[83]
	C18:0, C18:1	1.59E-002	
	C20:4, C22:4	3.39E-003	
	C18:2, C20:4	6.59E-003	
	C18:2, C20:3	4.07E-003	
	C18:2, C20:2	3.68E-003	
	C20:3, C20:4	3.77E-003	
Phosphatidylethanolamine (v_{pe})	C16:0, C16:1	2.99E-003	[83]
	C18:0, C18:1	1.84E-002	
	C20:4, C22:4	5.37E-003	
	C18:2, C20:4	5.41E-003	
	C18:2, C20:3	6.29E-004	
	C18:2, C20:2	7.27E-004	[83]
	C22:5, C22:6	3.85E-003	
	C20:3, C20:4	5.20E-003	
Sphingomyelin (v_{sm})	C18:1, C16:0	2.02E-004	[83]
	C18:0, C18:1	1.03E-004	
Ceramide (v_{cer})	C16:0, C18:0	4.60E-006	[84]
	C18:0, C18:0	4.60E-006	
v_{ATPase}	-	21.6	[86]

4.3 Computational results

This section summarizes the computational results from simulations of varied substrate availability. The cardiac efficiency is determined for each substrate composition while demanding a simplified and extended metabolic target function. Finally, predicted flux distributions are evaluated with respect to experimentally observed substrate and oxygen demands.

4.3.1 Efficiency of ATP formation in varied substrate availability

The dephosphorylation of ATP through myosin light chain kinase is an important step in the cross-bridge cycle to generate cardiac contraction [136, 137]. However, currently this dynamic process is not described in the reconstructed metabolic network of the human cardiomyocyte. Therefore, a simplified metabolic target functions was defined by demanding a baseline ATP consumption rate (v_{ATPase}) of 21.6 mmol $\cdot$ min$^{-1}\cdot$ (l cell)$^{-1}$ [86] to reflect this important cardiac functions.

$$v_t = v_{ATPase} \tag{4.28}$$

The oxidation of available substrates m should provide sufficient ATP synthesis to enable this ATP consumption rate (v_{ATPase}). These alternative energy-delivering substrates included glucose, oleate, acetoacetate and lactate, which can be taken up and oxidised by cardiomyocytes to generate ATP. The external uptake rate for each substrate is expressed by v_m (m=1,2,...,ns) and described as follows:

$$v_m = \beta_m \cdot v_s \tag{4.29}$$

where the coefficient β ($0 \leq \beta_m \leq 1$) denotes the relative share of the respective substrate m in the total substrate uptake flux v_s (see Chapter 4.2.1).

The coefficient β was modified on a fine grid of values between 0 and 1. The network boundaries were restricted to the import of the investigated substrates, cofactors (choline, ethanolamine) and oxygen while only the export of degradation products such as glutamine and NH3 was allowed (see Appendix, Table 2 or Additional file 5 of the SEM for all applied constraints).

In total, 176 851 flux minimisation computations were performed, while

Table 4.5: *Baseline ATP consumption.*

$\beta_{Glucose}$	β_{Oleate}	$\beta_{Acetoacetate}$	$\beta_{Lactate}$	v_{O_2}	v_s	C_{i^+}
0.00	1.00	0.00	0.00	4.1101	0.1626	0.6849
1.00	0.00	0.00	0.00	3.6007	0.6005	0.6576
0.00	0.00	1.00	0.00	3.9269	0.9806	0.2791
0.00	0.00	0.00	1.00	3.8124	1.2701	0.2091
0.79	0.21	0.00	0.00	3.8534	0.3823	0.7334
0.42	0.37	0.09	0.12	3.9830	0.3154	0.7000
0.33	0.19	0.43	0.05	3.9420	0.4536	0.6500
0.20	0.16	0.26	0.38	3.9485	0.5292	0.6000
0.46	0.03	0.46	0.05	3.7757	0.6847	0.5500
0.17	0.09	0.01	0.73	3.8880	0.7020	0.5000
0.20	0.04	0.41	0.35	3.8534	0.7841	0.4500
0.16	0.03	0.33	0.48	3.8448	0.8575	0.4000
0.06	0.05	0.03	0.86	3.8794	0.8942	0.3600
0.02	0.02	0.52	0.44	3.9010	0.9677	0.3000
0.07	0.00	0.07	0.86	3.7930	1.1556	0.2500
0.00	0.00	0.13	0.87	3.8297	1.2247	0.2070

All data is ranked by the calculated efficiency in descending order and given fully for exclusive utilisation of each substrate. Results for altered substrate availability are listed by the achieved efficiency with a value of: 0.25, 0.3,0.36, 0.4, 0.45, 0.5, 0.55, 0.6, 0.65 and 0.7. Rates for oxygen requirement (v_{O_2}) and total substrate uptake rates (v_s) are given in mmol $\cdot$ $min^{-1}\cdot$ (l cell)$^{-1}$. For all results, see Additional file 8 of the SEM.

minimising the sum of external uptake fluxes without restricting the oxygen supply (see Additional file 8 of the SEM for predicted flux values).

Each simulated substrate composition for glucose, oleate, acetoacetate and lactate meets the energy demand to enable the predefined ATP consumption rate (v_{ATPase}). Nonetheless, oxygen and substrate demands differed clearly between substrate combinations as presented in Figure 4.4. A minimal oxygen requirement for all simulations was v_{O_2}= 3.6007 mmol $\cdot$ $min^{-1}\cdot$ (l cell)$^{-1}$ and only reached in exclusive utilisation of glucose, as can be seen in Table 4.5 and Figure 4.5.

Simulating exclusive utilisation of oleate resulted in an increased oxygen uptake to a maximum of v_{O_2}= 4.1101 mmol $\cdot$ $min^{-1}\cdot$ (l cell)$^{-1}$, while only a minimal total substrate uptake rate was required (v_s=0.162 mmol $\cdot$ $min^{-1}\cdot$ (l cell)$^{-1}$). For each simulation an efficiency measure (C_{i^+}) was calculated based on two input criteria: (1) the oxygen demand and (2) the total substrate uptake rate. As illustrated in Figure 4.5, this measure enables to compare a given oxygen and total substrate demand to the best and worst achieved values within the total set of simulations. On the basis of C_{i^+}, the optimal substrate composition should

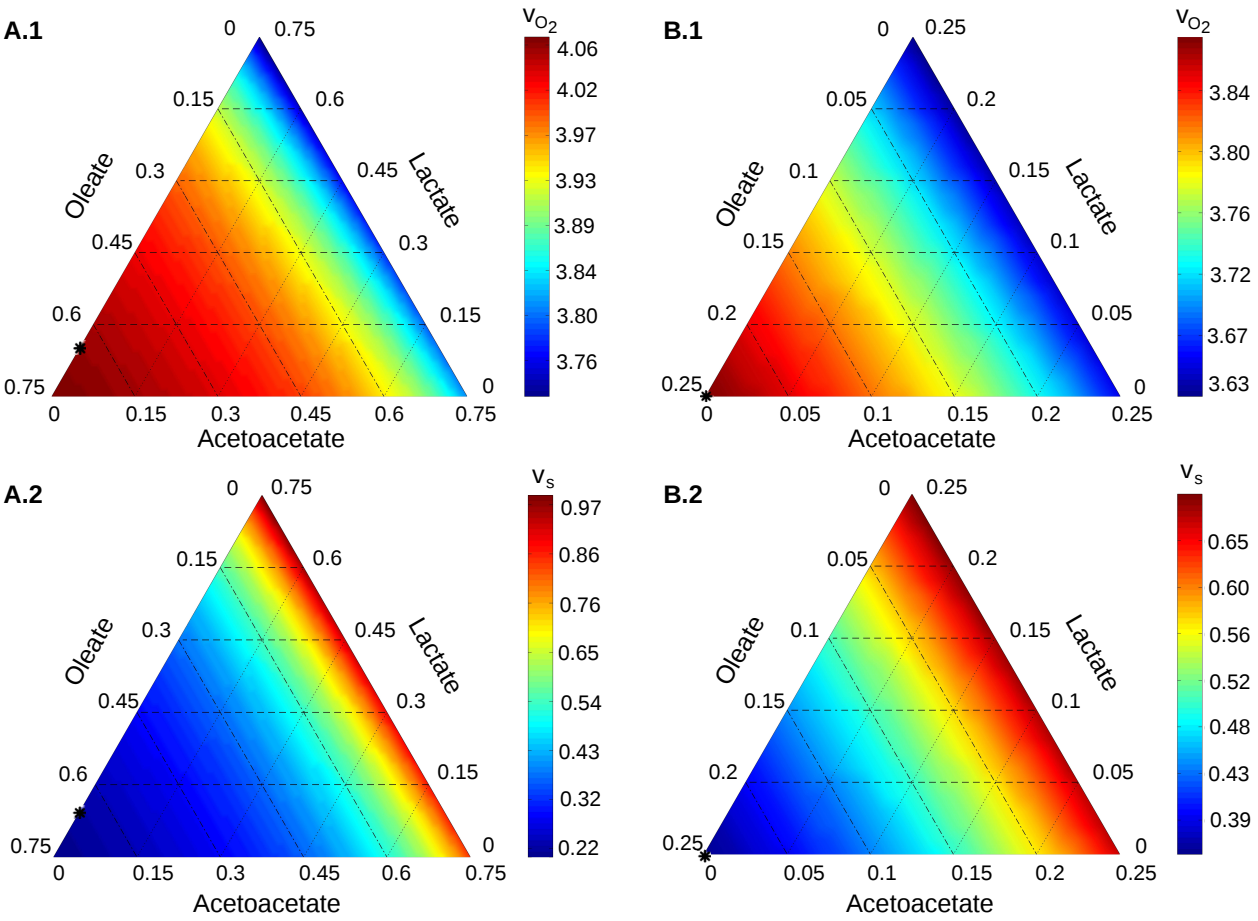

Figure 4.4: *Illustration of total substrate uptake rate (v_s) and oxygen demand (v_{O_2}) for a fixed glucose supply with (A) $\beta = 0.25$ and (B) $\beta = 0.75$. The panels A.1 and B.1 refer to the oxygen demand (v_{O_2}) for the given glucose proportion, while panels A.2 and B.2 refer to the total substrate uptake rate (v_s). The optimal substrate composition (*) is marked for each panel: (A) $v_{Glucose}$= 25%, v_{Oleate}= 64%, $v_{Acetoacetate}$= 0%, $v_{Lactate}$= 11%, (B) $v_{Glucose}$= 75%, v_{Oleate}= 25%, $v_{Acetoacetate}$= 0%, $v_{Lactate}$= 0%.*

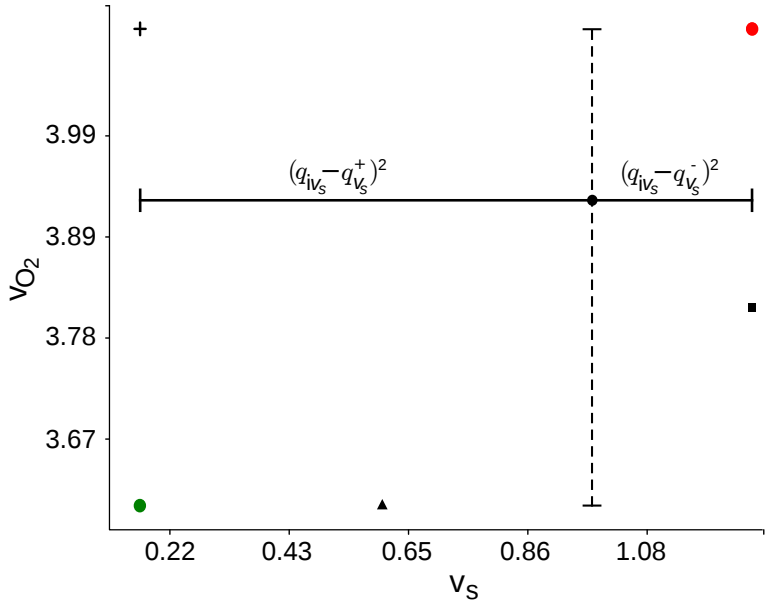

Figure 4.5: *Illustration of oxygen (v_{O_2}) and total substrate uptake rates (v_s) for exclusive utilisation of glucose (▲), oleate (+), acetoacetate (●) and lactate (■). Calculated distances for each criterion were visualized for acetoacetate, with dotted lines indicating distances to minimal and maximal oxygen uptake rates and straight lines to respective minimal and maximal total substrate uptake rates. Additional markers indicate theoretical values for best (green circle) and worst (red circle) solution. The efficiency index C_{i^+} is defined as the relative distance for each solution to the best-case solution: $C_{i^+} = \frac{s_{i^-}}{s_{i^+} + s_{i^-}}$.*

satisfy the metabolic target function, while requiring as little oxygen and substrates as possible, thus enabling an efficient cardiac metabolic performance.

In the extreme situation in which only one substrate is exclusively oxidised, glucose and oleate were almost identical efficient in terms of oxygen and total substrate demand according to our selected efficiency measure (C_{i^+}; Table 4.5, Figure 4.5). Simulating more physiological situations in which all four substrates could be utilised revealed that a combination of oleate and glucose in the percentage of 21% and 79%, respectively, provided an optimal nutritional supply for the cardiomyocyte (C_{i^+} 0.7334; see Table 4.5).

By contrast, the least efficient substrate supplies according to C_{i^+} include lactate. Especially sole lactate utilisation required a maximal total substrate uptake rate (v_s) of 1.2701 mmol $\cdot$ min$^{-1}\cdot$ (l cell)$^{-1}$, thus 7.84-fold higher than in case of oleate utilisation. We determined the lowest efficiency for a total substrate combination of 13% acetoacetate and 87% lactate (C_{i^+}= 0.2070, see Table 4.5).

To identify alternate flux solutions that can equally satisfy the problem, i.e. yield the same optimal solution, additional computations (see Chapter 4.2.3) were

performed. The optimisation problem was repeated for substrate combinations with the highest and lowest calculated efficiency. Here, four alternative distributions yielding the same optimal solution were determined for the substrate combination achieving the highest calculated efficiency (79% oleate, 21% glucose). The calculated distributions showed no significant difference from the original distribution (F= 135, Pr($>$F) $<$2e-16, p$\leq$0.001) and 90.70% of the fluxes were unique, thus the variance (s) equals zero (see Additional file 9 of the SEM for a complete overview of all calculated alternate flux values).

Furthermore, 11 alternative distributions were identified for the least efficient substrate combination showing no significant difference from the original distribution (F= 135, Pr($>$F) $<$2e-16, p$\leq$0.001) and 74.41% unique flux solutions (s=0). The largest variance (s=0.24) was found for flux rates of creatine and phosphocreatine transport into the mitochondrion as well as cytosolic and mitochondrial creatine kinase. However, all fluxes representing the external substrate and oxygen uptake were found with unique solutions.

4.3.2 Validation of calculated efficiency

To validate the theoretical observations, computations were performed by applying substrate compositions as determined in a recent experimental study [82] (see Chapter 2.2.2), which investigated the utilisation of glucose, lactate, oleate, acetate and ketone bodies (acetoacetate, (R)-3-hydroxybutanoate) in dependence on workload and insulin to improve the perfusion system for the isolated rat heart. Again the simplified metabolic target function with a baseline ATP consumption rate (v_{ATPase}) of 21.6 mmol $\cdot$ min$^{-1}\cdot$ (l cell)$^{-1}$ [86] was included in the optimisation problems. The network boundaries were set as given in Appendix Table 3.

The computational results, summarised in Table 4.6 and Figure 4.6, show that calculated flux rates are in good concordance with experimentally determined uptake rates and correspond in many cases. Compared to the experiment, the oxygen demand is underestimated in all simulations but in sole acetate oxidation. Moreover, the total substrate uptake rate is increased in simulations for sole utilisation of acetoacetate and in combined utilisation of acetate and glucose. Here, the ratio of calculated oxygen demand to total substrate uptake rate shows the greatest deviation from experimentally obtained values.
To further compare these estimations with the experiment, efficiency measures were determined for each substrate composition as described above. As depicted

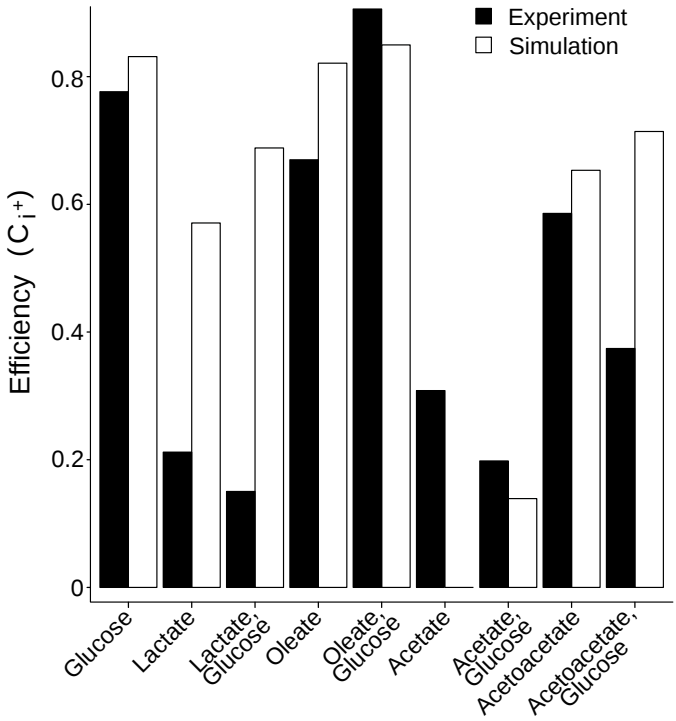

Figure 4.6: *Comparing calculated cardiac efficiency (C_{i+}) under experimental conditions [82] to theoretical simulations of altered substrate supply.*

in Figure 4.6, the calculated efficiency indices were almost identical except for simulations of lactate oxidation. Here, the required oxygen and substrate demand to satisfy the baseline ATP consumption rate obtained a more favourable relation as the calculated oxygen demand in sole oleate utilisation was clearly underestimated. Furthermore, the oxygen and substrate demand increased to a maximum (C_{i^+}= 0; see Table 4.6, Figure 4.6) in simulations of sole acetate utilisation. This explains the differences between calculated efficiency indices. In agreement with these simulations, oxidation of glucose and oleate showed to be more efficient in terms of oxygen demand and total substrate uptake rate.

The comparison of experimental results in the oxidation of acetoacetate with the computed ones is limited due to reduced cardiac work during the perfusion experiment and altered substrate application. The applied optimisation problems consider direct presence of acetoacetate and glucose, while in the experiment, glucose was added at a later time in the perfusion. The data, summarized in Table 4.6, show that sole utilisation of acetoacetate is less efficient than glucose or oleate oxidation, but demonstrate that oxygen and substrate uptake rates are more favourable than in the case of acetate and lactate.

Table 4.6: *Simulation of experimental substrate supply and comparison by calculated efficiency C_{i^+}.*

			Simulation				Experiment			
Exp.	**Substrate**	β_m	v_{O_2}	v_s	v_{O_2}/v_s	C_{i^+}	v_{O_2}	v_s	v_{O_2}/v_s	C_{i^+}
1	Glucose	1.00	3.60	0.60	6.00	0.83	4.28	0.55	7.84	0.78
2.1	Lactate	1.00	3.81	1.17	3.25	0.60	4.71	1.41	3.34	0.21
2.2	Glucose Lactate	0.23 0.77	3.73	0.96	3.89	0.69	4.70	1.59	2.96	0.15
3.1	Oleate	1.00	4.11	0.16	25.37	0.82	4.94	0.18	28.07	0.67
3.2	Glucose Oleate	0.54 0.46	4.02	0.24	16.75	0.85	4.36	0.21	20.57	0.91
4.1	Acetate	1.00	4.8	2.4	2	0	4.28	1.68	2.55	0.31
4.2	Glucose Acetate	0.05 0.95	4.6	2.11	2.19	0.14	4.69	1.46	3.21	0.2
5.1	Acetoacetate	1.00	3.93	0.98	4.00	0.65	4.20	0.53	7.89	0.59
5.2	Glucose Acetoacetate	0.26 0.74	3.81	0.86	4.41	0.71	4.95	1.01	4.91	0.37

Flux rates for v_{O_2} and v_s are given in mmol $\cdot$ min $^{-1}\cdot$ (l cell)$^{-1}$. v_{O_2} indicates oxygen demand; v_s, total substrate uptake rate; C_{i^+}, calculated efficiency.

4.3.3 Extending the metabolic target function and cardiac efficiency

Cardiomyocytes have to maintain an adequate ATP synthesis together with a multitude of metabolic functions including abundance of contractile proteins, membrane integrity and protection against reactive oxygen species. To reflect these metabolic features of the human cardiomyocyte, an extended metabolic target function (v_t) was defined by including not only the formation of ATP and important membrane lipids: ceramide (cer), cardiolipin (cl), phosphatidylcholine (pc), phosphatidylethanolamine (pe) and sphingomyelin (sm) (see Chapter 4.2) but also of NADPH.

$$v_t = v_{ATPase} + v_{cer} + v_{cl} + v_{pc} + v_{pe} + v_{sm} \tag{4.30}$$

The corresponding metabolic flux rates were obtained from experimentally determined synthesis rates of membrane lipids from tracer studies [83, 153]. To take into account possible short-term storage of energy, the synthesis of glycogen was allowed during simulations while restricting the degradation of glycogen to a maximal rate ($v_{GL;max}$ = 0.216 mmol $\cdot$ min$^{-1}\cdot$ (l cell)$^{-1}$) as determined in previous investigations [154].

The myocardial defence mechanisms against hypoxia are mostly represented by NADPH to maintain reduced glutathione. To consider this aspect, an initial simulation was performed to determine the basal NADPH formation in the case of unrestricted substrate supply. The cytosolic and microsomal glucose-6-phosphate dehydrogenase rate (G6PDH) assigned a rate of 2.13e-05 mmol $\text{min}^{-1}\cdot$ (l cell)$^{-1}$ and 3.05e-03 mmol $\cdot$ $\text{min}^{-1}\cdot$ (l cell)$^{-1}$, respectively, but no flux was found for the NADPH producing isocitrate dehydrogenase. The rate of cytosolic G6PDH was 0.08% of the hexokinase flux rate distribution. An overall NADPH production rate of 1.42e-05 mmol $\cdot$ $\text{min}^{-1}\cdot$ (l cell)$^{-1}$ was determined and included in the simulations as a minimal required rate of NADPH synthesis in addition to the metabolic target function.

In order to simulate varied substrate availability that corresponds more to physiological conditions, the set of available substrates (m=9) was extended by including saturated, medium-chain unsaturated and long-chain unsaturated fatty acids. The network boundaries were restricted to the import of the investigated substrates, cofactors (Choline, Ethanolamine) and oxygen. Only the export of degradation products such as glutamine, NH3 and urate was allowed (see Appendix, Table 4 and Additional file 5 of the SEM for all applied constraints).

In total, 218 618 computations were performed simulating altered supply of 9 different substrates (ns=9). As expected, no solutions were found in the case of absent α-linoleate and docosahexaenoate supply, thus these fatty acids are required as precursors of the biosynthesis of certain phospholipid species in the metabolic network and cannot be replaced by any other substrate [155]. For each simulation, the efficiency (C_{i^+}) was calculated to identify optimal substrate combinations based on three criteria: (i) oxygen demand (v_{O_2}), (ii) total substrate uptake rate (v_s) and (iii) endogenous glucose derived from glycogen turnover (v_{GL}).

The highest efficiency scores were calculated for substrate combinations with a major share of fatty acids and glucose, as presented in Table 4.7. Especially a substrate combination of 90% glucose, 5% of palmitate and 1.667% of α-linoleate, eicosapentaenoate and docosahexaenoate showed to be more favourable than any other substrate combination (v_{O_2}=6.9154 mmol $\cdot$ $\text{min}^{-1}\cdot$ (l cell)$^{-1}$; v_s=4.8859 mmol $\cdot$ $\text{min}^{-1}\cdot$ (l cell)$^{-1}$; C_{i^+}=0.8438). As expected, the efficiency (C_{i^+}) was directly proportional to an increasing share of glucose and fatty acids (Figure 4.7-A) and inversely proportional to an increasing share of acetoacetate and lactate (Figure 4.7-A).

In fact, a substrate combination of 95% acetoacetate and 5% fatty acids with a

share of 0.83% palmitate, 0.83% α-linoleate and 3.33% docosahexaenoate resulted to be least efficient to fulfil the demanded metabolic target function (see Table 4.7). A maximal oxygen demand (v_{O_2}=48.421 mmol $\cdot$ min$^{-1}\cdot$ (l cell)$^{-1}$) was estimated in predominately utilisation of acetoacetate (95%) supplemented by oleate (0.83%), α-linoleate (0.83%) and docosahexaenoate (3.33%). Similarly, a maximal total substrate supply (v_s= 10.2332 mmol $\cdot$ min^{-1} $\cdot$ (l cell)$^{-1}$) was calculated for a substrate combination of 45% acetoacetate, 35% lactate, 15% glucose, 1.67% oleate, 0.8% α-linoleate and 2.5% docosahexaenoate (see Additional file 10 of the SEM).

Again the optimisation problem was repeated to identify alternative flux solutions in substrate combinations with the highest and lowest calculated efficiency as described (see Table 4.7). Here, 202 alternative distributions were identified with 71.92% unique flux solutions (variance s=0) achieving the same objective for the substrate combination with the highest calculated efficiency (see Additional file 9 of the SEM). None of thel alternative distributions showed any significant difference to the original distribution (F=462, Pr($>$F) $<$2e-16, p$\leq$0.001).

Similarly, 216 alternative distributions with 56.96% unique flux solutions were found for the substrate combination with the lowest calculated efficiency. The calculated distributions showed no significant difference from the original distribution (F=278, Pr($>$F) $<$2e-16, p$\leq$0.001). The largest variance (s=29.83) was again found for flux rates of creatine and phosphocreatine transport into the mitochondrion as well as cytosolic and mitochondrial creatine kinase. In addition, variable flux rates were found for β-oxidation of fatty acids and ATP:nucleoside-diphoshate phosphotransferase. Each flux representing the glycogenolysis, external substrate and oxygen uptake was unique (s=0) in all simulations.

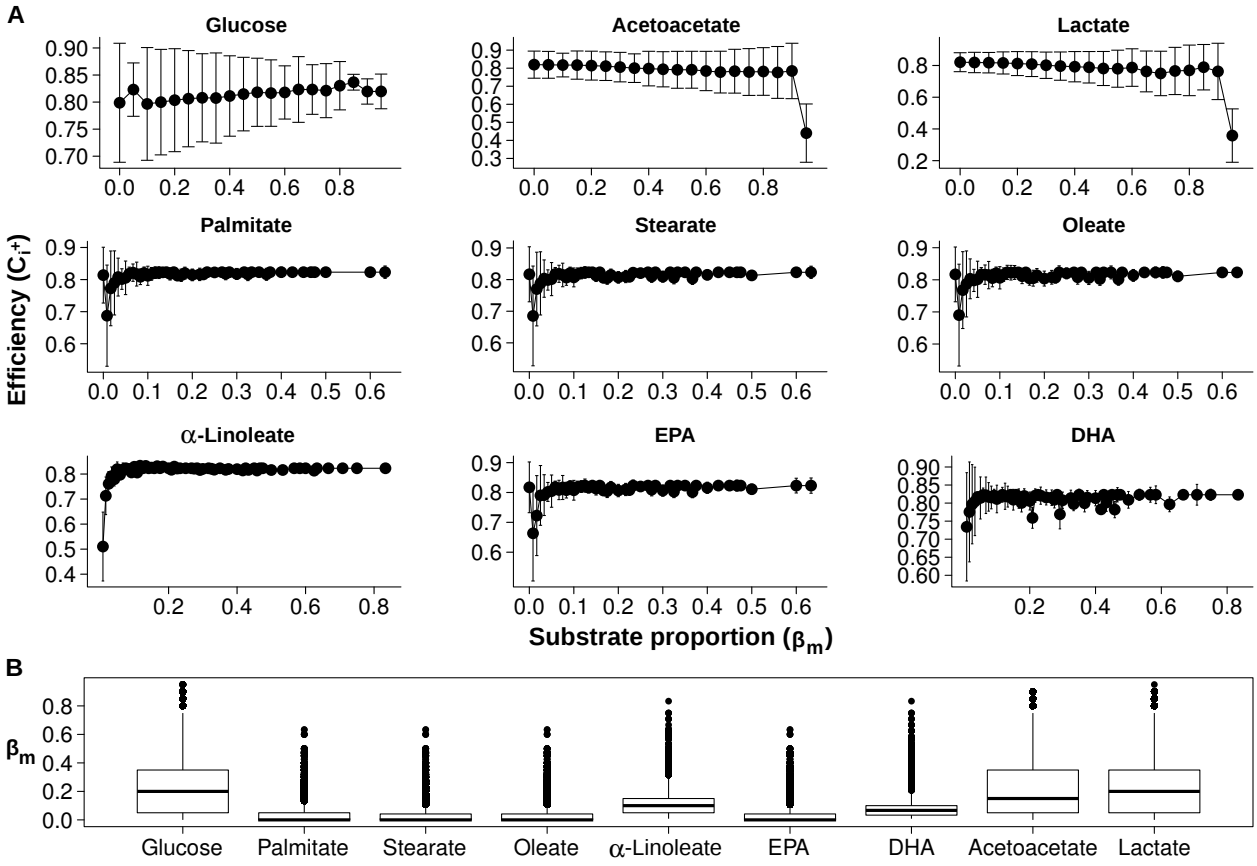

Figure 4.7: ***A.*** *Calculated efficency values for each substrate in varied share (β_m) of the total substrate uptake rate (v_t). Values are mean $\pm$ standard deviation.*
B. *Box and whisker plots of the proportion of substrates according to the total substrate uptake flux by efficiency score C_{i^+} greater than 0.8. The bold horizontal line in panels indicate mean. $C_{i^+} \geq 0.8$: n=76925. $\circ$ Outliers.*

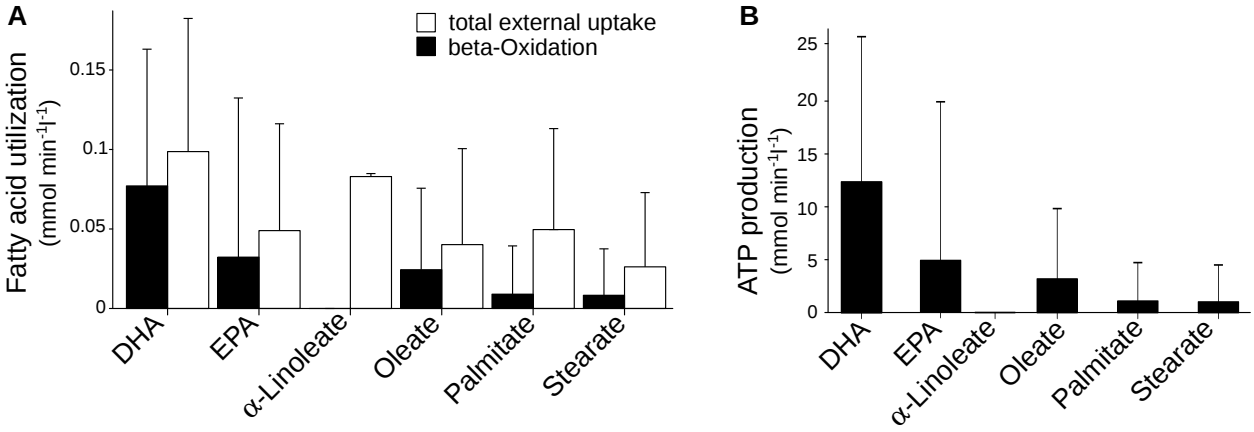

Figure 4.8: ***A.*** *Exogenous utilisation of fatty acids and contribution to ATP production by fatty acid β-oxidation.*
B. *Steady-state rates of ATP production from fatty acid β-oxidation. Data are expressed as boxplots.*

4.3.4 Contribution of fatty acids to ATP formation

The data, as illustrated in Figure 4.7-B, shows that the variability of substrate combinations with a large efficiency index ($C_{i^+} \geq 0.8$) increased with the advanced objective function. The mean share ($\beta_{\bar{x}}$) of glucose, fatty acids, acetoacetate and lactate was 0.231, 0.311, 0.221, and 0.237, respectively. The data, summarised in Figure 4.7-A, show for all fatty acids a similar pattern of calculated efficiency. Nonetheless, the contribution to ATP production differed between saturated, monounsaturated and polyunsaturated fatty acids. The mean rates of fatty acid utilisation and rates of ATP produced by fatty acid utilisation are summarised in Figure 4.8.

The ATP formation rate by fatty acid β-oxidation was calculated by assuming 120, 136, 134, 132, 142 and 156 moles of ATP derived from full oxidation of palmitate, stearate, oleate, α-linoleate, eicosapentaenoate and docosahexaenoate, respectively. The vast majority of palmitate, stearate and oleate contributed to phospholipid biosynthesis, while polyunsaturated fatty acids were mostly degraded via β-oxidation. As illustrated in Figure 4.8-A, α-linoleate was not degraded by β-oxidation, it therefore contributed fully to phospholipid biosynthesis. Additionally, degradation of docosahexaenoate and eicosapentaenoate through β-oxidation yielded a maximal ATP production (Figure 4.8-B) and this contribution rose up to 99.1% and 98.82% of utilised docosahexaenoate and eicosapentaenoate, respectively.

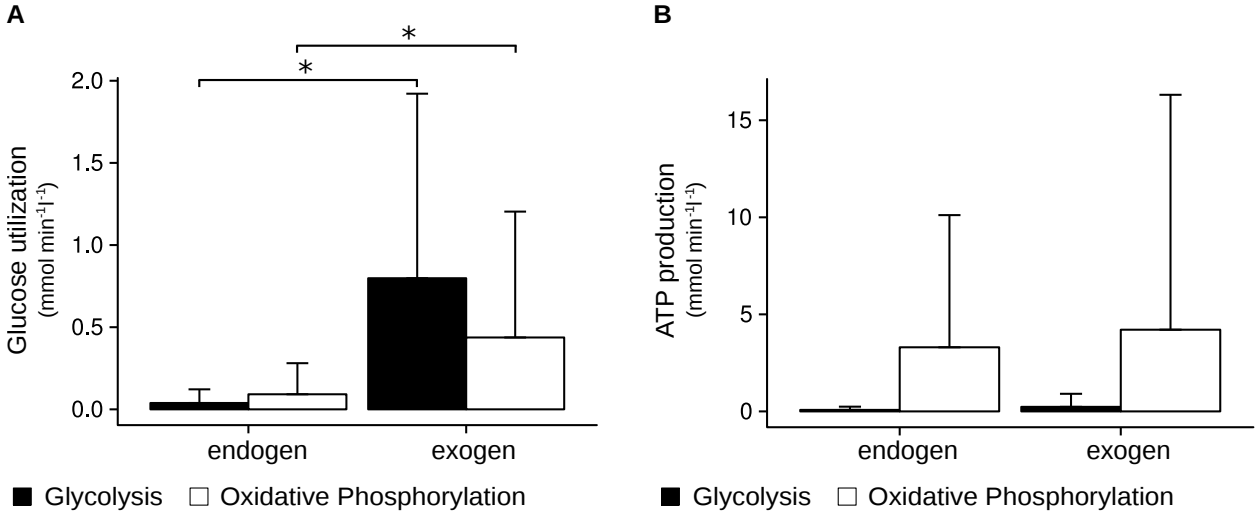

Figure 4.9: ***A.*** *Degradation of exogenous and endogenous glucose (glycogenolysis) by glycolysis and oxidative phosphorylation.*
B. *Steady-state rates of aerobic and anaerobic ATP production from glucose utilisation derived from exogenous glucose and glycogenolysis. Data are expressed as boxplots.* * *significant difference between endogenous and exogenous glucose.* $p<0.05$ *(unpaired t-test).*

4.3.5 Glycogen turnover

Glycogenolysis and glycogen synthesis occurred simultaneously throughout the simulations. In case of excessive glucose supply, which was not needed to fulfil the target function, glycogen was synthesized at a maximal rate of 0.887 mmol $\cdot$ $\text{min}^{-1}\cdot$ (l cell)$^{-1}$. Rates of exogenous glucose entering glycolysis were significantly greater than those from endogenous glycogen degradation (Figure 4.9-A; $p\leq0.05$). Following this, a large proportion of exogenous glucose was oxidised by oxidative phosphorylation and was also significantly greater than those from endogenous glycogen degradation (v_{exo}=0.437 $\pm$ 0.766 mmol $\cdot$ $\text{min}^{-1}\cdot$ (l cell)$^{-1}$; v_{endo}=0.091 $\pm$ 0.189 mmol $\cdot$ $\text{min}^{-1}\cdot$ (l cell)$^{-1}$; $p\leq0.05$).

In fact oxidative phosphorylation contributed most to cellular ATP production from exogenous and endogenous glucose utilisation (Figure 4.9-B), with glycogen accounting for 34.41% of ATP production (when glucose accounted for 50% of the total substrate uptake rate). The percentage of ATP production deriving from endogenous glucose oxidation by oxidative phosphorylation increased to 80.16% in a glucose share of less than 10% of the total substrate uptake rate. These results are supported by previous findings [156] showing a contribution of glycogen up to 41% of the total ATP production under experimental conditions.

Table 4.7: *Results for simulations of varied substrate availability of glucose, acetoactate, lactate and 6 different fatty aicids: palmitate, stearate, oleate, α-linoleate, eicosapentaenoate and docosahexaenoate.*

$\beta_{Glucose}$	$\beta_{Palmitate}$	$\beta_{Stearate}$	β_{Oleate}	$\beta_{\alpha\text{-Linoleate}}$	β_{EPA}	β_{DHA}	$\beta_{Acetoacetate}$	$\beta_{Lactate}$	v_{O_2}	v_s	v_{GL}	v_{GS}	C_{i+}
0.9000	0.0500	0.0000	0.0000	0.0167	0.0167	0.0167	0.0000	0.0000	6.9154	4.8859	0.0000	0.4027	0.8438
0.2500	0.0000	0.0000	0.0000	0.2083	0.0000	0.0417	0.0000	0.5000	4.0502	0.4093	0.1450	0.0000	0.8000
0.4500	0.0417	0.0000	0.0000	0.0417	0.0000	0.1667	0.3000	0.0000	11.4761	2.0466	0.0000	0.0000	0.7500
0.2500	0.0250	0.0000	0.0500	0.0250	0.0250	0.0250	0.5500	0.0500	14.9112	3.2573	0.0000	0.0690	0.7000
0.0000	0.0250	0.0000	0.0250	0.0250	0.0000	0.0750	0.1000	0.7500	17.3465	3.4111	0.0098	0.0000	0.6500
0.2500	0.0167	0.0167	0.0000	0.0167	0.0167	0.0333	0.6500	0.0000	20.2825	4.8859	0.0000	0.1150	0.6000
0.0500	0.0000	0.0333	0.0000	0.0167	0.0333	0.0167	0.4500	0.4000	22.5428	4.8859	0.0000	0.0103	0.5500
0.1500	0.0000	0.2250	0.0750	0.0750	0.0000	0.0750	0.1500	0.2500	25.2571	10.2332	0.0000	0.4532	0.5000
0.4000	0.0000	0.0167	0.0000	0.0083	0.0083	0.0167	0.3500	0.2000	27.6323	9.7718	0.0000	0.3434	0.4500
0.3000	0.0000	0.0000	0.0083	0.0083	0.0000	0.0333	0.0500	0.6000	29.8822	10.2332	0.0000	0.2629	0.4000
0.2500	0.0167	0.0083	0.0000	0.0083	0.0000	0.0167	0.3000	0.4000	32.3227	10.2332	0.0000	0.2266	0.3500
0.2500	0.0083	0.0083	0.0000	0.0083	0.0000	0.0250	0.5000	0.2000	34.8810	10.2332	0.0000	0.2266	0.3000
0.2000	0.0000	0.0250	0.0000	0.0083	0.0083	0.0083	0.7500	0.0000	37.2907	9.7718	0.0000	0.1757	0.2500
0.0000	0.0000	0.0083	0.0083	0.0083	0.0083	0.0167	0.3000	0.6500	38.8292	9.7718	0.2160	0.0000	0.2000
0.0000	0.0083	0.0083	0.0083	0.0083	0.0000	0.0167	0.4000	0.5500	41.2341	10.2332	0.2160	0.0000	0.1500
0.0000	0.0167	0.0000	0.0000	0.0083	0.0167	0.0083	0.9500	0.0000	44.3334	9.7718	0.0000	0.0029	0.1000
0.0000	0.0000	0.0083	0.0000	0.0083	0.0000	0.0333	0.9000	0.0500	47.5569	10.2332	0.0120	0.0000	0.0500
0.0000	0.0083	0.0000	0.0000	0.0083	0.0000	0.0333	0.9500	0.0000	47.9063	10.2332	0.2160	0.0000	0.0100

Results are ranked by the calculated efficiency C_{i+} in descending order and given for maximal and minimal calculated efficiency values. Further results are shown for each efficiency value of 0.3, 0.35, 0.4, 0.45, 0.5, 0.55, 0.6 and 0.65. Rates for oxygen requirement (v_{O_2}), total substrate uptake rates (v_s), glycogenolysis (v_{GL}) and glycogen synthesis (v_{GS}) are given in mmol $\cdot$ $min^{-1}\cdot$ (l cell)$^{-1}$. For a complete overview of all results, please see Additional file 10. GL indicates glycogenolysis; GS, glycogen synthesis; EPA, eicosapentaenoate; and DHA, docosahexaenoate

5 Discussion

This thesis aimed to present a comprehensive reconstruction of the human cardiomyocyte that accomplish a large set of metabolic and physiological functions to study cardiac metabolism. A basic approach has been developed to simulate a varying substrate supply and to analyse cardiac efficiency under nutritional stress. Calculated flux distributions are in compliance with an experimental study of the isolated working heart. Finally, optimal substrate compositions have been proposed for the cardiomyocyte to meet important cellular functions and maintain cardiac performance.

Metabolic network reconstruction

The reconstructed metabolic network of the human cardiomyocyte is based on previous human network reconstructions [6, 8, 96] by integrating gene expression data and available experimental evidence of metabolic reactions reported for cardiomyocytes. Using linear optimisation approaches, the ability of the network has been ensured to achieve a wide range of metabolic target reactions required for maintaining the structural and functional integrity of the cell [77, 108]. The consistency and functionality of CardioNet is a clear advantage compared to a previous automated reconstructed genome-scale network of the human heart [147], which lacks functionality.

CardioNet allows for an additional 228 mitochondrial reactions compared to two mitochondrial networks of the human cardiomyocyte reported previously [61, 146]. The metabolism of 26 distinct fatty acids is included to a greater extent, taking into consideration of variable acyl-chain composition of important phospholipids such as cardiolipin, phosphatidylserine and phosphatidylcholine.

The present reconstruction can serve as a reliable basis for the integration and analysis of different types of data to study important metabolic processes of the human cardiomyocyte. The estimation of flux rates from tracer kinetic data [157, 158] or prediction of flux changes inferred from changes in gene expression level

of metabolic enzymes [159] under pathological conditions are only a few examples of possible applications.

Optimisation-based concept of cardiac efficiency in varied substrate availability

Under normal physiological conditions, cardiomyocytes metabolise a wide range of substrates including fatty acids, glucose, lactate, pyruvate, ketone bodies and amino acids to meet the ATP demand for muscle contraction and further cellular mechanisms [31]. The rate of substrate utilisation is dependent on (i) substrate availability, (ii) requirement of ATP production for maintenance of cardiac contraction, (iii) oxygen supply and (iv) hormonal level of various hormones directly influencing substrate uptake, e.g. insulin and glucagon. By examining how variations in the relative proportions of glucose, fatty acids, lactate and ketone bodies may affect cardiac efficiency interesting results emerged.

Linear optimisation problems were defined with the objective to minimize the total substrate and oxygen demand, while the substrate availability was constrained and a metabolic target function of the cardiomyocyte was demanded. By calculating a Euclidean based-distance measure (C_{i^+}), optimal substrate combinations were identified based on the criteria: (i) oxygen demand, (ii) total substrate uptake rate and (iii) rate of endogenous glucose derived from glycogenolysis. On the basis of C_{i^+}, predominant oxidation of fatty acids (79%) supplemented by glucose (21%) were most effective in maintaining the required ATP production.

Additionally, in sole oleate utilisation, total substrate requirement and oxygen consumption were more favourable compared to sole utilisation of glucose, lactate and acetoacetate. By contrast, predominant utilisation of lactate and acetoacetate were least efficient in maintaing ATP production. These findings are supported by previous studies [82, 160] documenting reduced cardiac performance in a predominately supply of ketone bodies. In diabetic conditions with increased concentration of ketone bodies, cardiac activity improved with additional fatty acid supply, indicating the inadequacy of ketone bodies to efficiently maintain ATP production.

To further validate the theoretical observations, substrate proportions were simulated as presented in a previous study of the isolated working rat heart [82] and compared to calculated efficiency measures derived from experimental measurements. Applied substrates were ranked equally according to the

calculated efficiency C_{i^+} based on experimental and simulated data. During the experiment, cardiac performance declined in a sole ketogenic environment (acetoacetate, (R)-3-hydroxybutanoate), while a mixture of glucose and acetoacetate seemed to reverse this effect.

Similar efficiency measures were calculated for ketone body utilisation during simulations and with experimental values, supporting these previous findings. In addition, acetate showed the worst relation of oxygen demand to total substrate requirement in meeting the metabolic target, both in results from simulations and experimental measurements. Nonetheless, no decline in cardiac performance during the actual experiment has been reported. By contrast, lactate was less efficient in the experimental setting.

Differences between calculated and experimentally determined flux rates may be caused by the constraints applied, in particular by the simplified metabolic target function, possibly observational error in the experiment and substrate interactions, which cannot be considered by FBA simulations.

Determination of cardiac efficiency while demanding an extended metabolic target function

The simplified target function was extended by demanding the formation not only of ATP and of NADPH, but also of important membrane lipids: ceramide, cardiolipin, phosphatidylcholine, phosphatidylethanolamine and sphingomyelin. The fraction of fatty acids in the set of importable substrates was enlarged to include this broader set of lipids in the simulations. These modifications involved the consideration of saturated (palmitate, stearate), monounsaturated (oleate), long chain poly-unsaturated omega-6 (α-linoleate) and omega-3 (eicosapentaenoic acid, docosahexanoic acid) fatty acids.

Although long chain poly-unsaturated fatty acids (PUFA) predominately serve as membrane lipids [36, 39, 40], there is evidence for occurrence of Acyl-CoA dehydrogenase 9 (ACAD-9) in human cardiomyocytes [161]. ACAD-9 catalyses the initial step of mitochondrial fatty acid β-oxidation. Moreover, a previous study showed enzymatic activity for ACAD-9 with long-chain unsaturated acyl-CoA as substrate (e.g.:C22:6-CoA) [162]. This is in concordance with another study [163] measuring rates of fatty acid β-oxidation for palmitate and docosahexaenoate. Hence, it is reasonable to consider fatty acid -oxidation of PUFA for a systematic analysis of substrate utilisation in cardiomyocytes.

A physiological simulation of cardiomyocyte metabolism was ensured by demanding flux rates as reported in previous experimental studies of membrane lipids [83, 153] and integrating the fatty acid composition of phospholipids as reported by investigations in human heart tissue [151, 152]. Further, another important aspect of cardiac metabolism is defence mechanisms against hypoxia, which is mostly effected by NADPH to maintain reduced glutathione.

To include this process, an additional computation was performed to determine the basal NADPH formation rate by the G6PDH, the rate limiting enzyme of oxidative pentose phosphate pathway, in the case of unrestricted substrate supply. This estimated basal rate of NADPH production (1.42e-05 mmol $\cdot$ min$^{-1}\cdot$ (l cell)$^{-1}$) was applied as minimal requirement to maintain cellular protection against reactive oxygen species (ROS).

Additionally, cardiac short-term storage of energy, in particular glycogen was considered, which could act as a potential precursor of sn-glycerol, a known intermediate for phospholipid biosynthesis and ATP production. The synthesis of glycogen was not restricted while the glycogen degradation was limited to a maximal rate as has been determined in previous investigations [154].

Glycogen turnover and contribution of substrates to ATP formation

As shown in the present study, glycogen synthesis and glycogenolysis occurred simultaneously throughout the simulations, which is consistent with previous studies [154, 156] documenting the same pattern. In case the available glucose was not needed to fulfil the metabolic target function, glycogen was synthesized with a maximal rate of 0.887 mmol $\cdot$ min$^{-1}\cdot$ (l cell)$^{-1}$.

The vast majority of glucose utilised during simulations derived from exogenous uptake, indicating that endogenous glycogenolysis was only utilised in a decreased glucose supply. Both external and endogenous glucose substantially contributed to ATP production by oxidative phosphorylation. Previously, Henning et. al. [156] demonstrated that glycogen accounted for 41% of synthesized ATP in predominately glucose oxidation.

In agreement with these experimental findings, computations show a glycogen contribution to ATP synthesis from glucose oxidation, which is dependent on an exogenous glucose supply. In case glucose accounts for 50% of the total substrate uptake rate, 34.41% of the ATP production from oxidative phosphorylation is

related to glycogen. Consequently, this contribution increased to 80.16% in case of decreased glucose supply (25% of the total substrate uptake rate).

To ensure unique solutions for calculated flux rates, additional simulations were performed. Depending on the complexity of the target function, up to 90.70% fluxes with unique solutions were found, which included fluxes representing glycogenolysis and external substrate and oxygen uptake for every tested substrate combination. None of the identified alternate flux solutions showed significant difference from the original. Hence the efficiency analysis of substrate combinations is not compromised by this small variability.

Implications for substrate utilisation to improve cardiac efficiency

This is the first study examining the efficiency of a large set of substrates using simulations. Computations showed that a balanced utilisation of different substrate classes (fatty acids, carbohydrates) is associated with higher cardiac efficiency compared to sole utilisation of single substrates.

Here, predominant utilisation of fatty acids ($\beta_{\bar{m}}$= 0.311), especially long-chain unsaturated fatty acids, supplemented by glucose ($\beta_{\bar{m}}$= 0.231), acetoacetate ($\beta_{\bar{m}}$= 0.221) and lactate ($\beta_{\bar{m}}$= 0.237) was more favourable. Moreover, utilisation of predominantly saturated and C18 polyunsaturated fatty acids yielded higher efficiency C_{i^+} than a greater share of long-chain omega-3 poly-unsaturated fatty acids.

This is supported by a recent study [164] of isolated muscle fibers from diabetic hearts, where an increase of mitochondrial uncoupling was measured during exposure to fatty acid. The induced ROS production in cardiomyocyte mitochondria led to an activation of multiple adaptive mechanisms by which oxidative damage can be prevented. The ambivalent role of long-chain omega-3 poly-unsaturated fatty acids is supported by findings from other studies [39, 40] that showed beneficial metabolic effects in myocardial protection against oxidative damage by incorporation of long-chain omega-3 poly-unsaturated fatty acids into mitochondrial membrane phospholipids such as cardiolipin.

The presented results indicate that a switch from fatty acid utilisation to predominant glucose utilisation in situations with increased workload would not decrease the efficiency of cardiac metabolism. This is emphasised by a high efficiency (C_{i^+}= 0.8438) for a combination of 90% glucose, 5% palmitate,

1.67% α-linoleate, 1.67% eicosapentaenoate and 1.67% docosahexaenoate.

Further, computations revealed that polyunsaturated fatty acids contributed mostly to ATP production via β-oxidation, while the vast majority of palmitate, stearate and oleate were used for phospholipid biosynthesis. In fact, up to 99.1% of utilised docosahexaenoate and 98.82% of utilised eicosapentaenoate contributed towards ATP production, respectively. In addition, α-linoleate was not degraded through β-oxidation, but served as substrate in the biosynthesis of phospholipid.

By contrast, predominant utilisation of acetoacetate was least efficient in computations applying the extended metabolic target function. Here, the oxygen demand and mitochondrial oxygen consumption were greater than with any other substrate combination, thus, possibly increasing the flux through complex I of the mitochondrial oxidative phosphorylation, which is considered a main source of cellular ROS.

These observations suggest that under metabolic conditions with increased acetoacetate levels, e.g. diabetes, cardiac contractility is affected by decreased ATP formation and increased ROS formation, which is linked to mitochondrial dysfunction [165, 166]. Nonetheless, it is beyond the scope of this study to further analyse these mechanisms, but the presented network reconstruction might contribute towards further investigation by incorporation of gene expression level information of metabolic enzymes mediated by PPAR-α.

6 Conclusions

The motivation for this thesis was to develop a comprehensive reconstruction of the human cardiomyocyte. This model can be used to enable studies of cardiac metabolism under normal and pathological conditions, thereby enabling hypothesis-driven experimental studies. The present study benefits from previous large-scale network reconstructions in humans [6, 8], which provided the methodological basis and strategies. It was aimed to integrate all cellular processes involved in anabolic and catabolic reactions in cardiomyocytes. However, since the mechanism of the entire transcriptional and translational process in cellular systems is still not known to enable a full stoichiometric representation, none of these processes were included. Nonetheless, it is intended to expand the network reconstruction by adding further cellular functions such as signalling pathways, DNA transcription and translation and its regulation in the future.

The comparison of CardioNet to existing mitochondrial networks of the cardiomyocyte illustrated the need to reconstruct reactions which are only present during heart failure or myocardial hypertrophy in order to enable simulations of these pathological conditions. It is expected that sufficient information of components and biological reactions will become available through experimental studies, such as proteome or gene expression studies in animal models and from human heart tissues. Therefore, further extensions of the network can be obtained and integration with other cellular process should be possible.

The presented approach enables to evaluate cardiac efficiency and to identify optimal substrate compositions to ensure a supply of energy-rich phosphates and cellular integrity. Proteomic data and experimentally determined flux rates will presumably improve estimations for different cellular conditions. Together with an extended metabolic network for cardiomyocyte under heart failure and myocardial hypertrophy, these estimations could make an important contribution to unveiling unanswered questions of cardiac metabolism.

In summary, this study provides a comprehensive reconstruction of the metabolic network of the human cardiomyocyte (CardioNet) to study metabolic and

physiological functions of the cardiomyocyte. The evaluation of metabolic efficiency in substrate supply and utilisation necessitates consideration of oxygen and substrate demand and of endogenous glucose deriving from glycogenolysis. In aerobic conditions predominant utilisation of saturated and long-chain unsaturated fatty acids supplemented by glucose proved to be more favourable for efficient cardiac metabolism than utilisation of acetoacetate or lactate. In conclusion, CardioNet can serve as a reliable basis to study cardiomyocyte metabolism.

References

1. Cardiovascular diseases (CVDs) - WHO Factsheet. 2002. (Accessed April 11, 2011, http://www.who.int/mediacentre/factsheets/fs317en/).
2. Torabi A, Cleland J, Khan N, et al. The timing of development and subsequent clinical course of heart failure after a myocardial infarction. Eur Heart J 2008;29:859–70.
3. Armstrong A, Binkley P, Baker P, Myerkowitz P, and Leier C. Quantitative investigation of cardiomyocyte hypertrophy and myocardial fibrosis over 6 years after cardiac transplantation. J Am Coll Cardiol 1998;32:704–10.
4. Levkau B, Schäfers M, Wohlschlaeger J, et al. Survivin determines cardiac function by controlling total cardiomyocyte number. Circulation 2008;117:1583–93.
5. Huthmacher C, Hoppe A, and Holzhütter H. Antimalarial drug targets in Plasmodium falciparum predicted by stage-specific metabolic network analysis. BMC Syst Biol 2010;4:120.
6. Gille C, Bölling C, Hoppe A, et al. HepatoNet1: a comprehensive metabolic reconstruction of the human hepatocyte for the analysis of liver physiology. Mol Syst Biol 2010;6:1–13.
7. Mardinoglu A, Agren R, Kampf C, et al. Integration of clinical data with a genome-scale metabolic model of the human adipocyte. Mol Syst Biol 2013;9:649.
8. Duarte C, Becker S, Jamshidi N, et al. Global reconstruction of the human metabolic network based on genomic and bibliomic data. Proc Natl Acad Sci USA 2007;104:1777–82.
9. Mo M, Palsson B, and Herrgård M. Connecting extracellular metabolomic measurements to intracellular flux states in yeast. BMC Syst Biol 2009;3:37.

10. Feist A, Henry C, Reed J, et al. A genome-scale metabolic reconstruction for Escherichia coli K-12 MG1655 that accounts for 1260 ORFs and thermodynamic information. Mol Syst Biol 2007;3:121.

11. Shlomi T, Cabili M, Herrgård M, Palsson B, and Ruppin E. Network-based prediction of human tissue-specific metabolism. Nat Biotechnol 2008;26:1003–10.

12. Vilijoen K and Blackburn J. Quality assessment and data handling methods for Affymetrix Gene 1.0 ST arrays with variable RNA integrity. BMC Genomics 2013;14:14.

13. Johnson W and Li C. Adjusting batch effect in microarray expression data using empirical Bayes methods. Biostatistics 2007;8:118–27.

14. Becker S, Feist A, Mo M, Hannum G, Palsson B, and Herrgård M. Quantitative prediction of cellular metabolism with constraint-based models: the COBRA Toolbox. Nat Protoc 2007;2:727–38.

15. Thiele I and Palsson B. A protocol for generating a high-quality genome-scale metabolic reconstruction. Nat Protoc 2010;5:93–121.

16. Hoppe A, Hoffmann S, Gerasch A, and Holzhütter H. FASIMU: flexible software for flux-balance computation series in large metabolic networks. BMC Bioinformatics 2011;12:28.

17. Scheer M, Grote A, Chang A, et al. BRENDA, the enzyme information system in 2011. Nucl Acids Res 2011;39:670–6.

18. Kanehisa M and Goto S. KEGG: Kyoto Encyclopedia of Genes and Genomes. Nucl Acids Res 2000;28:27–30.

19. Saier M, Tran C, and Barabote R. TCDB: the Transporter Classification Database for membrane transport protein analyses and information. Nucl Acids Res 2006;34:D181–6.

20. Fahy E, Subramaniam S, Murphy R, et al. Update of the LIPID MAPS comprehensive classification system for lipids. J Lipid Res 2009;50:S9–S14.

21. Wishart D, Knox C, Guo A, et al. HMDB: a knowledgebase for the human metabolome. Nucl Acids Res 2009;37:D603–10.

22. Wittig U, Kania R, Golebiewski M, et al. SABIO-RK - database for biochemical reaction kinetics. Nucl Acids Res 2012;40:D790–6.

23. Wheeler D, Church D, Federhen S, et al. Database resources of the National Center for Biotechnology. Nucl Acids Res 2003;31:28–33.

24. Consortium TU. Ongoing and future developments at the Universal Protein Resource. Nucl Acids Res 2011;39:D214–9.

25. Hubbard T, Aken B, Ayling S, et al. Ensembl 2009. Nucl Acids Res 2009;37:D690–7.

26. Edgar R, Domrachev M, and Lash A. Gene Expression Omnibus: NCBI gene expression and hybridization array data repository. Nucl Acids Res 2002;30:207–10.

27. Hermann G and Decherd G. The chemical nature of heart failure. Ann Intern Med 1939;12:1233–44.

28. Neubauer S. The failing heart - an engine out of fuel. N Engl J Med 2007;356:1140–51.

29. Ingelsson E, Sundstrom J, Arnlov J, Zethelius B, and Lind L. Insulin resistance and risk of congestive heart failure. JAMA 2005;294:334–41.

30. Swan J, Anker S, Walton C, et al. Insulin resistance in chronic heart failure: relation to severity and etiology of heart failure. J Am Coll Cardiol 1997;30:527–32.

31. Neely J and Morgan H. Relationship between carbohydrate and lipid metabolism and the energy balance of heart muscle. Annu Rev Physiol 1974;36:413–59.

32. Doenst T, Goodwin G, Cedars A, Wang M, Stepkowski S, and Taegtmeyer H. Load-induced changes in vivo alter substrate fluxes and insulin responsiveness of rat heart in vitro. Metabolism 2001;50:1083–90.

33. Foryst-Ludwig A, Kreissl M, Sprang C, et al. Sex differences in physiological cardiac hypertrophy are associated with exercise-mediated changes in energy substrate availability. Am J Physiol Heart Circ Physiol 2011;301:H115–22.

34. Goodwin G, Taylor C, and Taegtmeyer H. Regulation of energy metabolism of the heart during acute increase in heart work. J Biol Chem 1998;273:29530–9.

35. Korvals C, Elvenes O, and Myrmel T. Myocardial substrate metabolism influences left ventricular energetics in vivo. Am J Physiol Heart Circ Physiol 2000;278:H1345–51.

36. Jezkova J, Novakova O, Kolar F, Tvrzicka E, Neckar J, and Novak F. Chronic hypoxia alters fatty acid composition of phospholipids in right ventricular mycoardium. Mol Cell Biochem 2002;232:49–56.

37. Pepe S and McLennan P. Cardiac membrane fatty acid composition modulates myocardial oxygen consumption and postischemic recovery of contractile function. Circulation 2002;105:2303–8.

38. Bordoni A, Lopez-Jimenez J, Spano C, Biagi P, Horrobin D, and Hrelia D. Metabolism of linoleic and alpha-linolenic acids in cultured cardiomyocytes:effect of different N-6 and N-3 fatty acid supplementation. Mol Cell Biochem 1996;157:217–22.

39. Siscovick D, Raghunathan T, King I, et al. Dietary intake and cell membrane levels of long-chain n-3 polyunsaturated fatty acids and the risk of primary cardiac arrest. JAMA 1995;274:1363–7.

40. Bei R, Frigiola A, Masuelli L, et al. Effects of omega-3-polyunsaturated fatty acids on cardiac myocyte protection. Front Biosci 2011;16:1833–43.

41. Razeghi P, Yound M, Alcorn J, Moravec C, Frazier O, and Taegtmeyer H. Metabolic gene expression in fetal and failing human heart. Circulation 2001;104:2923–31.

42. Cook G, Edwards T, Jansen M, Bahouth S, Wilcox H, and Park E. Differential regulation of carnitine palmitoyltransferase-I gene isoforms (CPT-I alpha and CPT-I beta) in the rat heart. J Mol Cell Cardiol 2001;33:317–29.

43. Lopaschuk G, Collins-Nakai R, and Itoi T. Developmental changes in energy substrate use by the heart. Cardiovasc Res 1992;26:1172–80.

44. Depre C, Shipley G, and Chen W. Unloaded heart in vivo replicates fetal gene expression of cardiac hypertrophy. Nat Med 1998;4:1269–75.

45. Fisher D, Heymann M, and Rudolph A. Myocardial consumption of oxygen and carbohydrate consumption in newborn sheep. Pediatr Res 1981;15:843–6.

46. Knaapen M, Vrolijk B, and Wenink A. Ultrastructural changes of the myocardium in the embryonic rat heart. Anat Rec 1997;248:233–41.

47. Pederson B, Chen H, Schroeder J, Shou W, DePaoli-Roach A, and Roach P. Abnormal cardiac development in the absence of heart glycogen. Mol Cell Biol 2004;24:7179–87.

48. Osorio J, Stanley W, Linke A, et al. Impaired myocardial fatty acid oxidation and reduced protein expression of retinoid X receptor-alpha in pacing-induced heart failureK. Circulation 2002;106:606–12.

49. Paolisso G, Gambardella A, Galzerano D, et al. Total-body and myocardial substrate oxidation in congestive heart failure. Metabolism 1994;43:174–9.

50. Liao R, Nascimben L, Friedrich J, Gwathmey J, and Ingwall J. Decreased energy reserve in an animal model of dilated cardiomyopathy. Circulation Research 1996;78:893–902.

51. Taylor M, Wallhaus T, and Degrado TR ea. An evaluation of myocardial fatty acid and glucose uptake using PET with [18F]fluoro-6-thia-heptadecanoic acid and [18F]FDG in patients with congestive heart failure. J Nucl Med 2001;42:55–62.

52. Park S, Cho Y, Finck B, Kim H, Higashimori T, and Hong Eea. Cardiac-specific overexpression of peroxisome proliferator-activated receptor-alpha causes insulin resistance in heart and liver. Diabetes 2005;54:2514–24.

53. Bird M and Saggerson E. Binding of malonyl-CoA to isolated mitochondria. Biochem J 1984;222:639–47.

54. Young M, Goodwin G, Ying J, et al. Regulation of cardiac and skeletal muscle malonyl-CoA decarboxylase by fatty acids. Am J Physiol Endocrinol Metab 2001;280:E471–9.

55. Chandler M, Stanley W, Morita H, et al. Short-term treatment with ranolazine improves mechanical efficiency in dogs with chronic heart failure. Circ Res 2002;91:278–80.

56. Augustus A, Buchanan J, Park T, et al. Loss of lipoprotein lipase-derived fatty acids leads to increased cardiac glucose metabolism and heart dysfunction. J Biol Chem 2006;281:8716–23.

57. Niu Y, Hauton D, and Evans R. Utilization of triacylglycerol-rich lipoproteins by the working rat heart: routes of uptake and metabolic fates. J Physiol 2004;558:225–37.

58. Zabkar J, Mozina M, Bratko I, and Demsar J. Learning qualitative models from numerical data. Artificial Intelligence 2011;175:1604–19.

59. Qian H and Elson E. Single-molecule enzymology: stochastic Michaelis-Menten kinetics. Biophys Chem 2002;101:565–76.

60. Brännströ A and Sumpter D. The role of competition and clustering in population dynamics. Proc R Soc 2005;272:2065–72.

61. Vo T, Greenberg H, and Palsson B. Reconstruction and Functional Characterization of the Human Mitochondrial Metabolic Network Based on Proteomic and Biochemical Data. J Biol Chem 2004;279:39532–40.

62. Giacomantomio C and Goodhill G. A boolean model of the gene regulatory network underlying mammalian cortical area development. PLoS Comput Biol 2010;6:e1000936.

63. Mendoza L and Zenarios L. A menthod for generation of standaridzed qualitative dynamic systems of regulatory networks. Theor Biol Med Model 2006;3:13.

64. Li F, Long T, Lu Y, Ouyang Q, and Tang C. The yeast-cell cylce network is robustley designed. Proc Natl Acad Sci USA 2004;101:4781–86.

65. Rapoport T, Heinrich R, and Rapopoprt S. The regulatory principles of glycolysis in erythrocytes in vivo and in vitro. Biochem J 1976;154:449–69.

66. Wolf J and Heinrich R. Effect of cellular interaction on glycolytic oscillations in yeast: a theoretical investigation. Biochem J 2000;345:321–34.

67. König M and Holzhütter H. Kinetic modeling of human hepatic glucose metabolism in T2DM predicts higher risk of hypoglycemic events in rigorous insulin therapy. J Biol Chem 2012;287:36978–89.

68. Kiebel S, Garrido M, and Friston K. Dynamic causal modelling of evoked responses: The role of intrinsic connections. Neuroimage 2007;36:332–45.

69. Hopfield J. Neural networks and physical systems with emergent collective computational properties. Proc Natl Acad Sci USA 1982;79:2554–8.

70. Vossel S, Mathys C, Daunizeau J, et al. Spatial attention, precision and bayesian inference: a study of saccadic response speed. Cerebral Cortex 2013;1:1–15.

71. Campo P, Garrido M, Moran R, et al. Remote effects of hippocampal sclerosis on effective connectivity during working memory encoding: a case of connectional diaschisis? Cerebral Cortex 2012;22:1225–36.

72. Friston K. The free-energy principle: a rough guide to the brain? Trends Cogn Sci 1995;13:293–301.

73. Dayan P, Hinton G, Neal R, and Zemel R. The Helmholtz machine. Nat Rev Neurosci 1995;7:889–904.

74. Guldberg C and Waage P. Über die chemische Affinität. Journal für Praktische Chemie 1879;19:69.

75. Michaelis L and Menten M. Über die chemische Affinität. Biochemische Zeitschrift 1913;49:333–69.

76. Johnson K and Goody R. The original michaelis constant: translation of the 1913 michaelis-menten paper. Biochemistry 2011;50:8264–9.

77. Holzhütter H. The principle of flux minimization and its application to estimate stationary fluxes in metabolic networks. Eur J Biochem 2004;271:2905–22.

78. Barrett T, Troup D, Wilhite S, et al. NCBI GEO: archive for functional genomics data sets - 10 years on. Nucl Acids Res 2011;39:D1005–10.

79. Su A, Cooke M, Ching K, et al. Large-scale analysis of the human and mouse transcriptomes. Proc Natl Acad Sci USA 2002;99:4465–70.

80. Wu C, Orozco C, Boyer J, et al. BioGPS: an extensible and customizable portal for querying and organizing gene annotation resources. Genome Biol 2009;10:R130.

81. Genomics of Cardiovascular Development, Adaptation, and Remodeling. 2013. (Accessed July 1, 2013, `http://www.cardiogenomics.org`).

82. Taegtmeyer H, Hems R, and Krebs H. Utilization of energy-providing substrates in the isolated working rat heart. Biochem J 1980;186:701–11.

83. Hatch G. Cardiolipin biosynthesis in the isolated heart. Biochem Journal 1994;297:201– 8.

84. Dobrzyn P, Dobrzyn A, Miyazaki M, and Ntambi J. Loss of stearoyl-CoA desaturase 1 rescues cardiac function in obese leptin-deficient mice. J Lipid Res 2010;51:2202–10.

85. Goodwin G, Arteaga J, and Taegtmeyer H. Glycogen turnover in the isolated working rat heart. J Biol Chem 1995;270:9234–40.

86. Wu F, Zhang E, Zhang J, Bache R, and Beard D. Phosphate metabolite concentrations and ATP hydrolysis potential in normal and ischaemic hearts. J Physiol 2008;586.17:4193–208.

87. Maglott D, Ostell J, Priutt K, and Tatusova T. Entrez Gene: gene-centered information at NCBI. Nucl Acids Res 2011;39:D52–7.

88. Kasprzyk A. BioMart: driving a paradigm change in biological data management. Database 2011;2011:1–3.

89. Vastrik I, D'Eustachio P, Schmidt E, et al. Reactome: a knowledge base of biologic pathways and processes. Genome Biol 2007;28:R39.

90. Caspi R, Altman T, Dreher K, et al. The MetaCyc database of metabolic pathways and enzymes and the BioCyc collection of pathway/genome databases. Nucl Acids Res 2012;40:D742–53.

91. Bolton E, Wang Y, Thiessen P, and Bryant S. PubChem: Integrated Platform of Small Molecules and Biological Activities. In: Annual Reports in Computational Chemistry, American Chemical Society, Washington, DC, 2008. Chap. 12:1–27.

92. Ren Q, Chen K, and Paulsen I. TransportDB: a comprehensive database resource for cytoplasmic membrane transport systems and outer membrane channels. Nucl Acids Res 2007;35:D274–9.

93. Gille C, Hoffmann S, and Holzhütter H. METANNOGEN: compiling features of biochemical reactions needed for the reconstruction of metabolic networks. BMC Syst Biol 2007;1:1–5.

94. Romero P, Wagg J, Green M, Kaiser D, Krummenacker M, and Karp P. Computational prediction of human metabolic pathways from the complete human genome. Genome Biol 2004;6:1–17.

95. Martens L, Hermjakob H, Jones P, et al. PRIDE: the proteomics identifications database. Proteomics 2005;5:3537–45.

96. Ma H, Sorokin A, Mazein A, et al. The Edinburgh human metabolic network reconstruction and its functional analysis. Mol Syst Biol 2007;3:135.

97. Forsythe RJ, Karp P, and Mavrovouniotis M. Estimation of equilibrium constants using automated group contribution methods. Comput Appl Biosci 1997;13:537–43.

98. Jankowski M, Henry C, Broadbelt L, and Hatzimanikatis V. Group contribution method for thermodynamic analysis of complex metabolic networks. Biophys J 2008;95:1487–99.

99. Cplex-Optimizer. 2012. (Accessed December 12, 2012, `http://www-01.ibm.com/software/integration/optimization/cplex-optimizer/`).

100. Inc. LS. LINDO API 5.0 - The Premier Optimization Engine. LINDO Systems Inc., 2007.

101. Becker S, Feist A, Hannum G, Palsson B, and Herrgard M. Quantitative prediction of cellular metabolism with constraint-based models: the COBRA Toolbox. Nat Protoc 2007;2:727–38.

102. Klamt S, Saez-Rodriguez J, and Gilles E. Structural and functional analysis of cellular networks with CellNetAnalyzer. BMC Syst Biol 2007;1:2.

103. Phalakornkule C, Lee S, Zhu T, et al. A MILP-based flux alternative generation and NMR experimental design strategy for metabolic engineering. Metab Eng 2001;3:124–37.

104. Lee S, Phalakornkule C, Domach M, and Grossmann I. Recursive MILP model for finding all the alternate optima in LP models for metabolic networks. Comput Chem Eng 2000;24:711–6.

105. Mahadevan R and Schilling C. The effects of alternate optimal solutions in constraint-based genome-scale metabolic models. Metab Eng 2003;5:264–76.

106. Gudmundsson S and Thiele I. Computationally efficient flux variability analysis. BMC Bioinformatics 2010;11:489.

107. Burgard A, Nikolaev E, Schilling C, and Maranas C. Flux coupling analysis of genome-scale metabolic network reconstructions. Genome Res 2004;14:301–12.

108. Hoffmann S, Hoppe A, and Holzhütter H. Prunnig genome-scale metabolic models to consistent ad functionem networks. Genome Inform 2007;18:308–19.

109. Galeva N and Altermann M. Comparison of one-dimensional and two-dimensional gel electrophoresis as a separation tool for proteomic analysis of rat liver microsomes: cytochromes P450 and other membrane proteins. Proteomics 2002;2:713–22.

110. Galeva N, Yakovlev D, Koen Y, Duzhak T, and Altermann M. Direct identification of cytochrome P450 isozymes by matrix-assisted laser desorption/ionization time of flight-based proteomic approach. Drug Metab Dispos 2003;31:351–5.

111. Nascimben L, Ingwall J, Lorell B, et al. Mechanisms for increased glycolysis in the hypertophied rat heart. Hypertension 2004;44:662–7.

112. Depre C, Rider M, and Hue L. Mechanisms of control of heart glycolysis. Eur J Biochem 1998;258:277–90.

113. Stankiewics-Choroszucha B and Gorski J. Effect of substrate supply and beta-adrenergic blockage on heart glycogen and triglyceride utilization during exercise in the rat. Eur J Appl Physiol 1980;43:11–17.

114. Bublitz C and Steavenson S. The pentose phosphate pathway in the endoplasmic reticulum. J Biol Chem 1988;26:12849–53.

115. Severin S and Stepanova N. Interrelationship between glycolysis and the anaerobic part of the pentose phosphate pathway of carbohydrate metabolism in the myocardium. Adv Enzyme Regul 1980;19:235–55.

116. Puisac B, Arnedo M, Casale C, et al. Differential HMG-CoA lyase expression in human tissues provides clues about 3-hydroxy-3-methylglutaric aciduria. J Inherit Metab Dis 2010;33:405–10.

117. Avogaro A, Nosadini R, Doria A, et al. Myocardial metabolism in insulin-deficient diabetic humans without coronary artery disease. Am J Physiol Endocrinol Metab 1990;258:E606–18.

118. Hasin Y, Shimoni Y, Stein O, and Stein Y. Effect of cholesterol depletion on the electrical activity of rat heart myocytes in culture. J Mol Cell Cardiol 1980;12:675–83.

119. Venter H, Genade S, Mouton R, Huisamen B, Harper I, and A L. Myocardial membrane cholesterol: effects of ischaemia. J Mol Cell Cardiol 1991;11:1271–86.

120. Khairallah R, Sparagna G, Khanna N, et al. Dietary supplementation with docosahexaenoic acid, but not eicosapentaenoic acid, dramatically alters cardiac mitochondrial phospholipid fatty acid composition and prevents permeability transition. Biochim Biophys Acta 2010;1797:1555–62.

121. Miyazaki M, Jacobson M, Man W, et al. Dietary supplementation with docosahexaenoic acid, but not eicosapentaenoic acid, dramatically alters cardiac mitochondrial phospholipid fatty acid composition and prevents permeability transition. Biochim Biophys Acta 2010;1797:1555–62.

122. Goodwin G and Taegtmeyer H. Regulation of fatty acid oxidation of the heart by MCD and ACC during contractile stimulation. Am J Physiol 1999;277:E772–7.

123. Awan M and Saggerson E. Malonyl-CoA metabolism in cardiac myocytes and its relevance to the control of fatty acid oxidation. Biochem J 1993;295:61–6.

124. Bester R and Lochner A. Sarcolemmal phospholipid fatty acid composition and permeability. Biochim Biophys Acta 1988;941:176–86.

125. Stam H, Broekhoven-Schokker S, and Hülsmann W. Characterization of mono-, di- and triacylglycerol lipase activities in the isolated rat heart. Biochim Biophys Acta 1986;875:76–86.

126. Ardail D, Privat J, Egret-Charlier M, Levrat C, Lerme F, and Louisot P. Mitochondrial contact sites: lipid composition and dynamics. J Biol Chem 1990;265:18797–802.

127. Hofgaard J, Banach K, Mollerup S, et al. Phosphatidylinositol-bisphosphate regulates intercellular coupling in cardiac myocytes. Eur J Physiology 2008;457:303–13.

128. Portois L, Peltier S, Sener A, Malaisse W, and Carpentier Y. Perturbation of phospholipid and triacylglycerol fatty acid positional location in the heart of rats depleted of n-3 long-chain polyunsaturates. Nutr Res 2008;28:51–7.

129. Turoczi T, Chang V, Engelman R, Maulik N, Ho Y, and Das D. Thioredoxin redox signaling in the ischemic heart: an insight with transgenic mice overexpressing Trx1. J Mol Cell Cardiol 2003;35:695–704.

130. Yamamoto M, Yang G, Hong C, et al. Inhibition of endogenous thioredoxin in the heart increases oxidative stress and cardiac hypertrophy. J Clin Invest 2003;112:1395–1406.

131. Mudge GJ, Mills RJ, Taegtmeyer H, Gorlin R, and Lesch M. Alterations of myocardial amino acid metabolism in chronic ischemic heart disease. J Clin Invest 1976;58:1185–92.

132. Dinkelborg L, Kinne R, and Grieshaber M. Transport and metabolism of L-glutamate during oxygenation, anoxia, and reoxygenation of rat cardiac myocytes. Am J Physiol 1996;270:H1825–32.

133. Hoffmann F, Hashimoto A, Lee B, Rose A, Shohet R, and Hoffmann P. Specific antioxidant selenoproteins are induced in the heart during hypertrophy. Arch Biochem Biophys 2011;512:38–44.

134. Caldarera C, Orlandini G, Casti A, and Moruzzi G. Polyamine and nucleic acid metabolism in myocardial hypertrophy of the overloaded heart. J Mol Cell Cardiol 1974;6:95–103.

135. Tantini B, Fiumana E, Cetrullo S, et al. Downregulation of the ornithine decarboxylase/polyamine system inhibits angiotensin-induced hypertrophy of cardiomyocytes through the NO/cGMP-dependent protein kinase type-I pathway. J Mol Cell Cardiol 2006;40:775–82.

136. Waldmüller S, Erdmann J, Binner P, et al. Novel correlations between the genotype and the phenotype of hypertrophic and dilated cardiomyopathy: results from the German Competence Network Heart Failure. Eur J Heart Fail 2011;13:1185–92.

137. Cheng Y, Li W, McElfresh T, et al. Changes in myofilament proteins, but not calcium regulation, are associated with a high fat diet-induced improvement in contractile function in heart failure. Am J Physiol Heart Circ Physiol 2011;301:H1438–46.

138. Russell R, Bergeron R, Shulman G, and Young L. Translocation of myocardial GLUT-4 and increased glucose uptake through activation of AMPK by AICAR. Am J Physiol 1999;277:H643–9.

139. Fox A, Reed G, Meilman H, and Silk B. Release of nucleosides from canine and human hearts as an index of prior ischemia. Am J Cardiol 1979;43:52–8.

140. Reibel D and Rovetto M. Myocardial adenosine salvage rates and restoration of ATP content following ischemia. Am J Physiol 1979;237:H247–52.

141. Olivetti G, Abbi R, Quaini F, et al. Apoptosis in the failing human heart. N Engl J Med 1997;336:1131–42.

142. Achterberg P, Stroeve R, and De Jong J. Myocardial adenosine cycling rates during normoxia and under conditions of stimulated purine release. Biochem J 1986;235:13–17.

143. Brown A, Raeside D, Bowditch J, and Dow J. Metabolism and salvage of adenine and hypoxanthine by myocytes isolated from mature rat heart. Biochim Biophys Acta 1985;845:469–76.

144. Hatefi Y and Galante Y. Dehydrogenase and transhydrogenase properties of the soluble NADH dehydrogenase of bovine heart mitochondria. Proc Natl Acad Sci USA 1977;74:846–50.

145. Hsu C, Oka S, Shao D, Hariharan N, and Sadoshima J. Nicotinamide phosphoribosyltransferase regulates cell survival through NAD+ synthesis in cardiac myocytes. Circ Res 2009;105:481–91.

146. Smith A and Robinson A. A metabolic model of the mitochondrion and its use in modelling diseases of the tricarboxylic acid cycle. BMC Syst Biol 2011;5:102.

147. Zhao Y and Huang J. Reconstruction and analysis of the human heart-specific metabolic network based on transcriptome and proteome data. Biochem Biophys Res Commun 2011;415:450–4.

148. Vockley J, Jenkinson C, Shukla H, Kern R, Grody W, and Cederbaum S. Cloning and characterization of the human type II arginase gene. Genomics 1996;38:118–23.

149. Heusch P, Aker S, Boengler K, et al. Increased inducible nitric oxide synthase and arginase II expression in heart failure: no net nitrite/ nitrate production and protein S-nitrosylation. Am J Physiol Heart Circ Physiol 2010;299:H446–53.

150. Jerby L, Shlomi T, and Ruppin E. Computational reconstruction of tissue-specific metabolic models: application to human liver metabolism. Mol Syst Biol 2010;6:401.

151. Rocquelin G, Guenot L, and Justrabo E. Fatty acid composition of human heart phospholipids: data from 53 biopsy specimens. J Mol Cell Cardiol 1985;17:769–73.

152. Rocquelin G, Guenot L, Astorg P, and David M. Phospholipid content and fatty acid composition of human heart. Lipids 1989;24:775–80.

153. Stanacev N, Stuhne-Sekalec L, Brookes K, and Davidson J. Intermediary metabolism of phospholipids. The biosynthesis of phosphatidylglycerophosphate and phosphatidylglycerol in heart mitochondria. Biochim Biophys Acta 1969;176:650–3.

154. Goodwin G and Taegtmeyer H. [5-3H]glucose overestimates glycolytic flux in isolated working rat heart: role of the pentose phosphate pathway. Am J Physiol 2001;280:E502–8.

155. Ohno Y, Suto S, Yamanaka M, et al. ELOVL1 production of C24 acyl-CoAs is linked to C24 sphingolipid synthesis. Proc Natl Acad Sci USA 2010;107:18439–44.

156. Henning S, Wambolt R, Schönekess B, Lopaschuk G, and Allard M. Contribution of glycogen to aerobic myocardial glucose utilization. Circulation 1996;93:1459–55.

157. Niklas J and Heinzle E. Metabolic Flux Analysis in Systems Biology of Mammalian Cells. Adv Biochem Eng Biotechnol 2012;127:109–32.

158. Sauer U. Metabolic networks in motion: 13C-based flux analysis. Mol Syst Biol 2006;2:62.

159. Hoffmann S and Holzhütter H. Uncovering metabolic objectives pursued by changes of enzyme levels. Ann N Y Acad Sci 2009;1158:57–70.

160. Wentz A, Avignin D, Weber M, et al. Adaption of myocardial substrate metabolism to a ketogenic nutrient environment. J Biological Chemistry 2010;285:24447–56.

161. Zhang J, Zhang W, Zou D, et al. Cloning and functional characterization of ACAD-9, a novel member of human acyl-CoA dehydrogenase family. Biochem Biophys Res Commun 2002;297:1033–42.

162. Ensenauer R, He M, Willard J, et al. Human acyl-CoA dehydrogenase-9 plays a novel role in the mitochondrial-oxidation of unsaturated fatty acids. Biol Chem 2005;280:32309–16.

163. Nada M, Abdel-Aleem S, and Schulz H. On the rate-limiting step in the beta-oxidation of polyunsaturated fatty acids in the heart. Biochim Biophys Acta 1995;1255:244–50.

164. Boudina S, Sena S, Theobald H, et al. Mitochondrial energetics in the heart in obesity-related diabetes: direct evidence for increased uncoupled respiration and activation of uncoupling proteins. Diabetes 2007;56:2457–66.

165. Paradies G, Petrosillo G, Pistolese M, Di Venosa N, Federici A, and Ruggiero F. Decrease in mitochondrial complex I activity in ischemic/reperfused rat heart: involvement of reactive oxygen species and cardiolipin. Circ Res 2004;94:53–59.

166. Li J, Romestaing C, Han X, et al. Cardiolipin remodeling by ALCAT1 links oxidative stress and mitochondrial dysfunction to obesity. Cell Metab 2010;12:154–65.

Appendix

1 Tables

Table 1: Constraints for the exchange of metabolites with the external (ext) and cytosolic (cyto) space.

Reaction: $m_{i,ext} \overset{v_i}{\longleftrightarrow} m_{i,cyto}$

Identifier	**Metabolite (m_i)**	**Constraint**
CC00237	Oxygen	$0 \leq v_i \leq +\infty$
CC00244	NH3	$-\infty \leq v_i \leq 0$
CC00287	Glutamine	$-\infty \leq v_i \leq 0$
CC00260	Glucose	$0 \leq v_i \leq +\infty$
CC00397	L-Lactate	$0 \leq v_i \leq +\infty$
CC00881	(R)3-Hydroxybutanoate	$0 \leq v_i \leq +\infty$
CC00379	Acetoacetate	$0 \leq v_i \leq +\infty$
CC01016	α-Linoleate	$0 \leq v_i \leq +\infty$
CC01977	Linolenate	$0 \leq v_i \leq +\infty$
CC00031	Docosahexaenoic acid	$0 \leq v_i \leq +\infty$
CC02174	LDL	$0 \leq v_i \leq +\infty$
CC00554	L-Isoleucine	$0 \leq v_i \leq +\infty$
CC00273	L-Lysine	$0 \leq v_i \leq +\infty$
CC00295	L-Methionine	$0 \leq v_i \leq +\infty$
CC00300	L-Tryptophan	$0 \leq v_i \leq +\infty$
CC00301	L-Phenylalanine	$0 \leq v_i \leq +\infty$
CC00341	L-Leucine	$0 \leq v_i \leq +\infty$
CC00353	L-Histidine	$0 \leq v_i \leq +\infty$
CC00394	L-Valine	$0 \leq v_i \leq +\infty$
CC00399	L-Threonine	$0 \leq v_i \leq +\infty$
CC00400	Ethanolamine	$0 \leq v_i \leq +\infty$

continues on next page

Table 1 – continued from previous page

Identifier	**Metabolite (m_i)**	**Constraint**
CC00452	Riboflavin	$0 \leq v_i \leq +\infty$
CC00488	Pyridoxine	$0 \leq v_i \leq +\infty$
CC00332	Choline	$0 \leq v_i \leq +\infty$
CC00369	Nicotinamide	$0 \leq v_i \leq +\infty$
CC00616	Folate	$0 \leq v_i \leq +\infty$
CC00788	Pantothenate	$0 \leq v_i \leq +\infty$

Table 2: Constraints for simulations of varied substrate availability with base line ATP consumption rate.

Reaction: $m_{i,ext} \overset{v_i}{\longleftrightarrow} m_{i,cyto}$

Identifier	**Metabolite (m_i)**	**Constraint**
CC00237	Oxygen	$0 \leq v_i \leq +\infty$
CC00244	NH3	$-\infty \leq v_i \leq 0$
CC00287	Glutamine	$-\infty \leq v_i \leq 0$
CC00260	Glucose	$0 \leq v_i \leq +\infty$
CC00730	Oleate	$0 \leq v_i \leq +\infty$
CC00397	L-Lactate	$0 \leq v_i \leq +\infty$
CC00379	Acetoacetate	$0 \leq v_i \leq +\infty$

Abbreviations used in the table for compartments are as following: ext, external; cyto, cytosol.

Table 3: Constraints for simulations of varied substrate availability as under experimental conditions [82]

Reaction: $m_{i,ext} \overset{v_i}{\longleftrightarrow} m_{i,cyto}$

Identifier	Metabolite (m_i)	Constraint
CC00237	Oxygen	$0 \leq v_i \leq +\infty$
CC00244	NH3	$-\infty \leq v_i \leq 0$
CC00287	Glutamine	$-\infty \leq v_i \leq 0$
CC00260	Glucose	$0 \leq v_i \leq +\infty$
CC00397	L-Lactate	$0 \leq v_i \leq +\infty$
CC00881	(R)3-Hydroxybutanoate	$0 \leq v_i \leq +\infty$
CC00379	Acetoacetate	$0 \leq v_i \leq +\infty$
CC00262	Acetate	$0 \leq v_i \leq +\infty$
CC00730	Oleate	$0 \leq v_i \leq +\infty$

Abbreviations used in the table for compartments are as following: ext, external; cyto, cytosol.

Table 4: Constraints for simulations of varied substrate availability (9 substrates) while satisfying the extended metabolic target function.

Reaction: $m_{i,ext} \overset{v_i}{\longleftrightarrow} m_{i,cyto}$

Identifier	Metabolite (m_i)	Constraint
CC00237	Oxygen	$0 \leq v_i \leq +\infty$
CC00244	NH3	$-\infty \leq v_i \leq 0$
CC00287	Glutamine	$-\infty \leq v_i \leq 0$
CC00530	Urate	$-\infty \leq v_i \leq 0$
CC00260	Glucose	$0 \leq v_i \leq +\infty$
CC00397	L-Lactate	$0 \leq v_i \leq +\infty$
CC00379	Acetoacetate	$0 \leq v_i \leq +\infty$
CC00446	Palmitate	$0 \leq v_i \leq +\infty$
CC01013	Stearate	$0 \leq v_i \leq +\infty$
CC00730	Oleate	$0 \leq v_i \leq +\infty$
CC01016	α-Linoleate	$0 \leq v_i \leq +\infty$
CC00025	Eicosapentaenoic acid	$0 \leq v_i \leq +\infty$
CC00031	Docosahexaenoic acid	$0 \leq v_i \leq +\infty$
CC00332	Choline	$0 \leq v_i \leq +\infty$
CC00400	Ethanolamine	$0 \leq v_i \leq +\infty$

Abbreviations used in the table for compartments are as following: ext, external; cyto, cytosol.

2 Overview of supplemental electronic material

Additional file 1: Gene expression annotation.
The identification of human heart tissue specific reactions requires a tissue specific gene expression profile. Gene expression samples have been obtained from different gene expression data available from Gene Expression Omnibus, including GDS181 and GSE1145. This table provides gene expression information annotated to metabolic reactions of the cardiomyocyte network. Each reaction identifier refers to a compartment localisation of the respective metabolic reaction. Furthermore, each entry in the table provides information about annotated Ensemble Gene ID, Geo Dataset ID, Geo Sample ID, Probeset ID, Gene ID, gene expression value and detection call. The information of gene expression status can be obtained from the column “Detection call”. Each expression is either categorized as present (P), absent (A) or M (marginal). Genes were considered as expressed for gene expression values with a cut-off greater than 100.
Format: XLS Size: 8.4MB

Additional file 2: Metabolites of the metabolic network.
Metabolites listed in this table occur in the metabolic network. For each entry a unique network identifier is given and provided with information of metabolite title, title synonym, metabolite sum formula and assigned compartment. Additionally cross-references to other databases are given and refer to the following databases: UniProtKB (UniProtKB entry), KEGG (Compound ID), Lipid Maps (LM ID), Pub Chem (CID) and Human Metabolome Database (HMDB ID). Abbreviations used in the table for compartments are as following, ext: external, cyto: cytosol, mito: mitochondrion, lyso: lysosome, peroxy: peroxisome and micro: microsome.
Format: XLS Size: 142KB

Additional file 3: References.
During the network reconstruction additional evidence for occurrence of metabolic reactions in the cardiomyocyte were obtained from previously reported studies. This table gives a full list of cross-references to PubMed identifier (PMID) providing evidence for included reactions of the metabolic network. Furthermore, directionality of reactions was set according to Gibbs energy ($\triangle G$, kJ/mol) and is provided with this table.
Format: XLS Size: 40KB

Additional file 4: Metabolic network of the human cardiomyocyte in SBML format.
Format: SBML Size: 982KB

Additional file 5: Definition and overview of objectives and constraints for simulation of metabolic and physiological functions of the cardiomyocyte.
To ensure consistency and full functionality of the metabolic network, a critical testing of physiological functions was performed based on knowledge of the cardiac metabolism by using flux balance analysis. The table lists all objectives and applied constraints as used in the optimization problem. Furthermore, constraints as used in functional pruning of the network are given. Abbreviations for constraints as used in simulations with FASIMU software are as follows: (+), secretion of the metabolite is allowed or the metabolite is product; (-), uptake of the metabolite is allowed or metabolite is substrate and (=), secretion and uptake of the metabolite is allowed or metabolites are either product or substrate.
Format: XLS Size: 125KB

Additional file 6: Flux distributions of metabolic and physiological functions of cardiomyocyte.
To ensure consistency and full functionality of the metabolic network, a critical testing of physiological functions was performed based on knowledge of the cardiac metabolism by using flux balance analysis. Abbreviations for compartments: ext - external, cyto - cytosol, mito - mitochondrion, lyso - lysosome, peroxy - peroxisome, micro - microsome.
Format: XLS Size: 1.86MB

Additional file 7: Testing functionality of Human heart model.
A comparison of the metabolic network to a previously reported genome-scale reconstruction of the human heart [147] was performed. The presented physiological functions of the cardiomyocyte (see Additional file 5) were applied to test the functionality of the partial network of the human heart and compare the performance of both networks. From 110 tested functions 53 were found to have no feasible solution, this included important cellular functions such as the citric acid cycle.
Format: XLS Size: 34KB

Additional file 8: Predicted metabolic fluxes of substrate uptake and oxygen demand for ATP expenditure in varied substrate availability.
Simulations of varied substrate availability were performed for four selected substrates, including glucose, oleate, acetoacetate and lactate while demanding a baseline ATP consumption rate (v_{ATPase}) of 21.6 mmol $\cdot$ $min^{-1}\cdot$ (l cell)$^{-1}$. This table lists uptake rates for oxygen, glucose, oleate, acetoacetate, lactate and the resulting total substrate uptake rate for each simulated substrate composition. Efficiency indices (C_{i+}) were separately calculated for each simulation.
Format: CSV Size: 26.7MB

Additional file 9: Alternate optima.
To identify alternate flux solutions that can equally satisfy the problem, i.e. yield the same optimal solution, additional simulations were performed. The MILP was re-solved after adding a constraint (z*) for a single flux of the original flux distribution which was set to either 1.01-fold (z_1^*) or 0.99-fold (z_2^*) of its original calculated flux value (v0).
The optimization problem was repeated with substrate combinations which were identified with the highest or lowest efficiency value while satisfying (1) a baseline ATP consumption rate and (2) a target function of the cardiomyocyte. This table includes all calculated flux solutions yielding the same optimal solution as with the original optimization problem. Furthermore, an overview is given of alternate flux solutions for fluxes representing external substrate and oxygen uptake. Statistical significance between flux solutions for the analysis of alternate flux solutions was determined by use of 1-way ANOVA.
Format: XLS Size: 2.65MB

Additional file 10: Predicted metabolic fluxes of substrate uptake and oxygen demand for fulfilling the metabolic target function in varied substrate availability.
Simulations of varied substrate availability were performed for nine selected substrates, including glucose, palmitate, stearate, oleate, α-linoleate, eicosapentaenoate, docosahexaenoate, acetoacetate and lactate. During the simulations, an ATP expenditure (v_{ATPase}) of 21.6 mmol $\cdot$ $min^{-1}\cdot$ (l cell)$^{-1}$ and a metabolic target flux were demanded, as specified in Additional file 6. Uptake rates for all nine substrates, the resulting total substrate uptake rate and oxygen consumption rate for all simulated substrate compositions which fulfilled the metabolic objective are given. Furthermore solutions for glycogen synthesis and

glycogenolysis as determined during simulations are shown.
Format: CSV Size: 24.2MB

Eidesstattliche Versicherung

„Ich, Anja Karlstädt, versichere an Eides statt durch meine eigenhändige Unterschrift, dass ich die vorgelegte Dissertation mit dem Thema:

„A systems biology approach to model cardiomyocyte metabolism“

selbstständig und ohne nicht offengelegte Hilfe Dritter verfasst und keine anderen als die angegebenen Quellen und Hilfsmittel genutzt habe.
Alle Stellen, die wörtlich oder dem Sinne nach auf Publikationen oder Vorträgen anderer Autoren beruhen, sind als solche in korrekter Zitierung (siehe „Uniform Requirements for Manuscripts (URM)“ des ICMJE -*www.**icmje**.org*) kenntlich gemacht. Die Abschnitte zu Methodik (insbesondere praktische Arbeiten, Laborbestimmungen, statistische Aufarbeitung) und Resultaten (insbesondere Abbildungen, Graphiken und Tabellen) entsprechen den URM (s.o) und werden von mir verantwortet.
Meine Anteile an etwaigen Publikationen zu dieser Dissertation entsprechen denen, die in der untenstehenden gemeinsamen Erklärung mit dem/der Betreuer/in, angegeben sind. Sämtliche Publikationen, die aus dieser Dissertation hervorgegangen sind und bei denen ich Autor bin, entsprechen den URM (s.o) und werden von mir verantwortet.

Die Bedeutung dieser eidesstattlichen Versicherung und die strafrechtlichen Folgen einer unwahren eidesstattlichen Versicherung (§156,161 des Strafgesetzbuches) sind mir bekannt und bewusst.“

Berlin, den 20.04.2013

Anteilserklärung

Frau Anja Karlstädt hatte folgenden Anteil an den folgenden Publikationen:

Publikation 1: Gille C., Bölling B., Hoppe A., Bulik S., Hoffmann S., Hübner K., Karlstädt A., Ganeshan R., König M., Rother K., Weidlich M., Behre J., Holzhütter H.G. HepatoNet1: a comprehensive metabolic reconstruction of the human hepatocyte for the analysis of liver physiology, Molecular Systems Biology 6:411, 2010.

Beitrag im Einzelnen:

Beteiligung an der Erstellung und Validierung des Stoffwechselnetzwerkes „HepatoNet1". Analyse und Annotation der verwendeten Genexpressionsdaten. Recherche thermodynamischer Parameter und Konzentrationsbereiche von Metaboliten zur Verwendung in mathematischen Simulationen. Beteiligung am Verfassen des Manuskripts.

Publikation 2: Karlstädt A., Fliegner D., Kararigas G., Sanchez Ruderisch H., Regitz-Zagrosek V., Holzhütter H.G. „CardioNet: A human metabolic network suited for the study of cardiomyocyte metabolism. BMC Systems Biology 2012;6:114".

Beitrag im Einzelnen:

Erstellung, Validierung und Prüfung des Stoffwechselnetzwerkes. Annotation und Analyse verwendeter Genexpressionsdaten. Konzeption, Planung und Durchführung der mathematischen Simulationen. Verfassung des Manuskripts.

Berlin, den 20.04.2013

Curriculum vitae

Mein Lebenslauf wird aus datenschutzrechtlichen Gründen in der elektronischen Version meiner Arbeit nicht veröffentlicht.

Publications

Peer-reviewed Publications

2012 **Karlstädt A**, Fliegner D, Kararigas G, Sanchez Ruderisch, Regitz-Zagrosek V, Holzhütter HG. CardioNet: A human metabolic network suited for the study of cardiomyocyte metabolism. BMC Systems Biology 2012;6:114

2010 Gille C, Bölling C, Hoppe A, Bulik S, Hoffmann S, Hübner K, **Karlstädt A**, Ganeshan R, König M, Rother K, Weidlich M, Behre J, Holzhütter HG. HepatoNet1: a comprehensive metabolic reconstruction of the human hepatocyte for the analysis of liver physiology. Mol Syst Biol 2010;6:411

Conference presentations

2013 **Karlstädt** A, Fliegner D, Kararigas G, Sanchez Ruderisch H, Regitz-Zagrosek V, Holzhütter HG. CardioNet: A human metabolic network suited for the study of cardiomyocyte metabolism. Poster presentation: Heart Failure conference, Lisbon, May 2013

2013 **Karlstädt** A, Fliegner D, Kararigas G, Sanchez Ruderisch H, Regitz-Zagrosek V, Holzhütter HG. CardioNet: A human metabolic network suited for the study of cardiomyocyte metabolism. Poster presentation: DZHK Meeting “Epigenetics and system biology in cardiovascular diseases”, Berlin, April 2013

2012 **Karlstädt** A, Fliegner D, Kararigas G, Sanchez Ruderisch H, Regitz-Zagrosek V, Holzhütter HG. CardioNet: A human metabolic network suited for the study of cardiomyocyte metabolism. Poster presentation: Conference of Systems Biology of Mamalian Cells (SBMC) 2012, Leipzig, July 2012

Acknowledgements

I would like to express my gratitude to several people. First and foremost, I would like to thank my adviser Prof. Hermann-Georg Holzhütter, who gave me this topic. I appreciate the time he spent to discuss research topics with me. I also would like to thank Prof. Vera Regitz-Zagrosek and her team for fruitful discussions and their contribution to this thesis.

I wish to acknowledge my colleagues at the Holzhütter lab and Regitz-Zagrosek lab for their support and academic discussions. In particular, I would like to thank Daniela Fliegner, Sylvia Albrecht and Bernd Binder for a thorough review of this thesis and Christoph Gille for his support during the network reconstruction.

I am thankful for my friends, including Preety Anand and Jike Chui. Their support and open-mind kept me grounded and motivated. I am indebted to my family for the love and encouragement during these years in Berlin. Without my parents and grandparents I could not have accomplished this thesis.

Finally, this thesis would not have been possible without the financial support of the German Research Foundation (DFG) and the Konrad-Adenauer Foundation.